POLITECNICO DI TORINO

Department of Mechanical and Aerospace Engineering

Master of Science in Automotive Engineering

Development and analysis of a suspension control logic for motorcycling application

Supervisor:

Prof. Alessandro Vigliani

Co-Supervisors:

Ing. Angelo Domenico Vella
Prof. Lorenzo Peroni

Candidate:

Stefano Luca Parravicini

Academic Year 2023/2024

Contents

List of Figures

List of Tables

Acknowledgements

I would like to express my profound gratitude to Professor Vigliani and Ing. Vella for their support in developing this thesis, patience, and advice. In addition, I would like to express my appreciation to IPG for supplying me with the essential software, which greatly facilitated the completion of this work.

1 Abstract

The genesis of *intelligent* suspensions can be traced back to the latter part of the last century when the concept of isolating oscillations was applied to automotive suspensions. This sparked a wave of research and development focused on creating suspensions capable of providing controlled responses. Differently from the automobile industry, motorcycle makers and OEMs have shown interest towards active suspension systems only in recent years, limited by the technological challenges that the implementation of these systems presents in the motorcycle field. Foremost among these are weight, space, and energy constraints. Therefore, the mass production of motorbikes equipped with live-tunable suspension settings is restricted to the so-called *semi-active* suspension layouts. Differently from an *active* suspension system, a semi-active prototype requires a considerably lower amount of energy, but on the other hand, is limited by the passivity constrain. In the current thesis project, pre-existing control logics applied to semi-active suspension layouts are investigated and compared. The principal observation will point out the conflict between comfort and handling, a limiting factor of the traditional passive systems and semi-active suspension control strategies. In recent years, more sophisticated control rationales able to minimize such dispute have been presented. The more and more dynamic environment of premium motorcycles opting for semi-active suspension schemes, motivates the research of an alternative solution to control semi-active suspension systems for 2-wheeled vehicles. In the current thesis project, the author focused on the possibility of designing a simpler control logic based on a blend of pre-existed control rationales able to minimize the handling-comfort duality. The backbone of the control logic is represented by two separate control logics; one able to master the handling, and a second capable of maximising comfort indexes. The suspension control unit will be finally responsible for identifying the motorcycle riding condition and thus, select to which extent to focus the orientation of the controller towards comfort to the detriment of the handling, or vice-versa. From this perspective, the innovative Hybrid control logic is indeed able to overcome the comfort-handling conflict. Different indexes exploited in the literature to measure comfort and road-holding are presented and used to measure coherently the performance of the Hybrid control logic. The design of the controller will be pursued through the simulation of the suspension through a quarter-car model in a Matlab-Simulink environment. Successively the control rationale is optimized in a 4DOF motorcycle model and the resulting performances are shown. To conclude the thesis project a test and validation of the controller is performed via the *IPG MotorcycleMaker* vehicle simulator.

2 Introduction

In the dynamic landscape of the automotive industry, the quest for creating captivating products that resonate with consumers is ever-present. At the forefront of this pursuit lies the optimization of vehicle attributes, specifically geared towards achieving a harmonious blend of road and ride performance. The pivotal challenge in this venture revolves around striking the right equilibrium between ensuring optimal comfort and road-holding properties. Original Equipment Manufacturers (OEMs) are dedicated to refining these aspects, making a thorough exploration of suspension systems essential in automotive engineering. In the last century, the industry in a close relationship with technical universities and more in general, with research institutes, has structured a novel method to approach the suspension design. Starting from the 1960s, with the introduction of the hydro-pneumatic suspension system engineered by Citroen [8], the innovative concept of 'active' suspension was presented to automotive manufacturers. Nowadays, the idea of controlled suspensions is taken to a completely different level. More in detail, due to the impressive progress that electronics has faced in the last decades, the idea of electronically controlled suspension has undergone significant advancements. These innovations have enabled automotive engineers to push the limits of suspension systems further than ever before. The promising future ahead of non-passive suspensions was also demonstrated by the continually increasing number of car manufacturers who research, design and develop controllable spring-damper systems [12]. To testify the high expectations and research around this topic, noticeable is the parenthesis in F1 from the 80s to the 90s, when the active suspensions made multiple appearances [10]. Anyway, 'intelligent' suspension layouts have faced mass production just limited, due to the multitude of complications the active systems imply. Another crucial role was covered by the great performance achieved by the traditional passive suspension in the last years with the adoption of non-linear characteristics and fine-tuning. Anyway, semi-active and active systems nowadays represent the finest and the prime product in terms of suspension performance.

2.1 Motivations and goals

This research aims to uncover the functionalities and the performances of well-known control strategies and to define a competitor control logic. The literature is plenty of study of rationales applied to 4-wheeled vehicles and off-road machines. On the other hand, it is less likely to face control logics applied to motorcycles. Therefore the present project aspires to define an innovative control strategy suitable for the mass production of 2-wheeled vehicles. The motivations that drives the thesis project lies in the possibility to develop a real-implementable control scheme able to asses

both comfort and handling, overcoming the conflict that generally characterises the suspension systems. Regarding innovative active and semi-active suspension controllers, in the landscape of current logics, it is common to encounter sophisticated control schemes adept at addressing this double objective, such as MPC, Neural networks and deep learning algorithms. As a consequence, the object of research is to implement an easier semi-active competitor control logic, based on simpler rules, without the need to derive the motorcycle plant model or extensive tuning. The ideal results are expected to demonstrate an improvement in passengers' comfort, riding feeling and safety compared to standard passive suspensions. The controller will be immersed in the restricted market of available suspension control algorithms for motorcycles. Indeed, the genesis of suspension control logics finds its roots in the early 2010s, with the Ducati Skyhook Suspension (DSS), one of the first rationale adopted to manage motorcycle riding comfort, to the more recent examples of electronically controlled suspensions, such as the Ohlins TTX-EC, DCD-Continuous Damping Control produced by ZF technologies or the KECS-Kawasaki Electronic Control Suspension [15] [1] [11].

2.2 Suspension fundamentals

In order to face properly the proposed topic of the research it is important to underline crucial key factors. First of all, it is necessary to introduce the fundamentals of the suspension design. The suspensions are intended as all the elements that compose the support of the vehicle body over the wheels. Therefore, it is possible to state that 'the suspension is what links the wheels to the vehicle body and allows relative motion'[16]. The necessity of a compliance element able to uncouple the so-called 'sprung' and 'unsprung' masses, i.e. the suspended and non-suspended masses over the spring-damper system, can be straightforward: enhancing the comfort of the users. It is imaginable that for the majority of the cases, the road profile is uneven, presenting irregularities and discontinuities. The smallest bumps are successfully absorbed by the tyres, which deform under the weight of the vehicle proceeding over an obstacle or small corrugations of the pavement. On the other hand, for larger disturbances the presence of the suspension is mandatory. A second crucial role may be interpreted as less intuitive and more complex: the road holding or handling. Normally it is referred to handling as the capability of the vehicle to ensure grip and adherence to the road pavement. Consequently, a supplementary aspect, as important as the comfort properties of the vehicle, is required to ensure the tyres are supplied by enough weight to guarantee the desired adherence. It is possible to summarize the main goals of the suspension assembly as follows[2]:

- Ensure optimal isolation from road disturbances enhancing the comfort of the

occupant

- Facilitate optimal tire-ground adherence, ensuring traction during braking, acceleration, and secure turning manoeuvres
- Impose the desired trim for the different manoeuvres

The suspension layouts adopted in the motorcycling industry are substantially different from the common automotive McPherson scheme. The limited space, the stringent ergonomics properties and the weights that refer to such types of vehicles, led the motorcycle suspension specialists to develop alternative solutions. The most common front suspension system is the so-called 'telescopic' suspension, composed of an inner and an outer tube coupled in a prismatic joint. The system is completed by a steering system composed of a bearing on the motorcycle chassis. The motion of the inner and outer tube is regulated by a spring and damper system, with the intent of uncoupling the vehicle body and the road asperities. The telescopic layout, in the majority of the cases implemented in the 'upside-down' version, i.e. with the outer tube in the uppermost position, has earned the title of the principal suspension layout due to the limited weight and inertia, as well as compactness and dynamic properties. As soon as the motorcycle body is subjected to longitudinal accelerations, for instance in case of a braking or an acceleration manoeuvre, the front suspension will compress or extend. Accordingly, the sprung mass will perceive a pitch motion. It follows that the front trail and the wheelbase will vary. The resulting variation of geometries is, indeed, a desired property of the telescopic suspension system: due to the reduction of the front trail in braking condition, the motorcycle results more rapid changing direction, a positive feeling when entering the turn. On the other hand, when the motorcycle is subjected to a strong acceleration, the front trail will increase, resulting in more stability. The panorama of rear suspension solutions in the motorcycle sector is wider. The principal goal of the rear suspension system is the isolation of the occupants by absorbing the road bumps and providing an optimal spring deformation. To accomplish this task, engineers have developed multiple solutions based on different mechanisms, resulting in an optimal suspension stroke and a wider possibility of tuning. Anyway, the swingarm layout composed of a spring and damper interconnecting the swingarm beam and the motorcycle body is one of the wider-spread solutions, due to its simplicity, large spring strokes and limited reaction forces. In figure 1 an example of the common suspension systems adopted in recent years is illustrated, where the front suspension is a traditional telescopic upside-down fork, and the rear suspension scheme presents a swingarm.

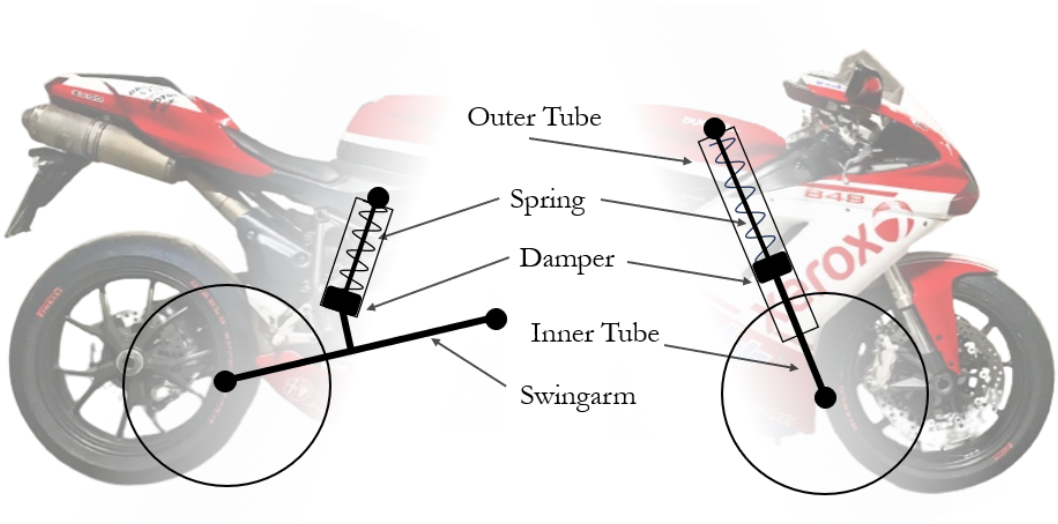

Figure 1: Common motorcycle suspension layouts: front telescopic fork, and rear swingarm

As previously mentioned, one of the first goals of the suspension mechanism is to isolate the occupants from the road asperities. Consequently, the principal element of a suspension is the spring. Such deformable element is represented by a torsional coil spring interposed between the sprung and unsprung masses, as visible from figure 1. The most generic guideline suggests a soft spring as possible to guarantee comfort, in order to anticipate the natural frequencies of the suspensions. Adopting this solution, the wheel motion and the rider seat will be uncoupled even at low speeds. On the other hand, a reduced spring stiffness will affect the in-plane motorcycle dynamics: excessively soft suspensions will be excited by the accelerations and forces to which the vehicle is subjected when riding, inducing variation of the vehicle geometries and excessive load transfers. Oppositely, immoderate stiff suspensions will induce adherence reduction and minor comfort. As imaginable the choice of the spring stiffness is a function of the motorcycle's weight, geometry, available power, load distribution, and available wheel travel space. More importantly, the choice of the suspension stiffness is a trade-off between comfort and handling properties[3]. To tune the wheel travel response to different road bumps, usually a progressive suspension characteristic is adopted. More in detail, generally, when the wheel motion is limited, the force exerted by the spring has a linear trend along with the suspension travel. However, when the spring reaches excessive deformations the suspension force perceived evolves into a non-linear behaviour. Typically the suspension behaviour drifts into a more rigid spring response. The so-called 'progressive' springs help ensure comfort and to limit the possibility of reaching the bump stop. A spring characterisation is shown in figure 2.

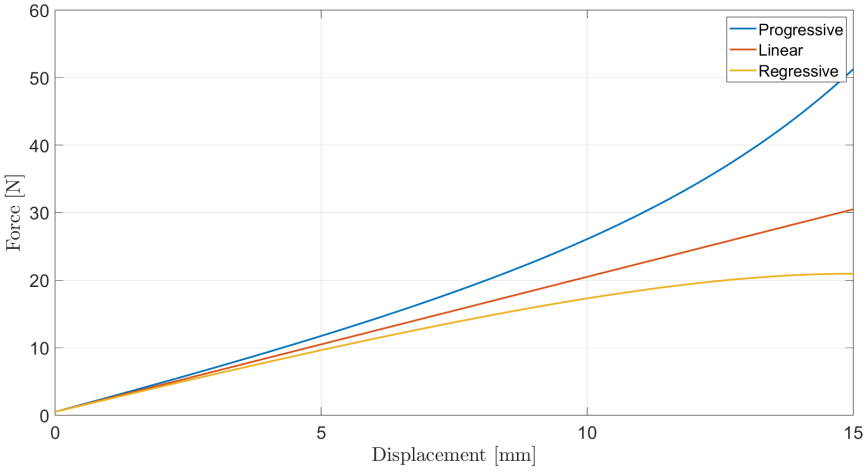

Figure 2: Spring force characteristics

The second crucial element of a suspension assembly is the damper. Differently from the spring, a damper will react as a function of the travel speed. The dampers aim to dissipate the oscillation the spring will induce. The tuning of the dampers is therefore critical since they heavily affect the vehicle's response to a road disturbance. Regularly, the damping coefficient in compression is reduced compared to the rebound phase to ensure a proper passage over a bump or a step[4]. The characteristic curve of the dampers is reported in figure 3.

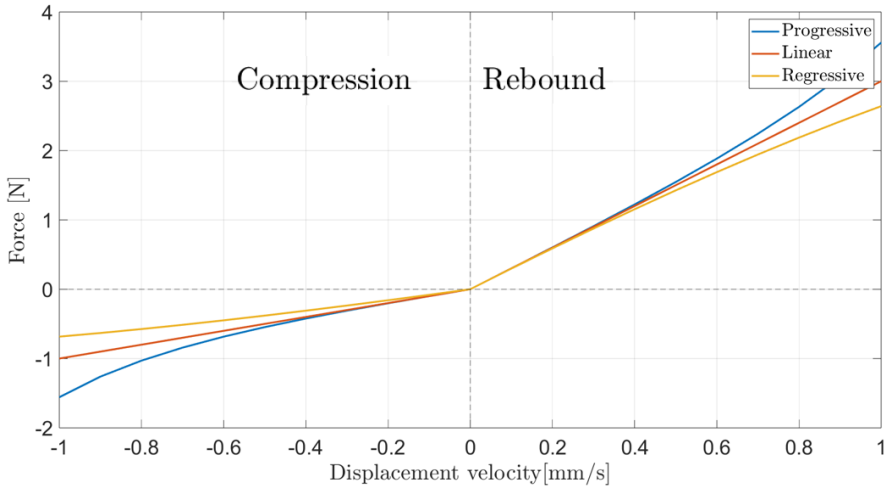

Figure 3: Damper force characteristics

The damper manufacturing solutions are multiple. In most cases, the damping is obtained through a reed valve which permits the passage of a viscous oil. Damping is guaranteed through the dissipation of energy as the oil passes through the valve orifices . Commonly, in the recent damping cartridge solutions the damping is different in compression and in the extension phase, for the reasons cited previously. This characteristic was achievable through the incorporation of valves with varying attributes, directing the flow of oil in response to the motion of the suspension. A real suspension system is visible in figure 4.

Figure 4: Common suspension layout for motorcycle applications. Left: Front suspension assembly. Right: Rear suspension assembly

2.3 Comfort - Handling trade-off

In paragraph 2.1 it was briefly mentioned the contraposition between the comfort of riding, and the road holding. In the current paragraph this contraposition will be investigated more deeply. The main goals of the suspension go unfortunately in opposite directions since the comfort properties are ensured by softer springs and dampers, whereas optimal vehicle trim, geometries and adherence are enhanced by stiffer suspension settings. One initial approach for addressing this issue involves considering the comfort problem through the analysis of the Frequency Response Function (FRF) of a quarter car model. A quarter-car model is a simple representation of a suspension, and it is useful to investigate the behaviour of the system when subject to particular road inputs. It is possible to imagine, as a first approximation,

the suspension as composed of two masses suspended over a spring and divided by a damper and a second spring in parallel. From the frequency response function in figure 5, retrieved for three different damping values, it is evident the comfort is ensured by a softer suspension since it allows to decouple the sprung mass from the wheel mass and the road. A softer suspension setting, indeed, anticipates the natural frequency related to the sprung mass filtering any further higher-frequency component, thus inducing better comfort. On the other hand, it is straightforward that in the vicinity of the resonance frequency of the suspended mass, the response is magnified. Handling, differently, is focused on the response of the unsprung mass which determines the reaction forces the vehicle exchanges with the ground. The main goal to ensure good handling properties is a low-variant tire-ground force. From the frequency response function of figure 5 it is evident how a more damped solution will induce a more regular reaction force transfer function, hence providing better handling and road holding. It is important to underline how the second peak of figure 5 is linked to the unsprung natural frequency, and it is not particularly affected by the choice of suspension damping regarding comfort. It is instead extremely sensitive when considering the vertical tire-ground forces.

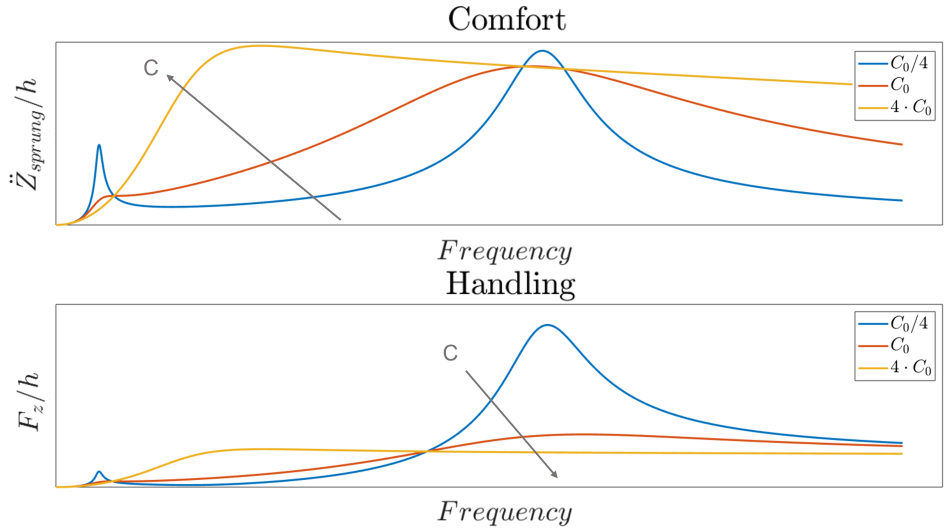

Figure 5: Up: Comfort frequency response function, Down: Handling frequency response function

An intuitive further consideration is then possible taking into consideration the variation of the geometries and trim of the vehicle. An important quantity, as mentioned, is the centre of gravity height, which affects significantly the riding behaviour of the motorcycle. The front trail also plays an important role in the manoeuvrability

of the vehicle, the turning capabilities and the stability of the motorcycle. Consequently, any variation of such quantities is critical and must be controlled. One of the main reasons a soft suspension is unsuitable for ensuring handling is that, when subjected to the forces experienced during driving, it deflects excessively, leading to a substantial variation in the aforementioned parameters. It is evident that the setting of the motorcycle suspension is a trade-off between comfort and handling. To better visualise the complexity of the problem, figure 6 is proposed which shows the variation of the root mean square value of the sprung mass acceleration and the tire-ground contact forces, for different suspension settings. The optimal comfort is ensured by soft springs and damping, whereas the ideal handling behaviour is enhanced by a stiffer spring, therefore as mentioned, it is evident that it is not possible to ensure both comfort and handling at the same time. It is worth mentioning that the curves proposed in the graph avoid the southwest side of the chart, corresponding to the optimal condition of minimised accelerations and force variation. It is therefore straightforward how difficult can result the setting of the suspension damping.

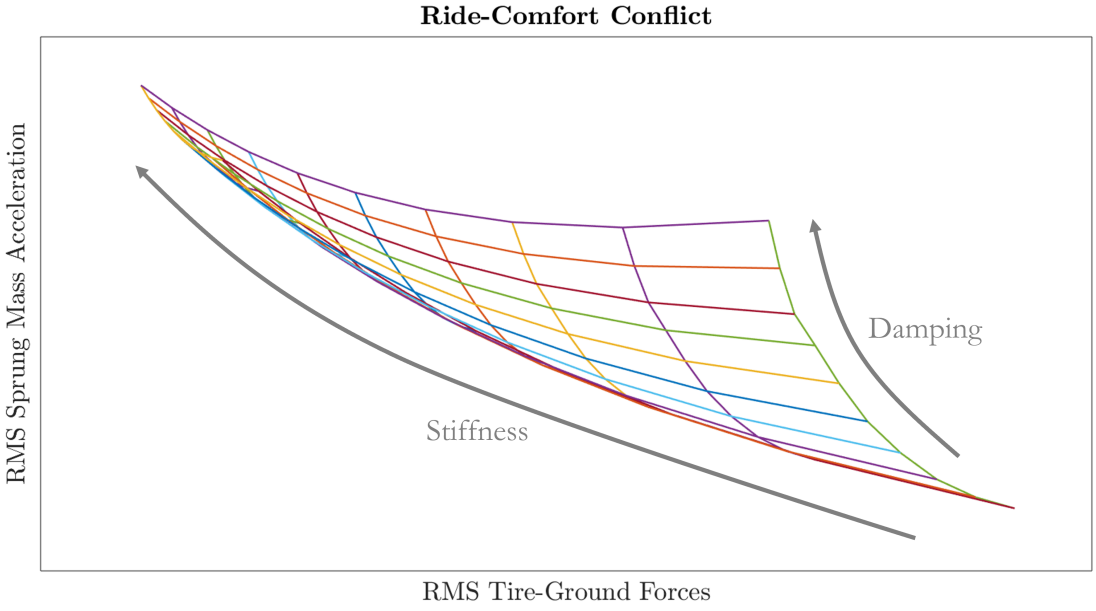

Figure 6: Comfort-handling conflict

This analysis elucidates the potential utility of implementing a variable-damping suspension system. Adjusting damping characteristics as needed can be advantageous, allowing for optimization based on specific requirements, whether emphasizing

handling or prioritizing comfort, depending on the driving situation.

2.4 Passive and Active suspensions

Based on the findings outlined in the previous chapter, automotive engineers began exploring technical options for adjustable suspension settings. The most intuitive solution considers an actuator interposed between the sprung and unsprung masses, placed in parallel with the spring. This layout, called 'active suspension system', unveiled numerous setting possibilities, realising a completely tunable response of the suspension adaptable to any situation. A multitude of control logics was developed, but more in particular, this solution provided the opportunity to dynamically correct the vehicle attitude, enhancing comfort but more importantly, handling, as mentioned in chapter 2. The main drawback of such implementation was the difficulty of retrieving the necessary amount of energy to feed the force actuators. It is, indeed, one of the major problems when this concept is applied to 2-wheeled vehicles, since the space available on the motorcycle is extremely limited, and the harvesting of energy represents a difficult engineering challenge. An alternative solution is to vary the damping setting, extracting only the energy required to dynamically change the suspension damping characteristic. The aforementioned layouts are commonly described as 'semi-active suspension systems'. Such solutions are particularly versatile but have to face a crucial drawback. The possibility of actively changing the amount of damping implies the so-called 'passivity constraint', which means it is not possible to introduce energy to the suspension systems. It is only possible to tune the energy dissipation per unit of time. The principal semi-active solutions are realised with the following technologies [20]:

- Solenoid/servo valve dampers
- Magnetorheological dampers
- Electromagnetic dampers

As mentioned in 2.2, the damping effect is obtained by forcing a working fluid through a series of orifices machined in a valve. It is thus possible to vary the flow area of the valves to change the effective damping coefficient of the dampers. One possibility involves using a solenoid valve, which once energized, moves a spool forced by a spring to change its relative position with the external housing. Due to the variation of the spool position, a different overlap between the passages of the oil through the housing and the spool is perceived [20]. Another possibility takes into consideration a servo electro-hydraulic system, enhancing a prompter response of the valve [17]. Servo systems on the other hand are more expensive and complex. Solenoid actuators are the optimal solution when the damping does not require a continuous variation,

but instead involves two different states of the damper, i.e. high damping value or low damping value. In the aforementioned case, the solenoid valve can easily open or close a bypass thus changing the actual damping [21].
Magnetorheological dampers are innovative systems based on non-Newtonian fluid which can change their viscosity when subjected to an electromagnetic field [22]. An interesting aspect of this technology is the speed of the response. As soon as the controller sends a command signal, the variation of the fluid viscosity is a matter of milliseconds [22].
The electromagnetic dampers are based on the interaction of a moving coil with a magnetic field, normally produced by a permanent magnet. The electric coil is linked to an external resistor, which on the basis of its value changes the damping action of the suspension. Therefore, through the variation of the external resistance perceived by the coil it is possible to control the damping of the semi-active system.

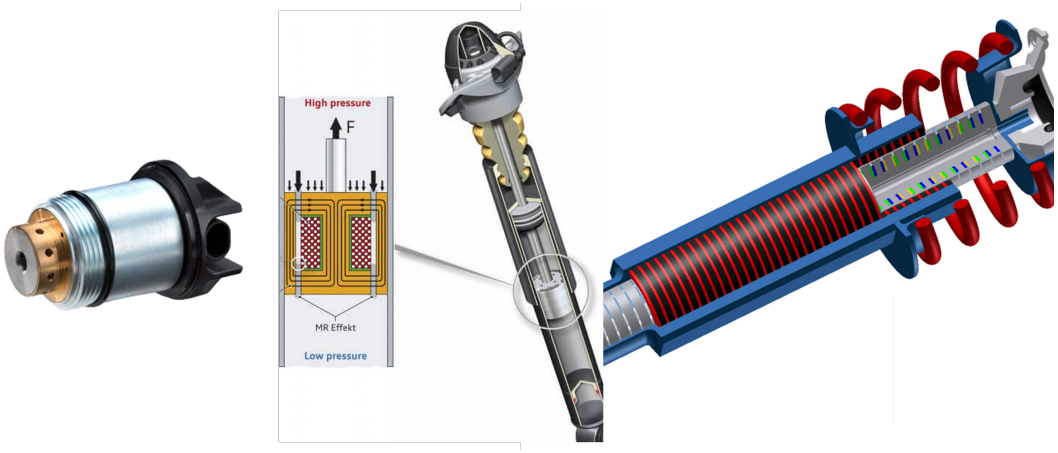

Figure 7: Left: Solenoid Valve manufactured by RAPA. Centre: MR fluid semi-active damper. Right: Electromagnetic suspension

3 Semi-active suspensions: State of the art

Alongside the system's layout presented in the previous paragraphs, a suspension control unit, the '*brain*' of the semi-active suspension, is necessary. Therefore an extensive literature on suspension control logics has been developed in recent years. In the current section, the primary controllers of the semi-active suspension system are presented. The focus of the project, as will be presented in future chapters, is limited to the semi-active control systems and as a consequence, the pre-existing controllers taken into account as possible competitors, and presented in this chapter, are non-active logics only. The first control strategy taken into account is one of the first rationales developed, the Skyhook control strategy, invented by Karnopp in 1974 with the intention to isolate a structure from the oscillations imposed by external inputs [13].

3.1 Skyhook control strategy

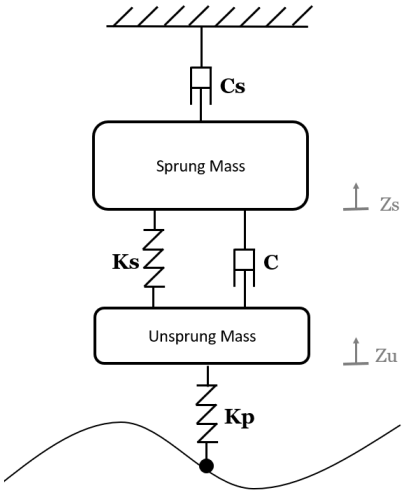

Figure 8: Skyhook configuration

3.1.1 Ideal Skyhook

The first method presented is the widely spread *Skyhook* control method. This suspension scheme aims to minimize the disturbances and oscillations that the occupants of the vehicle, or the rider, may perceive. It is then straightforward why the Skyhook control method is defined as a 'comfort-oriented' control strategy[27].

A standard quarter-car model with 2 DOF is exploited and represented in figure 8 to represent the system in question. As the term may suggest, the *skyhook* system refers to an ideal scheme, supposed to reduce the sprung mass vibrations through a second shock absorber attached between an inertial frame and the sprung mass [9][27]. The aforementioned system can be described by the equation of motion:

$$\begin{bmatrix} m_s & 0 \\ 0 & m_u \end{bmatrix} \begin{Bmatrix} \ddot{z}_s \\ \ddot{z}_u \end{Bmatrix} + \begin{bmatrix} c_s + c & -c \\ -c & c \end{bmatrix} \begin{Bmatrix} \dot{z}_s \\ \dot{z}_u \end{Bmatrix} + \begin{bmatrix} k_s & -k_s \\ -k_s & k_s + k_p \end{bmatrix} = \begin{Bmatrix} 0 \\ k_p h \end{Bmatrix} \tag{1}$$

where m_s and m_u are the sprung and unsprung masses respectively, c_s is the damping characteristic of the Skyhook shock absorber in question, and c is the damping coefficient of the traditional damper. The suspension and radial stiffness of the tyre are represented with ideal springs of characteristic k_s and k_p respectively. To study the behaviour of the system, the quarter-car model is simulated with a chirp sine wave input road signal. A comparison between the passive and ideal Skyhook systems is represented in figure 9, where the sprung mass acceleration is plotted with respect to time and frequency:

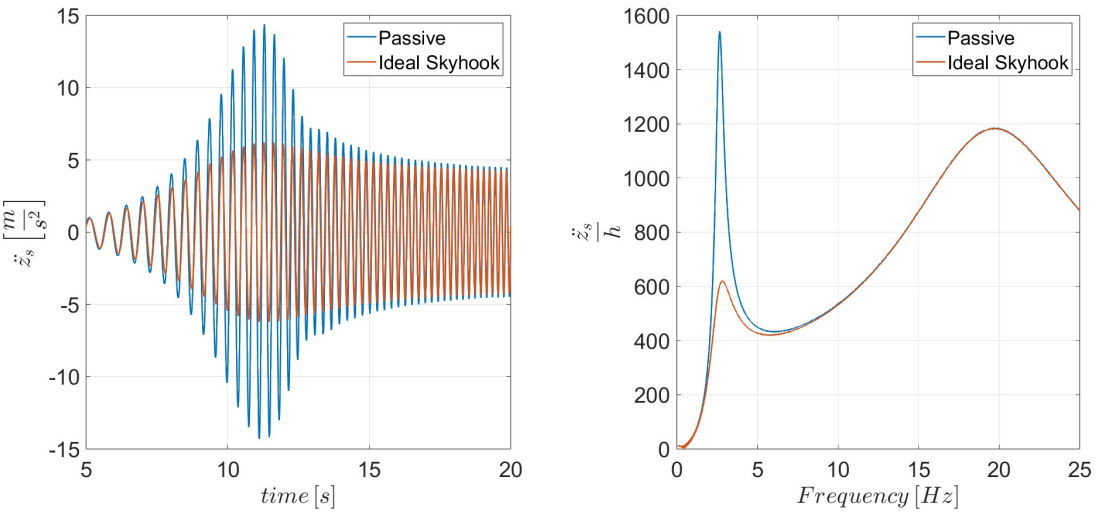

Figure 9: Acceleration response to a sweep signal in input

As it is visible, the active system is effectively able to reduce the displacement of the motorcycle body to an input disturbance. However, it is also important to analyse the response of the sprung mass velocity in order to highlight the system's vibrational characteristics. Indeed, figure 10 represents the transfer function and the

time response of the sprung mass velocity of both systems considered, passive and Ideal Skyhook, when the input signal is a sine wave sweeping from 0.01 to 25 Hz.

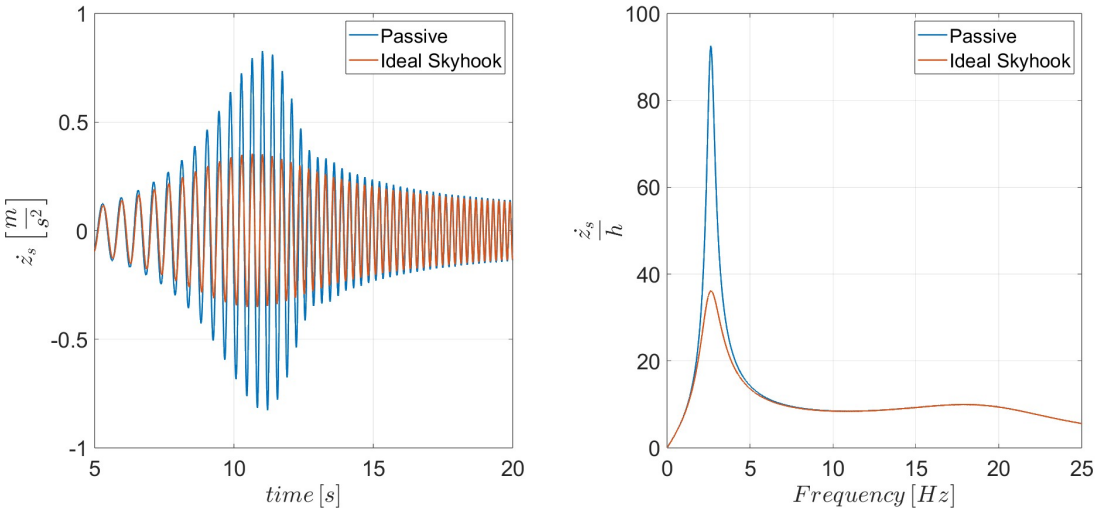

Figure 10: Velocity transfer function and time response of the Skyhook and passive systems

3.1.2 Active Skyhook

Unfortunately, the ideal skyhook is not practically achievable, due to the impossibility of disposing a fixed frame above the sprung masses, able to absorb the chassis vibrations [9]. As a consequence, a multitude of 'real-world' solutions is available. One possible layout provides that the shock absorber element is replaced with an active damper between the two masses [13]. The system shown in figure 11 can replicate the skyhook damper actions and can be defined as an 'Active suspension system'. The aforementioned Skyhook active version represents a 'real-implementable' solution, given the active damper provides an equivalent force to the fictitious Skyhook shock absorber. In the following equation 2, is represented the overall force the dampers actuate to the sprung mass.

$$F_{sprungmass} = -C_{skyhook}\dot{z}_s + c(\dot{z}_u - \dot{z}_s) \tag{2}$$

The velocity-dependent force elements are therefore the Skyhook damper and the shock absorber interposed between the sprung and unsprung mass. It is possible to represent the force of the actuator as the product between the suspension stroke velocity and a variable active damping coefficient C_{active}, as shown in figure 3.

$$F_{active} = C_{active}(\dot{z}_u - \dot{z}_s) \tag{3}$$

From the equality of the terms F_{active}=$F_{sprung\ mass}$, it is possible to finally obtain C_{active}:

$$C_{active} = -\frac{\dot{z_s}}{\dot{z_u} - \dot{z_s}} C_{skyhook} + c \tag{4}$$

From figure 4 it is possible to conclude that the real active suspension scheme requires distinctive qualities. Firstly, such a solution must consider continuously variable damping characteristics, and the response of the actuator should be rapid enough to suit the fast-varying conditions of the input road. But more importantly, it is evident that the damping coefficient can be negative, and this is the reason why such a solution is an *active* solution, since it is required not only to regulate the dissipation of energy but also to provide it subform of an external force.

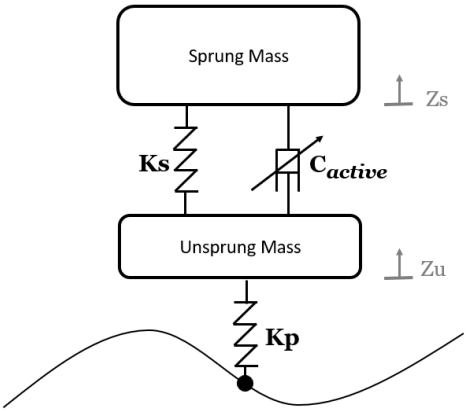

Figure 11: Active system configuration

More in detail, equation 4 shows that anytime the sprung mass velocity and the difference of the sprung and unsprung mass speed have the same sign, the damping coefficient may assume a negative value. The behaviour of the ideal skyhook logic is consequently implementable only by an active system able to provide and deliver power to the system analysed, as a four-quadrant actuator [9][23]. However, those types of suspension layouts are perfectly replacing the skyhook shock absorber only on a conceptual framework. Indeed, when $\dot{z}_u$ and $\dot{z}_s$ have the same value the equivalent damping should reach infinite values since the denominator goes to zero. To conclude, it is possible to resemble the Skyhook system adopting a four-quadrant actuator, while it is definitely impossible to perfectly replicate its response. In addition, the unsprung masses are influenced by such an alternative solution since they are affected by the opposite force the active damper actuates on the sprung mass.

3.1.3 Semi-active Skyhook

The high cost and energy demand of the active system approximating the Skyhook technology are concerning. Consequently, another interesting solution consists of replacing the traditional shock absorber located between the sprung and unsprung mass, no more with an active actuator, but with a 'semi-active' damper. The semi-active version of the Skyhook strategy consists of modulating the damping coefficient in different configurations to replicate the original Skyhook system [9]. As mentioned in 2.4, a passive or semi-active damper, does not require harvesting nor storage of energy, limiting the complexity of the system. The energy requirements are critical aspects during the vehicle development phase since designers have to deal with manufacturing costs and feasibility issues. Such an aspect is even more pronounced in motorcycle productions where the space available for additional actuators is extremely limited[27]. The semi-active Skyhook solution is an approximation of the ideal system: the unsprung masses are still influenced by the action of the semi-active damper, and in addition, the damping characteristic is no longer continuously modulating, but differently it switches from a low damping state to a high damping one following the law [13]:

$$C_{semi-active} = \begin{cases} C_{min} & if \quad \dot{z_s}(\dot{z_s} - \dot{z_u}) \leq 0 \\ C_{max} & if \quad \dot{z_s}(\dot{z_s} - \dot{z_u}) > 0 \end{cases} \tag{5}$$

The aim of the proposed solution is to define a simple and implementable scheme that replicates the active version of the skyhook control design. As a matter of fact, the shock absorber is only switching between two different conditions, making the controller much simpler. The purpose of such a control strategy is to implement a dissipative state when the vehicle body and the unsprung mass are moving towards the same direction. Differently, an ideal zero-dissipative condition is adopted when the sprung mass and the unsprung one are going in opposite directions[23]. The working states of the semi-active damper are mapped in figure 12. As mentioned in advance, by exploiting such a control strategy it is possible to implement an approximation of the ideal skyhook system in a real framework. More in detail, the characteristics plotted are achievable with magnetorheological fluids, or standard shock absorbers equipped with control valves suitable to change the damping coefficient[9]. Finally, in figure 13 the two systems equipped with the actuator and the controlled damper are compared. The differences between the transfer functions are straightforward, as well as the different behaviour of the suspensions with respect to time. It is important to underline how the active system is particularly effective at lower frequencies, where the transfer function peaks are more smoothed. Differently, at higher frequencies the trend is inverted, and a better response is provided by the semi-active version. The

same aspects are confirmed in the time domain plots.

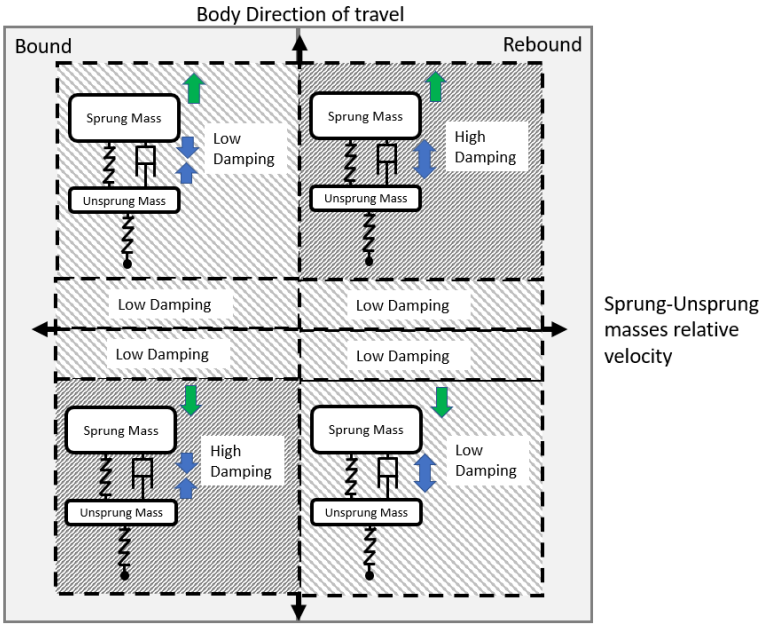

Figure 12: Damping control strategy

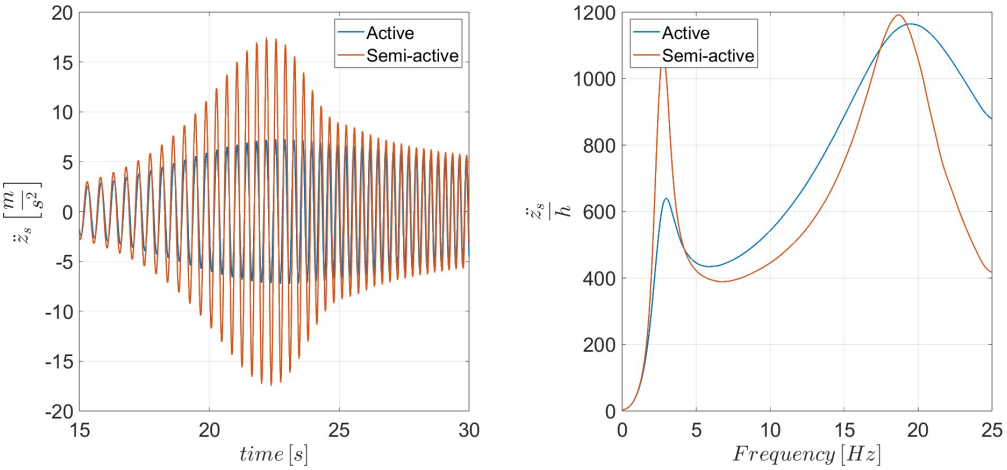

Figure 13: Comparison of the time response and transfer function of the semi-active and active suspension layout

Takenori, Kazuhiro, Hideyuki and Taro developed an innovative method to realise

the Skyhook system. As mentioned in the analysis of this active system, it is necessary to retrieve the sprung and unsprung mass velocities to perform the control logic, as well as the body acceleration. Accordingly, an expensive sensor layout is required, composed of linear transducers and accelerometers. Then, the authors demonstrated that the suspension stroke speed is possible to recover just from the sprung mass acceleration. The Skyhook system is consequently implementable by exploiting only a couple of accelerometers or a single gyroscope [27]. The control law becomes:

$$C_{active} = \begin{cases} C_{min} & if \quad \dot{z}_s \ddot{z}_s \leq 0 \\ C_{max} & if \quad \dot{z}_s \ddot{z}_s > 0 \end{cases} \tag{6}$$

it is then important to underline how the velocity of the masses located above the suspensions is retrieved from an integration of the acceleration.

3.2 Groundhook control strategy

Another approach deserving attention is the *Groundhook* suspension system. From the previous analysis, it was possible to underline how the Skyhook concept was developed to absorb the sprung masses' oscillations but was definitely not oriented in damping the unsprung masses. The layout presented in the current section is an alternative solution designed to take into account the large oscillations of the wheels, and more in general, of the unsprung masses. Consequently, the system is called 'handling-oriented' since the sprung masses are limitedly affected by the action of the active system, and correspondingly, the vehicle body accelerations are not damped out. Differently, the aim of the Groundhook system is to reduce the tyre contact force variability, inducing better rider confidence, and obviously, more reliable handling properties.

3.2.1 Ideal Groundhook

The system presented in figure 14 represents the ideal Groundhook suspension system. The main idea that supports the current system is the minimisation of tyre contact forces through the minimization of tyre deflection [9]. This is the reason why differently from the Skyhook, in the Groundhook approach the shock absorber is placed between the unsprung mass and the ground in order to dampen the oscillations. It is valuable to point out the dissimilarities with the previous model, where the damping of the tyre was neglected. This choice is motivated by the need to analyse the behaviour of the tire and focus on its vibrations, therefore is important to consider the damping, even if it is generally deficient compared to the tire radial

stiffness. The system's response to a sweep sine in input, representing the road irregularities, is shown in the following passage. The main feature of the input signal is the wide band of frequencies considered, from 0.01 to 25 Hz. The target of the study is to represent the unsprung mass oscillations as well as the tire-ground forces derived from the road surface. The wide frequency range is adopted to ensure that all the possible road conditions are taken into account.

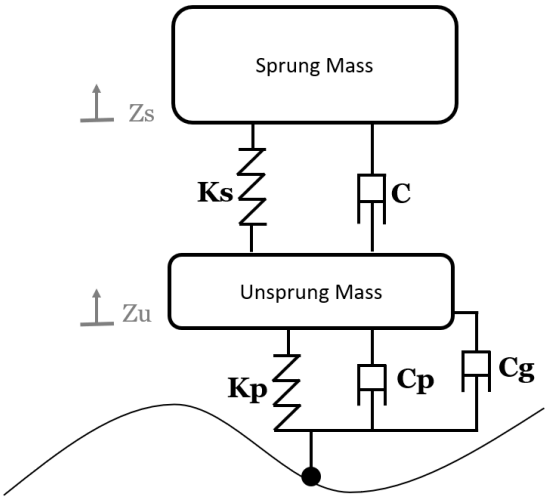

Figure 14: Groundhook suspension system

As proposed in 3.1.1, the equation of motion is retrievable by applying the second low of the dynamics to the system analysed, obtaining the equation 7

$$\begin{bmatrix} m_s & 0 \\ 0 & m_u \end{bmatrix} \begin{Bmatrix} \ddot{z}_s \\ \ddot{z}_u \end{Bmatrix} + \begin{bmatrix} c & -c \\ -c & c + c_p + c_g \end{bmatrix} \begin{Bmatrix} \dot{z}_s \\ \dot{z}_u \end{Bmatrix} + \begin{bmatrix} k_s & -k_s \\ -k_s & k_s + k_p \end{bmatrix} \begin{Bmatrix} z_s \\ z_u \end{Bmatrix} = \begin{Bmatrix} 0 \\ (c_p + c_g)\dot{h} + k_p h \end{Bmatrix} \tag{7}$$

where the term c_p is the tyre damping property that, as anticipated, was considered in this layout. In figure 15 it is possible to notice the principal effect of introducing a shock absorber interposed between the wheel hub and the ground. The wheel vibrations are largely damped out along the whole frequency band. Anyway, it is possible to highlight the peaks before 5 and around 15 Hz, i.e. in correspondence with the natural frequencies of the system. In 15 is also possible to state that the active system is more effective around the second resonance peak, where the system

response is more critical and the additional shock absorber is damping out most of the mass vibrations. Outside such a region, the Groundhook system does not show major benefits. The suspensions partially mediate the unsprung mass shaking, but on the other hand, the forces the tyre is exchanging with the ground are critical. It is clearly understandable how such vibrations are strongly connected to motorcycle handling, and as a consequence, to rider sensations and to the possibility of performing demanding manoeuvres. Tire-ground vertical reaction forces are represented by the equation 8.

$$F_{tire-ground} = (c_p + c_g)(\dot{h} - \dot{z_u}) + k_p(h - z_u) \tag{8}$$

It is possible to retrieve the relationship shown considering the forces exchanged by the tyre as the result of the tyre deflection and its velocity of deformation. The symbols involved represent c_p: tyre damping coefficient, c_g: groundhook damper characteristic, $\dot{h}$ and h: velocity of ground surface variation and ground profile, k_p: tyre radial stiffness, z_u and $\dot{z_u}$: unsprung position and velocity respectively. From 8 it is possible to compute the contact force on the bases of the tyre deformation. In figure 16 are plotted the aforementioned forces with respect to time a), and their frequency response function b). In 16 b) is strongly highlighted a particularly critical condition for adherence at high frequencies due to high force variability, as well as the small influence of the Groundhook system within the low-frequency band.

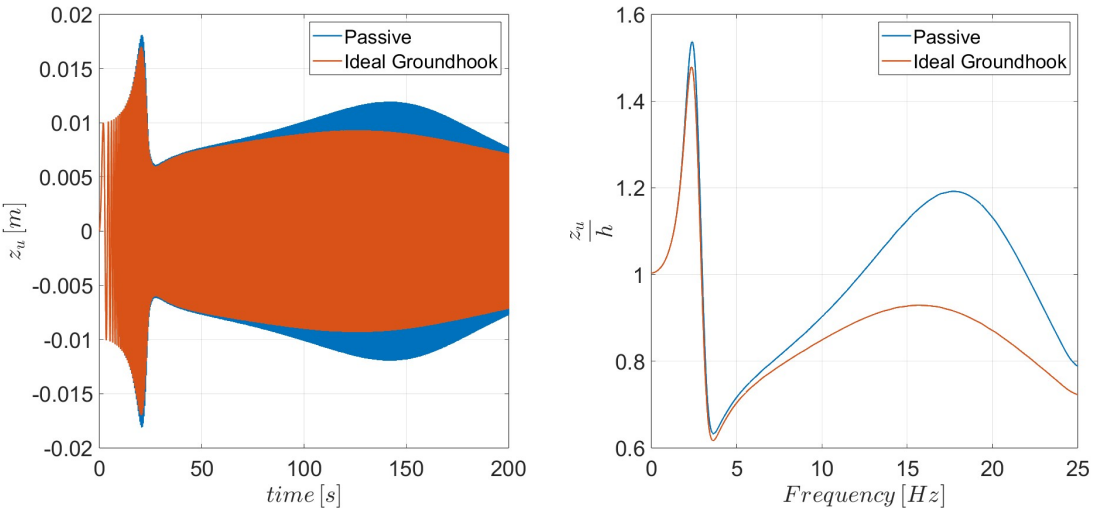

(a) (b)

Figure 15: Unsprung mass position response to a sweep input signal

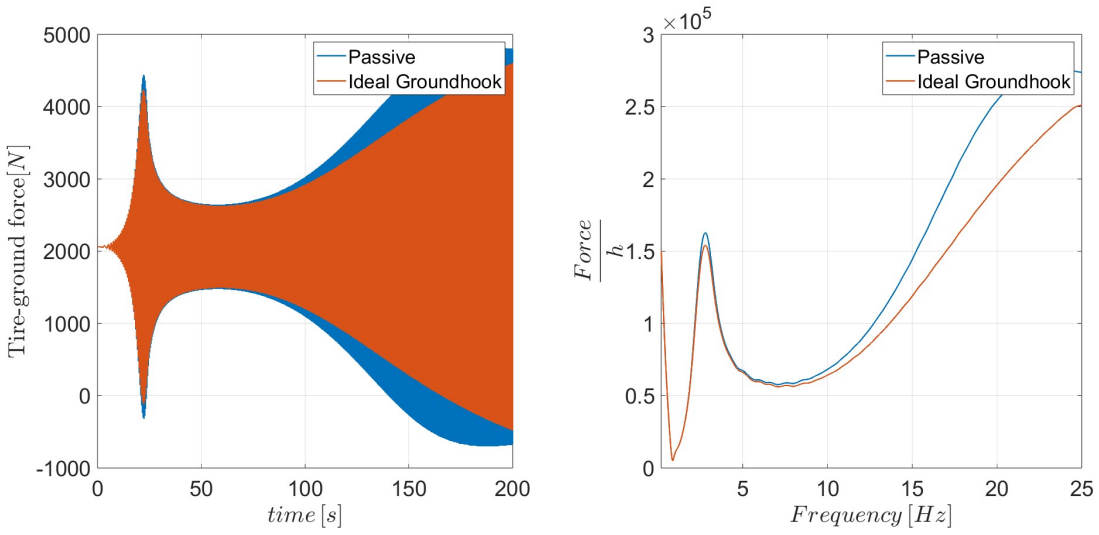

(a) (b)

Figure 16: Tyre-ground force comparison between Ideal Groundhook and Passive system

3.2.2 Semi-active Groundhook

The system analysed does not apply to the real world. Related to such a suspension layout, negative consequences are unavoidable. One drawback comes from the technical feasibility of introducing a specific damping characteristic between the unsprung mass and the ground. Anyway, the most concerning aspect of a high damping coefficient of the tire is the high energy dissipation linked to the rolling of the wheel, and as a consequence, to the resulting unacceptable rolling resistance. The Groundhook system that actually finds a real-world application is the same as the one presented in figure 11. The critical aspects related to such a design are the resulting opposite forces on the sprung mass that will influence the riding comfort. A chirp signal is provided to the suspension model, equipped with a semi-active shock absorber specifically controlled with the following strategy:

$$C_{active} = \begin{cases} C_{min} & if \quad -\dot{z_u}(\dot{z_s} - \dot{z_u}) \leq 0 \\ C_{max} & if \quad -\dot{z_u}(\dot{z_s} - \dot{z_u}) > 0 \end{cases} \tag{9}$$

The simulations performed are shown in figure 17 and 18.

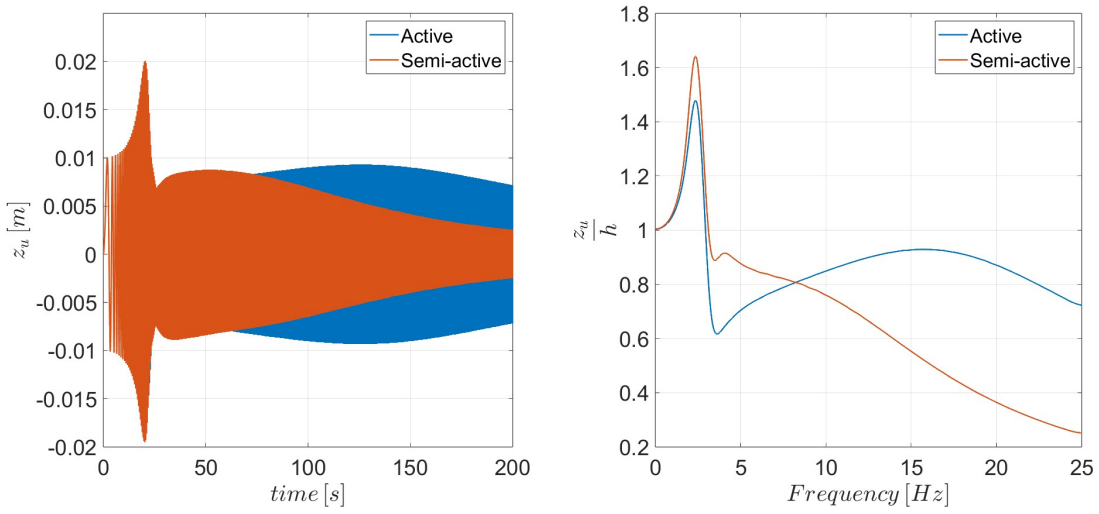

Figure 17: Unsprung mass deflection comparison between the ideal (active) and semi-active Groundhook control

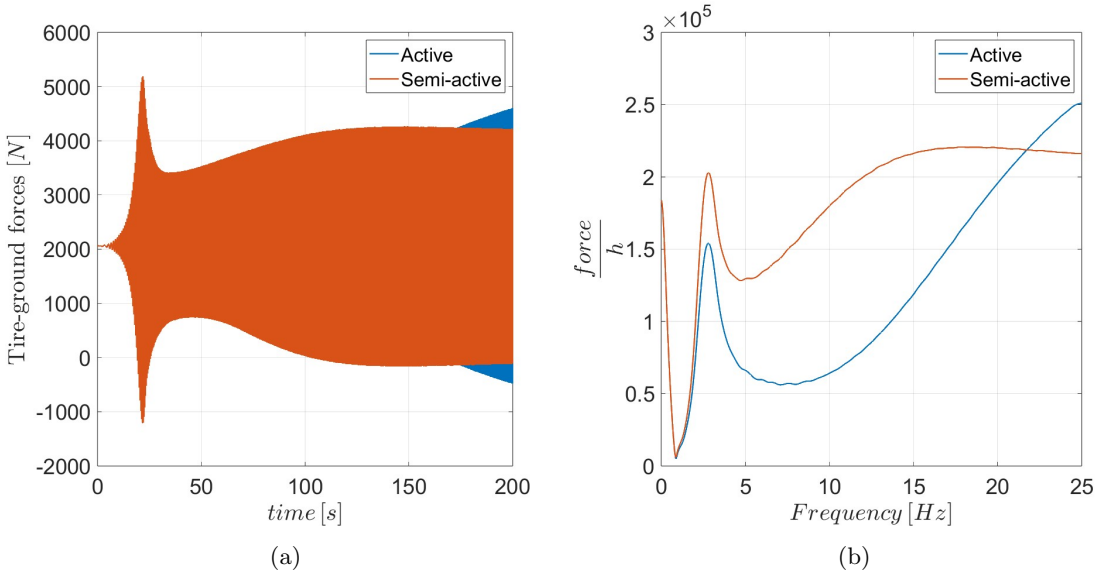

Figure 18: Semi-active VS active Groundhook tyre-ground forces

It is clearly visible how the ideal Groundhook approach allows for better performances, reducing the ground force variability and unsprung masses oscillations.

Anyway, the semi-active version is the only implementable real-world Groundhook approximation that does not imply the adoption of an energy-demanding active system.

3.3 Acceleration Driven Damper (ADD)

The most common comfort-oriented suspension control strategy is the previously presented Skyhook control. The Acceleration-driven damper is a novel optimized strategy based on the Skyhook algorithm. The proposed layout replicates the system adopted to simulate the Skyhook and the Groundhook control logics in 12. Therefore, the semi-active damper is still meant to be placed between the sprung and the unsprung masses. It is possible to demonstrate that the ADD controller is the optimal comfort-oriented control strategy, which means it is the most efficient control scheme to minimize the sprung mass accelerations. Savaresi and co-authors, indeed, developed this policy by minimizing, through the Maximum Principle of Pontyagin, a cost function aimed at reducing the sprung mass acceleration [18]. The optimal control strategy found is [18]:

$$C_{active} = \begin{cases} C_{min} & if \quad \ddot{z_s}(\dot{z_s} - \dot{z_u}) \leq 0 \\ C_{max} & if \quad \ddot{z_s}(\dot{z_s} - \dot{z_u}) > 0 \end{cases} \tag{10}$$

It is important to underline that the current control scheme was proven to be the optimal control strategy when the controller is comfort-oriented, the road surface is unpredictable, and the optimization is based on a single-step horizon only [18][19]. Anyway, it is straightforward the resemblance with the original Skyhook control, the main difference is just related to the body measurements which are only linked to the sprung mass acceleration and no more to the speed. Consequently, the sensor layout can be substantially the one exploited with the Skyhook strategy: a single accelerometer [18] and a linear transducer. In figure 19 a comparison between the two main comfort-oriented strategies, Skyhook and ADD is shown. To complete the analysis of figure 19, two opposite passive damper settings are provided, the maximum damping and minimum damping passive shock absorber. Figure 19 presents an approximation of the frequency response function of the body acceleration from the road surface input. It is clearly visible the dual behaviour of the controllers. The Skyhook provides a remarkable attenuation around the body's natural frequency, the first peak. Differently, beyond that resonant frequency the ADD control provides better results in terms of vibration reduction. It is therefore possible to introduce the ADD-SH crossover frequency; the frequency where there is an inversion in the optimality of the controller. Before the crossover frequency the Skyhook appears to be the optimal comfort-oriented controller, whereas after that specific point, the ADD

represents the optimal control strategy [19]. Finally, it is visible that with respect to the softer passive suspension system, the Skyhook provides much better results in the frequency region that precedes the first resonant peak. It is not possible to come to such a conclusion if a stiffer damper is considered; there are little or no improvements in adopting a Skyhook rationale if the shock absorber is characterized by a high value of damping, since the two curves are mainly overlapped before the first peak of the graph. On the other hand, this setting provides the worst response after the ADD-SH crossover frequency.

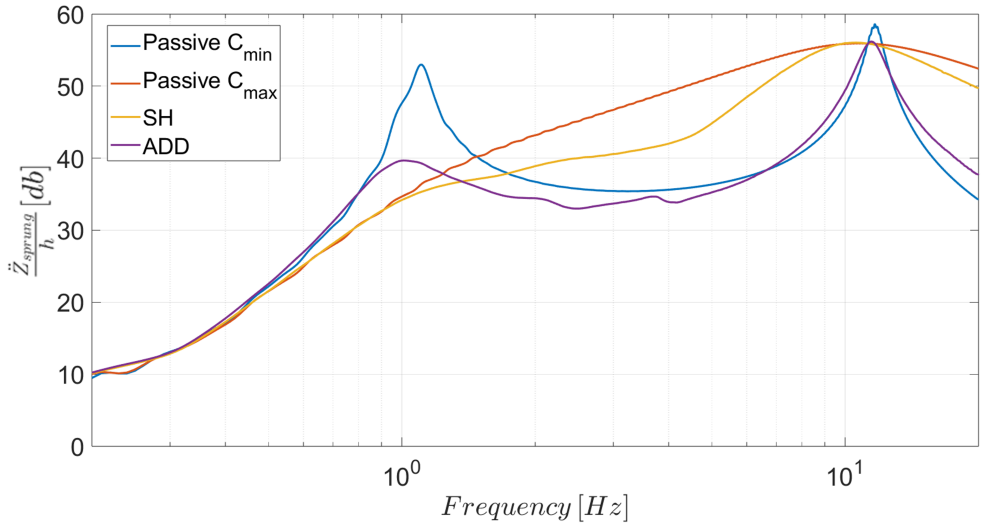

Figure 19: Frequency response function magnitude from road surface to body acceleration

As a matter of fact, the major benefits of introducing the Skyhook when a stiff damper is mounted are visible along the frequencies between the two peaks, where the semi-active version presents a great reduction in the sprung mass oscillations. Also in this case the relation between the softer open-loop system and the Skyhook is opposite compared to the stiffer one. It is possible to sum up by referring to the conclusion drawn by Savaresi and co-authors: the improvements of increasing the passive damping coefficient improve the suspension response limited to a specific frequency region, reducing the efficiency of other bandwidths. The semi-active control logic instead; gives the possibility of implementing optimal suspension characteristics by reducing vibrations somewhere in the frequency region without paying a worse behaviour somewhere else [19]. It is also important to underline how the signal of the acceleration is retrieved by the accelerometer sensor mounted on the motorcycle body which is highly affected by noise, principally linked to the engine vibrations, that can

easily induce chassis oscillations. The frequency of the noise may be even high but nevertheless, the magnitude of the disturbance is generally expected to be low. In this case, the noise is not actually a problem, since the zero-crossing condition is far. The most concerning condition may happen when riding on a flat surface, where noise induces oscillations around zero and consequently may cause high-frequency switching in the damper characteristics[19][18]. A possible solution is to consider an exclusion zone, where the controller is not sensible to signal variations, around the zero value.

3.4 Mixed Skyhook and ADD control strategy

As mentioned previously in section 3.3, a specific analysis of the performances of Skyhook and ADD shows that the behaviour of the two controllers is characterized by a strong duality. More in detail, the crossover SH-ADD frequency separates the region of action of the optimal controllers. Consequently, it is a straightforward necessity to implement a dedicated rationale able to switch behaviour from Skyhook in the region preceding the crossover frequency, to ADD after that point. This concept is the base of the Mixed SH-ADD controller [19]. The control law, given a two-state damper is:

$$C_{in} = \begin{cases} C_{max} \quad if \quad [(\ddot{z_s}^2 - \alpha^2 \dot{z_s}^2) \leq 0 \wedge \dot{z_s}(\dot{z_s} - \dot{z_u}) > 0] \\ \qquad\qquad \vee [(\ddot{z_s}^2 - \alpha^2 \dot{z_s}^2) \geq 0 \wedge \ddot{z_s}(\dot{z_s} - \dot{z_u}) > 0] \\ C_{min} \quad if \quad [(\ddot{z_s}^2 - \alpha^2 \dot{z_s}^2) \leq 0 \wedge \dot{z_s}(\dot{z_s} - \dot{z_u}) \leq 0] \\ \qquad\qquad \vee [(\ddot{z_s}^2 - \alpha^2 \dot{z_s}^2) > 0 \wedge \ddot{z_s}(\dot{z_s} - \dot{z_u}) \leq 0] \end{cases} \tag{11}$$

where the term α represents the crossover frequency between SH and ADD, and as a consequence is usable as a sort of tuning knob. Figure 20 represents the frequency response function magnitude of the main controllers considered. In detail, the Skyhook system and the ADD are compared with the Mixed control strategy. Savaresi, Spelta and co-authors demonstrated that the mixed control method provides excellent results and is extremely close to the results of the optimal control strategy, the one able to minimize the comfort cost function, which as a consequence represents a lower bound. In this sense, it is possible to state that the '*Mix control strategy*' layout provides a quasi-optimal solution, and it is practically impossible to evaluate a better controller oriented in minimizing the sprung vibrations[19]. It is meaningful to analyse the time response as well; such a study is performed in figure 21 where two different road disturbances of 1.25 and 4 Hz are taken into account.

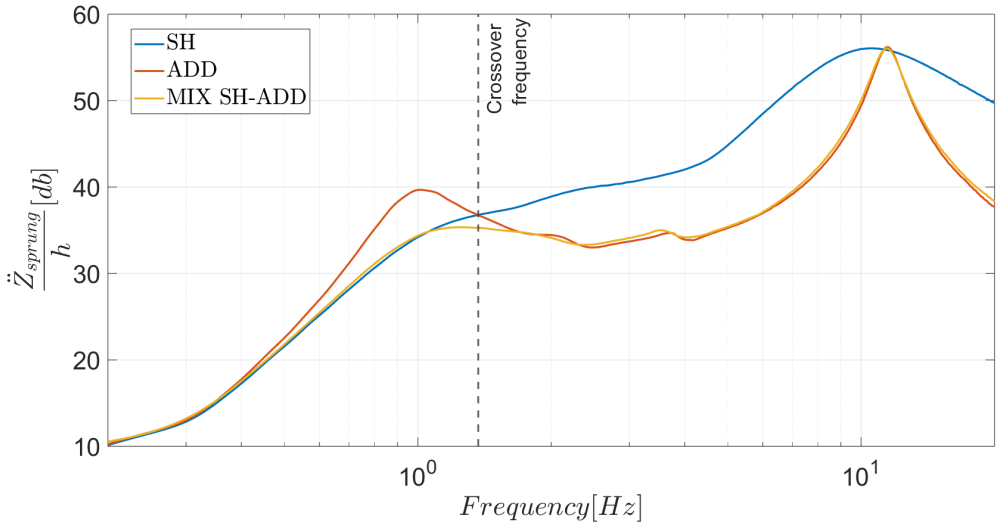

Figure 20: Frequency response function magnitude from road excitation to body acceleration. SH, ADD and mixed control algorithms are displayed

The study undertaken by Savaresi and Spelta shows a high non-linear behaviour, and similar conclusions to the one stated in the frequency response analysis can be drawn: the Skyhook control shows slightly better performances around the body resonance frequency (figure 21 a)), but the Mix-1 strategy is actually able to outperform the SH at higher frequencies (figure 21 b)).

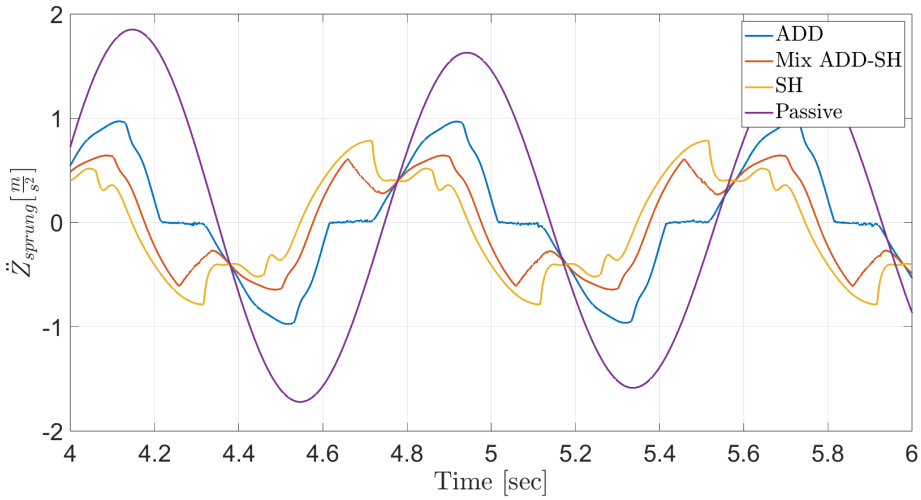

(a) 1.25 Hz

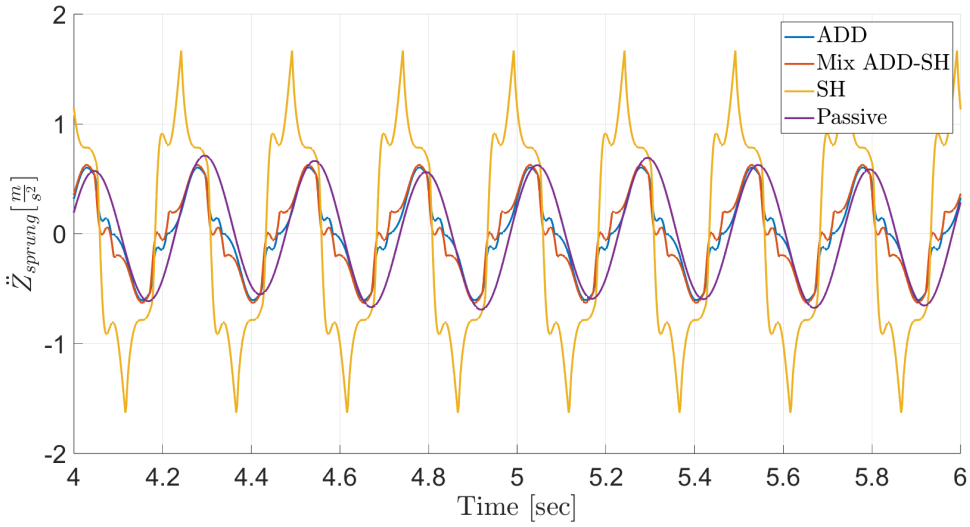

(b) 4 Hz

Figure 21: Sprung mass acceleration time responses from monotone road disturbance

To conclude, it is important to underline how the comfort object requires opposite suspension characteristics with respect to handling, and consequently, it is recommendable to consider and control the road-holding performance even if the controller is comfort-oriented to ensure a global optimal behaviour. The analysis performed by the authors shows suitable handling indexes as well.

3.5 Mix-1-sensor control strategy

Regarding the sensors' layout, the motorcycle environment implies a series of critical aspects in particular concerning the space available and the cost; as mentioned in advance in section 3.1.3 and in 2.4, the cost of a motorcycle is much lower with respect to a luxury car, where more likely the electronic suspensions will be mounted on. In addition, the space available in the periphery of the front assembly is extremely limited; in particular around the front fork and the unsprung masses. It is evident the advantage of exploiting a control strategy based on a limited number of sensors, more in detail, a single accelerometer. As a matter of fact, an accelerometer actually allows the implementation of a reliable control algorithm, even if it is limited the amount of data it can retrieve. It is also located in a more favourable region of the motorcycle compared to the linear suspension stroke transducers. The Mix-1-sensor control strategy is based on the idea of reducing the sprung mass accelerations by exploiting only an accelerometer. In order to reach such objective the Mix-SH-ADD

rationale is properly modified [25]:

$$C_{in} \begin{cases} C_{max} & if \quad (\ddot{z}^2 - \alpha^2 \dot{z}^2) \leq 0 \\ C_{min} & if \quad (\ddot{z}^2 - \alpha^2 \dot{z}^2) > 0 \end{cases} \tag{12}$$

The term α represents a 'tuning knob' to properly adjust the crossover frequency between the SH and the ADD control rationale [25]. There is also an alternative version of the single-sensor control logic of the Mix-1 rationale; the Mix-1-stroke. The main idea of the presented alternative logic is to reduce the number of sensors mounted on the vehicle by exploiting only a linear transducer to measure the suspension stroke [25], instead of an accelerometer. This strategy is based on the same controller proposed in 12, but to guarantee the expected results, the control strategy is coupled with a dynamic non-linear observer shown in equation 13 to estimate the sprung mass acceleration.

$$\begin{cases} \hat{\ddot{z}}(t) = -k/M(z(t) - z_t(t)) - c(t)/M(\dot{z}(t) - \dot{z}_t(t)) \\ \ddot{c}(t) = \alpha \dot{c}(t) + \beta c(t) + \gamma c_{in}(t - \tau) \end{cases} \tag{13}$$

The proposed system is a non-linear dynamic observer of the quarter car model exploited to represent the behaviour of the vertical motion of the motorcycle. The inputs are the suspension stroke and the delayed damping request $c_{in}(t\text{-}\tau)$. The experimental results evaluated by authors Spelta, Savaresi and Fabbri are recalled in the following passage, where in figure 22 are shown the main controller's logic compared. In figure 22 are compared all the controllers presented in this chapter, the ADD, the SH, the SH-ADD mix, and finally, two versions of the *Mix-1* control logic. The Mix-1 is implemented in two different configurations, on a single accelerometer (Mix-1) and a single linear transducer (Mix-s). It is possible to observe that the non-linear observer ensures optimal behaviour, since the frequency response functions of Mix-1 and Mix-s algorithms are very close[25]. Finally, it is evident the potentiality of such rationales since the sensors needed are very simple and the results are great. Anyway the observer non-linearity may induce different results if different road profiles are provided as inputs[25]. In the same graph of figure 22, the results presented in the previous paragraph are confirmed: the SH fashion is particularly able to damp the mass oscillation in the firsts frequency regions, anticipating the first natural frequency of the system. Beyond the resonance frequency the ADD logic predominates. The optimal performance of the Mix-1 control rationale are therefore straightforward: the adoption of such system can minimize the sprung mass, enhancing the best comfort-oriented control strategy and requests a limited sensor scheme.

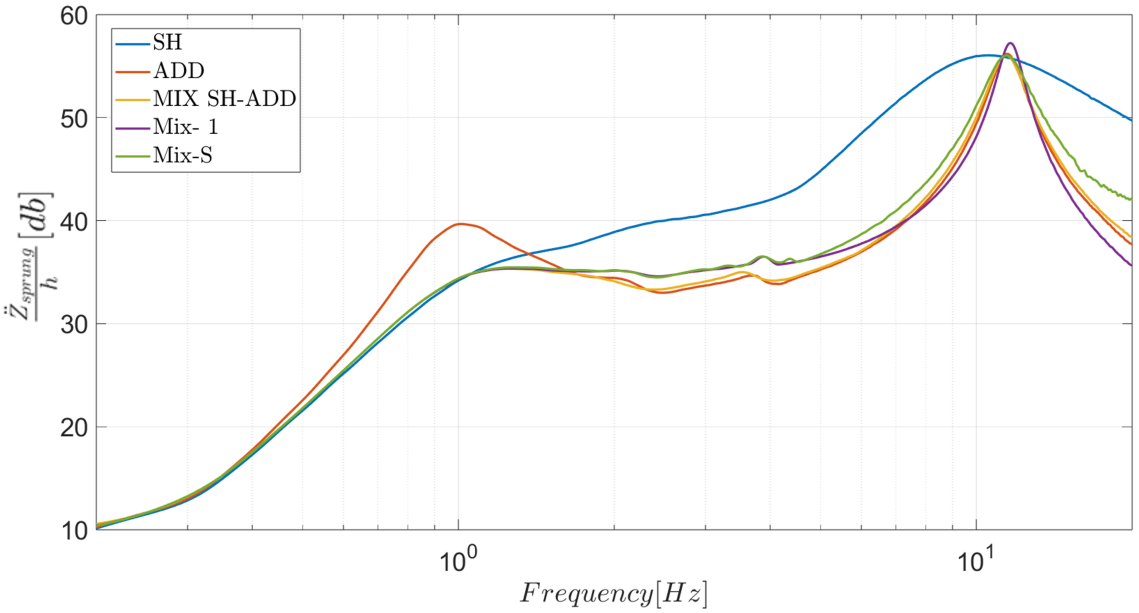

Figure 22: Frequency response function of SH, ADD, Mix SH-ADD, Mix-1 and Mix-s, from road profile to sprung mass acceleration

3.6 Mix-Pitch control strategy

To study the comfort of a suspension assembly the so-called Quarter-car is widely spread. As mentioned in the previous sections, such a mathematical model is able to properly describe the behaviour of the suspension in a heave excitation condition, it is totally unable to take into account the pitch motion. As a matter of fact, it is also important to consider the pitch motion to correctly retrieve a complete overview of the comfort problem. It is stated in ISO 2631-1 that the pitch motion can affect the vibration sickness and the weighting functions of generic rotational vibration comfort indexes reach their maximum around 0.6 Hz [26]. Such vibration frequencies are normally reached during the riding of a motorcycle, and as a consequence, it is recommendable to perform analysis considering no more the quarter-car model, but a more complex system represented by the half-car model. Figure 23 depicts such a mathematical representation. The model in figure 23 can be described by a 6 differential equations non-linear system of the 10_{th} order. Four equations are the linear differential equations used to describe the rotational dynamics of the sprung mass, the vertical translations of the front and rear unsprung masses, and the sprung mass's vertical motion. The other two equations represent the damper dynamics of both the front and rear shock absorbers, described by non-linear differential equations [24].

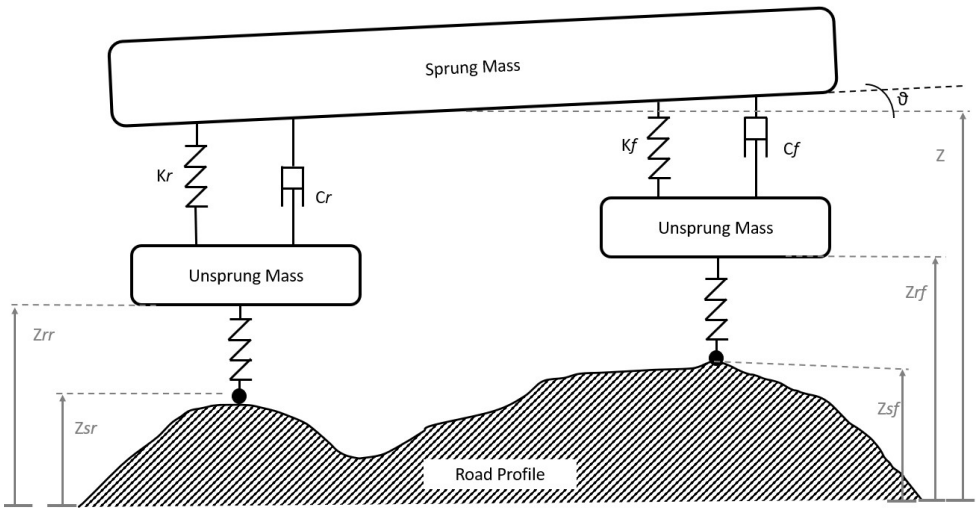

Figure 23: Half-car model

To analyse the system presented in figure 23 the authors have considered two different inputs; a simultaneous road excitation $z_{rr} = z_{rf}$ to simulate the heave movements and an opposite road excitation where z_{rr} = -z_{rf} to take into account the pitch motion. Both of them are sweep signals ranging from 0 to 50 Hz. The results evaluated by Savaresi, Delvecchio and Spelta are summed up in figure 24, where the passive system and the Mix-1 control strategy are compared. Considering the graph of figure 24, it is evident the presence of one resonance peak linked to the sprung mass natural frequency, and one related to unsprung mass excitation frequency, respectively at 2 and 13 Hz [24]. Similarly to the conclusions stated in the previous sections, the hard and soft passive damper settings present complementary behaviour; the soft characteristic accentuates the body resonance peak, whereas the hard one induces an increment of the oscillations at higher frequencies. To ensure the optimal response possible the mix-1 control logic can be applied to the half-car model presented in figure 23, which as mentioned in section 3.6, provides the best performances representing a trade-off between a Skyhook and an ADD control strategy [24]. Taking into consideration the pitch excitation, the resonance peak is moved to a higher frequency; about 5-6 Hz. Also in this case the passive shock absorber is limited to the "traditional comfort trade-off", where the soft damping allows a good filtering of the medium-high frequency vibrations, but it is far from an optimal characteristic when analysing the resonance peak attenuation. Differently, the hard version of the damper provides a remarkable reduction of the maximum peak but is a non-optimal solution when taking into consideration the high-frequency region [24]. From these conclusions, the authors developed an innovative strategy, aimed at

taking into consideration the pitch motion as well as the heave. The rationale novel rationale is presented in equation 14.

$$\begin{cases} C_{h,f} = \begin{cases} C_{max} & if \quad (\ddot{z_f}^2 - {\alpha_f}^2 \dot{z_f}^2) < 0 \\ C_{min} & if \quad (\ddot{z_f}^2 - {\alpha_f}^2 \dot{z_f}^2) \geq 0 \end{cases} \\ C_{h,r} = \begin{cases} C_{max} & if \quad (\ddot{z_r}^2 - {\alpha_r}^2 \dot{z_r}^2) < 0 \\ C_{min} & if \quad (\ddot{z_r}^2 - {\alpha_r}^2 \dot{z_r}^2) \geq 0 \end{cases} \\ C_{\theta} = \begin{cases} C_{max} & if \quad (\ddot{\theta}^2 - {\alpha_\theta}^2 \dot{\theta}^2) < 0 \\ C_{min} & if \quad (\ddot{\theta}^2 - {\alpha_\theta}^2 \dot{\theta}^2) \geq 0 \end{cases} \\ C_{in,f} = max(c_{h,f}(t), c_{\theta}(t)) \\ C_{in,r} = max(c_{h,r}(t), c_{\theta}(t)) \end{cases} \tag{14}$$

It is interesting to analyse the content of the equation presented above. The rationale is thought to damp the most prevailing motion between heave and pitch. More in detail in this case, given that the model is considering both suspensions, the damping of the front and rear shock absorbers are now defined following the Mix-1 algorithm shown in section 3.6. To consider the pitch damping another rationale is included in the system 14, indeed C_θ is thought to reduce the pitch motion by exploiting the same structure of the rationale Mix-1-Sensor, but in this case is not considering the reduction of the linear oscillations of the suspension strokes, but is aimed to damp the angular vibrations of the sprung mass θ. Finally, the front and rear shock absorbers' damping will be defined by selecting the maximum value among the heave and pitch damping. As mentioned above, in this manner it is possible to select the damping accordingly to the most relevant vibration between heave and pitch [24]. The results found by the authors are represented in figure 25. Considering the Heave excitation (figure 25 a)) it is possible to conclude that the Mix-Pitch algorithm is not actually improving the comfort and the best results are still provided by the Mix-1-sensor algorithm. Anyway, as expected, the greatest improvements are visible in Figure b), where the pure pitch excitation is considered. In this case, the Half-Car-Mix-Pitch rationale shows the best pitch oscillation attenuation as the maximum peak is strongly reduced in amplitude and provides good performance over the entire frequency range compared to the other suspension control policies, except for the soft passive suspension at medium-high frequencies, which anyway pays a great bill around the first resonance peak.

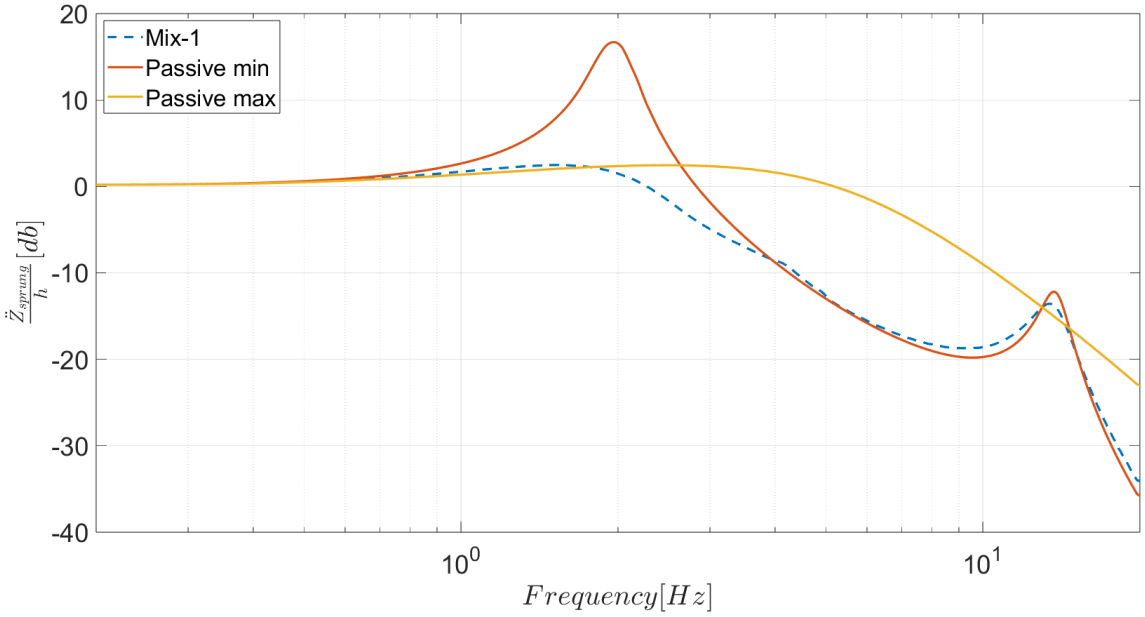

(a) Heave

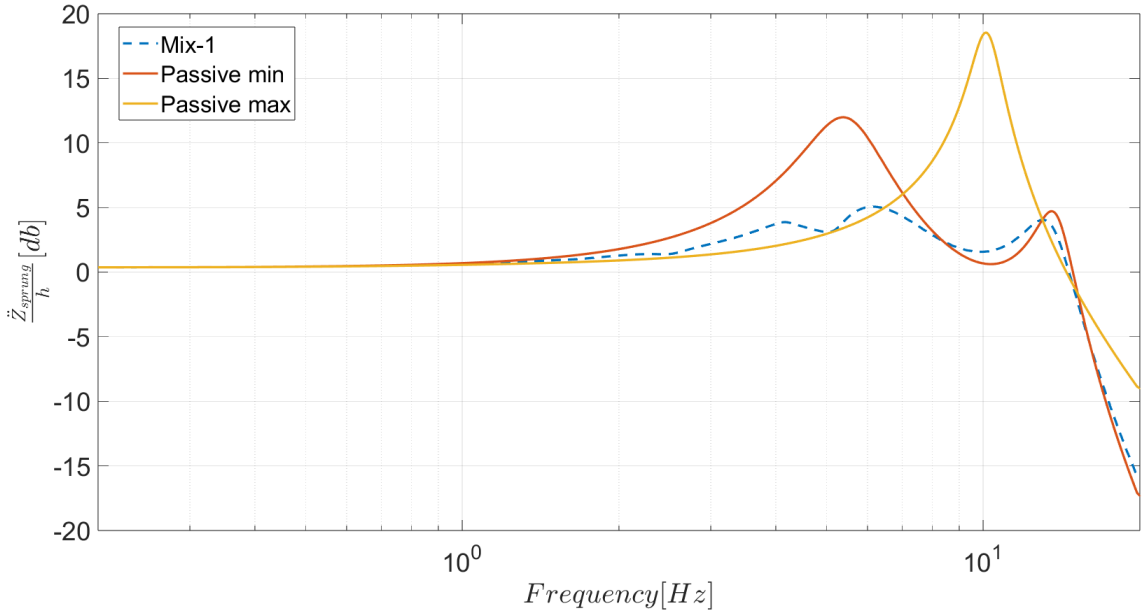

(b) Pitch

Figure 24: Approximate frequency response of body motion from different excitation: a) heave, b) pitch

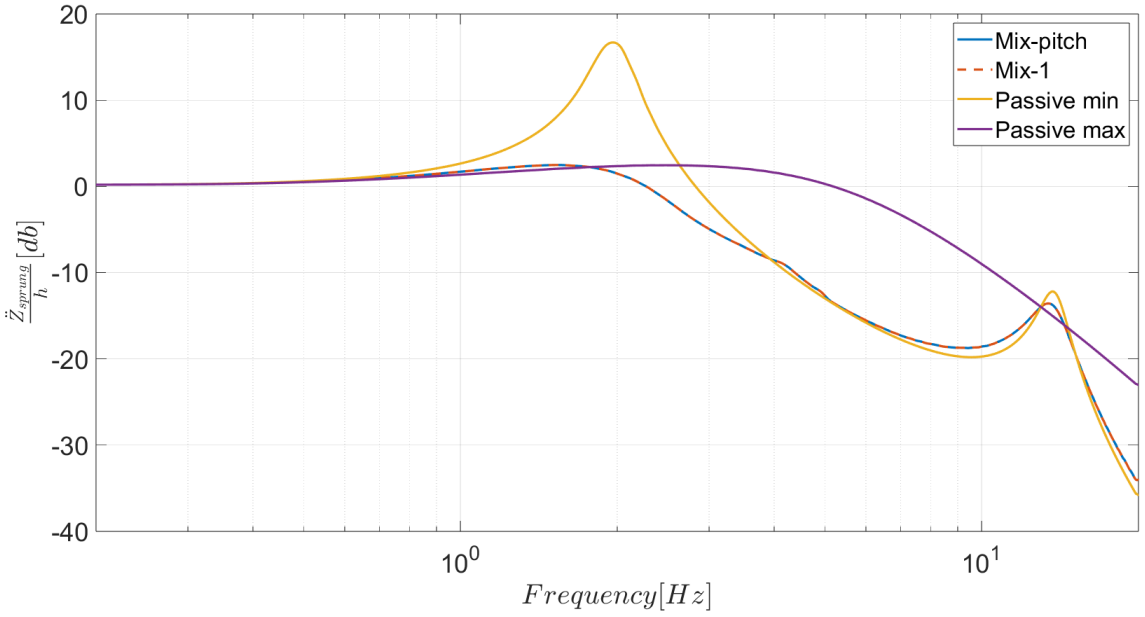

(a) Heave

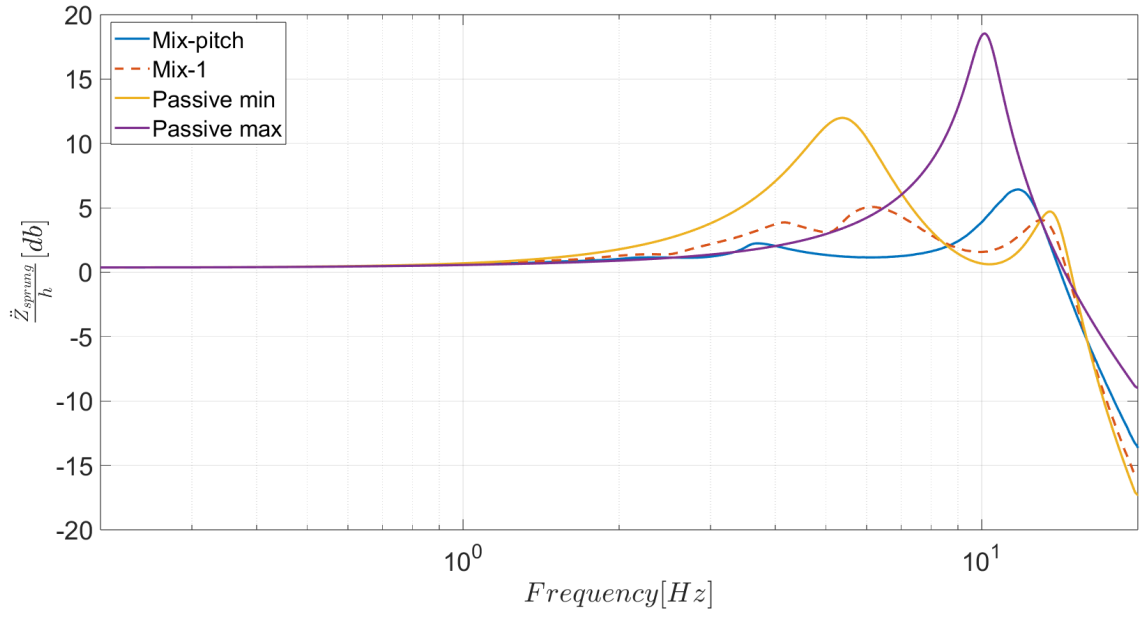

(b) Pitch

Figure 25: Frequency response function comparison of the different algorithms proposed: a) Heave, b) Pitch excitation

4 Project Overview and Preliminary Discussions

As shown in the previous chapters, the suspension system is afflicted by the handling-comfort conflict, which determines a substantial limit of the suspension's overall performance. In the first chapter was abundantly treated how active suspensions represented a pivotal technology able to overcome the aforementioned contraposition. Also discussed was the rationale behind why these solutions pose a formidable challenge today in terms of their feasibility and practical implementation. From this statement, the principal semi-active solutions presented in the suspension control panorama were presented. It was pointed out the optimal comfort-oriented control strategy; a blend of sub-optimal comfort rationales. The road holding was outlined in the only handling-oriented controller presented, the Groundhook control logic. From a comparison of both controllers, the optimal comfort-oriented rationale Mix SH-ADD control logic, and the handling controller Groundhook, is still visible the conflict that arises when considering in the same context the road holding and the comfort of passengers: while the two optimal controllers excel within their respective domains, they fall short of being globally optimal when evaluating the overall performance. The focal point of this project revolves, therefore, around devising a cutting-edge solution, able to master the comfort of the occupants and the handling of the vehicle. As introduced in chapter 2, the goal of the project is to introduce a suspension solution for the 2-wheeled vehicle market, where the preexisting semi-active suspensions are still limited. Therefore the innovative rationale may represent a real turning point in the motorcycle mass production industry.

4.1 Simulations and indexes

The suspension setting is in a close relationship with the vehicle characteristics, it is irrational to expect a single suspension layout matching a wide variety of vehicles. Therefore it is important to establish a unique vehicle set of characteristics, a vehicle capable of embodying a standard motorcycle. The characteristics was chosen based on the main feature of a common middleweight naked motorcycle, or at least a sport tourer motorbike, the most shared two-wheeler of recent years. Moreover, it can represent a revolving marketing aspect focusing the suspension control on a really appealing motorcycle class. The target vehicle characteristics are reported in table 1. The motorcycle characteristics presented are based on a standard motorbike. To ensure these characteristics reflect the typical features of motorcycles, they were compared with benchmark quantities provided by Cossalter's 'Motorcycle Dynamics' handbook, and meticulously evaluated against the main dynamic parameters to en-

sure they fall within appropriate ranges. Therefore, the resulting key parameters of the motorcycle are provided in table 2. The suspension stiffness is checked based on a widely adopted index, the *rider SAG*, a metric used to assess the compatibility of suspension with motorcycle parameters indicating the extent of suspension compression under the weight of the rider in full gear. In the literature, it is possible to find guidelines suggesting the optimal suspension stroke when the occupant is aboard, facilitating the determination of suitable suspension characteristics to ensure optimal rider comfort. An important characterisation of the suspension is also provided by the reduced natural frequency of the suspensions. In fact, the front and rear suspension was firstly reduced to a simplified single degree of freedom mass-spring-damper system and finally, the Cossalter's manual was exploited to verify the coherence of the resulting frequencies with those of a standard two-wheeled vehicle[5]. In order to quantify appropriate suspension damping, the formula for the 'optimal damping coefficient' was selected. Illustrated in equation 15, this formula derives the optimal passive damping value from the quarter-car simplified vehicle model. It determines the suspension damping required to achieve an optimal acceleration transfer function, thus ensuring comfort.

$$C_{optimal} = \sqrt{\frac{m \cdot (k_{susp,f} + k_{susp,r})}{2} \cdot \frac{k_{tyre,f} + k_{tyre,r} + 2 \cdot (k_{susp,f} + k_{susp,r})}{k_{tyre,f} + k_{tyre,r}}} \tag{15}$$

To provide an extensive analysis of the model and the simulations outlined in this chapter, it is important to specify that the suspension passive damping setting is selected by a proportional rule. More in detail, the front and rear suspension damping values were set as proposed in the following equation:

$$C_{f,r} = c_{opt} \cdot \frac{k_{f,r}}{k_f + k_r} \tag{16}$$

Differently from the suspension setting, the tyre radial stiffness of the accounted motorbike is a property derived from an expected wheel-hop resonance frequency[6]. The Vehicle body mass property takes into account also the rider's weight, therefore it is considerable as the overall sprung mass the suspension has to sustain. As visible from table 2, the reduced bounce natural frequency is smaller compared with the pitch one, hence providing the correct in-plane dynamic of the vehicle. Thus aspect is ensured by a meticulous characterisation of the geometries and the suspension setting. To conclude the presentation of the vehicle, it is possible to affirm that the motorcycle presented is a standard road motorbike, correctly tailored to meet the ride requirements of such a vehicle.

Vehicle body mass	265	Kg
Front unsprung mass weight	12	Kg
Rear unsprung mass weight	14	Kg
Pitch moment of inertia of vehicle body	82	$Kg \cdot m^2$
Wheelbase	1.485	m
Front semi-wheelbase	0.81	m
Rear semi-wheelbase	0.675	m
Front suspension stiffness	20e3	$\frac{N}{m}$
Rear suspension stiffness	30e3	$\frac{N}{m}$
Front tyre radial stiffness	100e3	$\frac{N}{m}$
Rear tyre radial stiffness	150e3	$\frac{N}{m}$
Front suspension damping coefficient	1218	$\frac{N \cdot s}{m}$
Rear suspension damping coefficient	1827	$\frac{N \cdot s}{m}$
Front tyre radial damping coefficient	500	$\frac{N \cdot s}{m}$
Rear tyre radial damping coefficient	600	$\frac{N \cdot s}{m}$

Table 1: Main vehicle parameters

Reduced bounce natural frequency	2	Hz
Reduced pitch natural frequency	2.6	Hz
Front-wheel hop frequency	14.5	Hz
Rear-wheel hop frequency	16.5	Hz
Square radius of inertia	0.55	$\sqrt{Kg \cdot m}$
Reduced front suspension natural frequency	2.0	Hz
Reduced rear suspension natural frequency	2.3	Hz

Table 2: Main vehicle in-plane dynamic characteristics

The analyses of the motorcycle are performed through the adoption of MATLAB-Simulink. Different models of the vehicle under investigation will be analyzed in the next chapter, and the main results will be discussed. In this paragraph, instead, the simulation setting and the conditions of the analysis are here reported. To evaluate the performance of the motorcycle it is necessary to indicate meaningful simulations,

and to ensure a correct comparison of the suspension control logics, always the same manoeuvres are taken into consideration.
To have an insight into the suspension behaviour it is possible to derive the frequency response function of the suspension, from the road profile to the indexes considered. The analyzed indices vary depending on the specific topic to be emphasised, more in detail:

- Comfort: the transfer function from the road profile to the motorbike body vertical acceleration is taken into account. When possible, the measurement will be referred to the rider seat position.
- Handling: the transfer function from the static contact force to the tyre-ground vertical force is taken into account.

The goal of the simulation is to outline the main behaviour of the suspension setting, in fact, even if it is a steady-state analysis, it is possible to draw some key aspects, such as the resonance or any cut-off frequencies. This simulation requires a steady-state increasing frequency input, therefore, in the following analysis a slowly linearly-increasing-frequency chirp sine wave signal is adopted. To ensure the stationarity of the signal, the simulation time is chosen high enough to exclude from the results any transient phenomenon. An approximation of the Frequency Response Function (FRF) is provided by the MATLAB command *tfestimate*. With such action it is possible to derive the transfer function response of the system by exploiting Welch's averaged periodogram method. To test the suspension layouts additional simulations will be taken into account.
A meaningful test is represented by the step analysis, where the vehicle model is fed with a step road profile of height of 0.05 m. In this manner, it is possible to highlight the response of the suspension to a sudden road excitation, and eventually retrieve an estimation of the free response of the vehicle. In this context, to have an insight into the comfort of the rider and the road-holding properties of the two-wheeler vehicle following a step road, the following indexes are exploited.

- Comfort: standard deviation of the sprung mass acceleration during the whole analysis. When possible, the measurement will be referred to the rider seat position.
- Handling: The standard deviation of the tyre-ground vertical reaction force.

Eventually, it is possible to adopt the Root Mean Square (RMS) value of the sprung mass acceleration to assess the comfort of the vehicle.
Finally, to provide the behaviour and the performance of the vehicle during real-exercise conditions, a road profile that resembles a real driving condition is adopted.

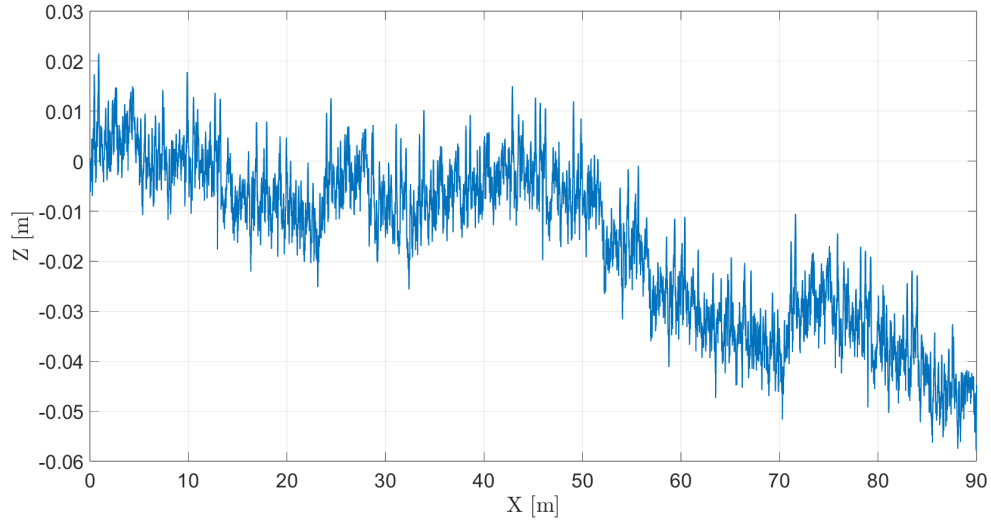

(a) Belgian block input signal provided to the simulation. It is the projection of the road on the X-Z plane

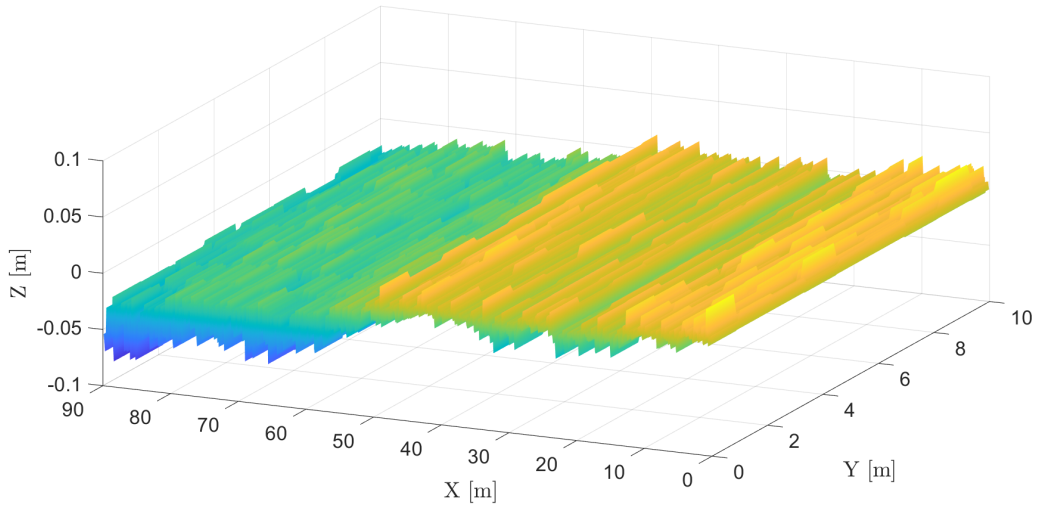

(b) Pitch

Figure 26: Reconstruction of the whole Belgian block pavement

To consider such an aspect, a real *Belgian block* pavement profile is extrapolated and fed to the motorcycle model. In this manner, it is possible to furnish a representation of the motorcycle suspension response when a real rough road is faced. The Belgian block road profile adopted in the simulations, i.e. its projection on the X-Z plane, is shown in figure 26 a), while figure 26 b) provides the representation

of the reconstructed road pavement. In relation with the Belgian block analysis, it is necessary to implement a specific metric to successfully represent the behaviour of the motorcycle. Different indexes are exploited to provide meaningful feedback regarding the handling and comfort of the vehicle:

- Comfort: The averaged mean value of the acceleration perceived by the rider, conforming to the ISO 2631 norm.
- Handling: Multiple indexes are adopted: the standard variation of the tyre-ground vertical force, the flying time and the RMS of the vertical ground forces.

The indexes exploited in the simulations are discussed in the current paragraph for sake of clarity. The standard variation, as presented in equation 17 is a statistical approach adopted to quantify *how much* a quantity is oscillating around a steady state value. Moreover, it can be exploited to have a direct rough measurement of comfort when applied to the sprung mass acceleration. The same mathematical operator is useful to establish to which extent the tyre-ground vertical forces vary and oscillate around the static reaction forces. It is an indication of the handling of the vehicle since a high variation of such forces may represent a loss in traction and an unpredictable motorcycle response. The mathematical formula of the standard deviation is reported in 17

$$std = \sqrt{\frac{1}{N-1}\sum_{i=1}^{N}|x_i - \mu|^2} \tag{17}$$

where x_i is the i^{th} element of the vector analysed, and μ is the mean value of the vector.
The Root-Mean-Square value (RMS) represents the mean constant value of the signal analysed. Such value has a deeper meaning when applied to the road-tyre forces. In fact, it is possible to rearrange the Root-Mean-Square value of the tyre-ground forces as presented in equation 18, in order to retrieve a road-holding coefficient, described as the RMS of the difference between the tyre reaction vertical forces and the static tyre-ground forces. Finally, such value is normalised with respect to the static load of the vehicle. The presented index is referred to a single tyre when the vehicle model features two different suspension structures. An increase in the aforementioned quantity may represent an increase in the mean value of the tyre-ground forces or a greater variation of the tyre vertical reactions. Those aspects induce different conclusions regarding road holding, therefore such quantity is adopted along with the standard deviation of the tyre-ground contact forces. In this manner it is possible to have a complete representation of the trend of the tyre-ground vertical forces, hence

a deeper analysis of the handling.

$$Road \quad Holding \quad coef. = \frac{rms(F_z - F_{z,static})}{F_{z,static}} \tag{18}$$

To complete the assessment of the handling, a measurement of the loss of contact between the tyre with the ground is considered. Therefore, the *flying time* index is introduced as the summation of the instants where the tyre-ground vertical forces are null. The mathematical definition of the aforementioned parameter is presented in equation 19

$$Flying \quad time = \sum \Delta t_{F_z=0} = N \cdot ts \tag{19}$$

where $\Delta t_{F_z=0}$ is the time window when the tyre contact force is zero. It follows that such index can be defined as the multiplication between N, the number of samples in which the vertical contact forces are null, and ts, the sample time.
As mentioned previously, when the Belgian block road proposed in figure 26 is fed to the motorcycle model, the averaged mean acceleration perceived by the rider over the whole simulation is adopted to quantify the level of comfort. Such quantity is properly calculated following the regulation of ISO 2631 reported in equation 20

$$a_w = \sqrt{\frac{1}{T}\int_{t_0}^{T} a_w^2 dt} \tag{20}$$

where the term a_w is the frequency-weighted acceleration of the rider seat. Therefore, to apply the equation 20 it is necessary to filter the rider-perceived acceleration through the transfer function represented in figure 27, as described in norm ISO 2631.

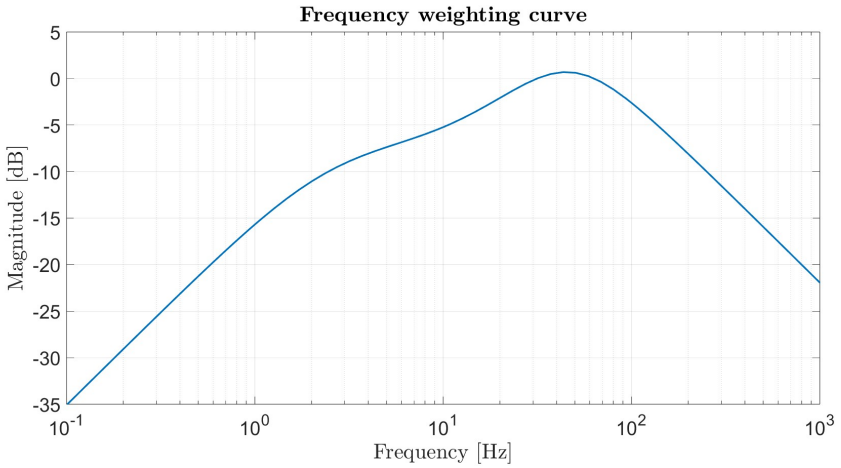

Figure 27: ISO 2631 norm weighting function of the rider-perceived acceleration

5 Hybrid control logic: Quarter-car model Simulation

5.1 Quarter-car model parameters

To investigate the desired behaviour of the innovative control, and to design a competitive rationale able to master both the comfort and the handling properties of the vehicle, a simplified model of the motorcycle is exploited. The scheme utilised for this purpose is commonly referred to as the *Quarter-car model*. Anyway, it is worth specifying that the quarter-car model in this concept is not a *quarter of a 4-wheeled vehicle*, it is more precisely a model of *half of the motorcycle* taken into consideration, but the physical scheme is equivalent, a two degree of freedom model composed by:

- one mass, representing the sprung masses supported over the suspensions: The vehicle body with the engine, gearbox and tank, the fairings, the upper portion of the suspensions and the rider
- a parallel scheme of a damper and a spring, to represent the suspensions.
- a second mass, positioned underneath the suspension scheme representing the unsprung masses, i.e. all the bodies not supported by the springs and dampers: rim and tyres, the braking system, and the lower portion of the suspensions (for instance the swingarm or the inner tubes of the front forks)
- a second parallel scheme of a damper and spring, positioned between the road surface and the unsprung masses, representing the tyre radial stiffness and its damping.

The quarter-car model is exploited due to its simplicity and intuitiveness, providing the opportunity to comprehensively study the characteristics of suspensions and the control logic. It is important to underline that the suspension damper is replaced with a controllable damping actuator in the semi-active version of the model as presented in figure 28. The motorcycle's properties adopted in the simulations reflect the may vehicle characteristics of table 1. To obtain a suspension model that approximates the performance of the motorbike prototype proposed, the quarter-car parameters of table 3 are exploited.

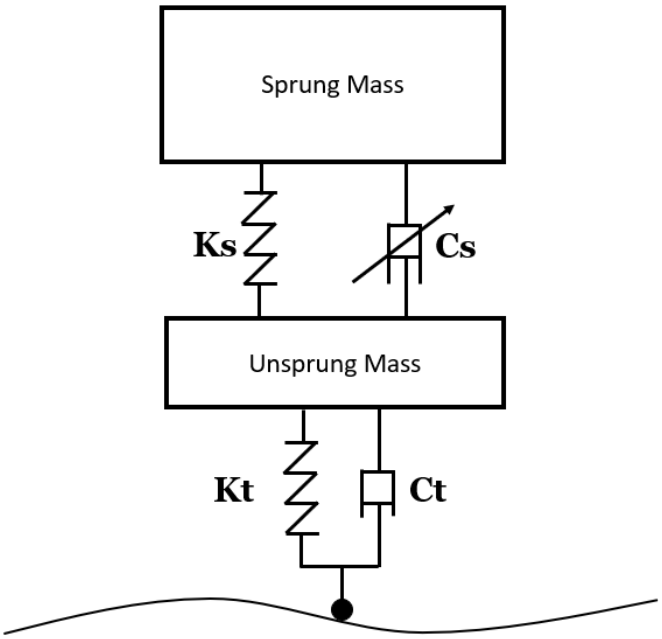

Figure 28: Representation of the quarter-car model adopted in the simulations

The suspension stiffness is defined as the mean value of the front and rear suspension stiffness of the vehicle of table 1. The same procedure is exploited to evaluate the tyre's radial stiffness and damping: the average of its front and rear value. To obtain a coherent model it is necessary to assign to the sprung and unsprung masses of the quarter-car model, half of the weight of their respective masses in the full-scale version of the vehicle. The damping of the system is a parameter of the simulations. In fact, for each controller scheme, the damping value is chosen as a consequence of the control logic, and compared to the optimal damping value of the passive system. The optimal damper setting is retrieved as the damping value that provides an optimal comfort-oriented response of the suspension[29], by applying the equation 21

$$c_{optimal} = \sqrt{\frac{m_s \cdot k_s}{2} \cdot \frac{k_t + 2 \cdot k_s}{k_t}} \tag{21}$$

where m_s is the sprung mass weight, k_s is the suspension stiffness and k_t the tyre radial stiffness. The semi-active suspension performances resulting from the implementation of different control logics will be discussed in subsection 5.2, whereas the current paragraph concludes with an analysis of the passive suspension layout, in order to provide a complete and exhaustive reference frame for the successive analyses.

Sprung mass weight	m_s	132.5	Kg
Unsprung mass weight	m_u	13	Kg
Suspension stiffness	k_s	25e3	$\frac{N}{m}$
Radial tyre stiffness	k_t	125e3	$\frac{N}{m}$
Suspension damping coefficient	c_s	1523	$\frac{N \cdot s}{m}$
Tyre radial damping	c_t	550	$\frac{N \cdot s}{m}$

Table 3: Quarter-car model characteristics

In figure 29 the frequency response function of the passive suspension system is presented. The graph of figure 29 shows the optimal damping value in contraposition with two opposite suspension settings: a softer ($\frac{c_{optimal}}{2}$), and a harder one ($(2 \cdot c_{optimal})$. The optimal damping provides a horizontal tangent in the inverting point of the transfer function, thus enhancing the optimal comfort setting [29]. A harder shock absorber shows, as expected, a more damped resonance frequency in the vicinity of the sprung mass natural pulsation, but pays a greater oscillation transmission at higher frequencies. The very opposite trend is visible adopting a softer damper. Differently, considering the tyre-ground forces it is noticeable that a harder damper allows a more constant reaction forces transfer function, improving the handling of the motorcycle: the comfort-handling conflict is perfectly perceivable.

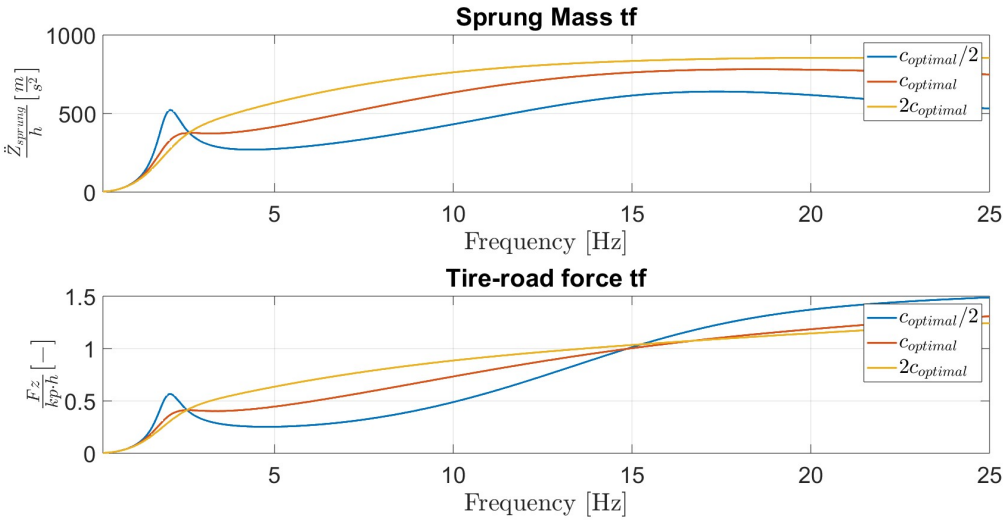

Figure 29: Frequency response function of the passive suspension system, with three different damping levels

From the graph of figure 29 it is possible to retrieve a characterisation of the passive suspension, differently, in figure 30 it is represented the step analysis performances of the system. Also in this case the optimal damping provides the optimal suspension stroke and sprung mass displacement.

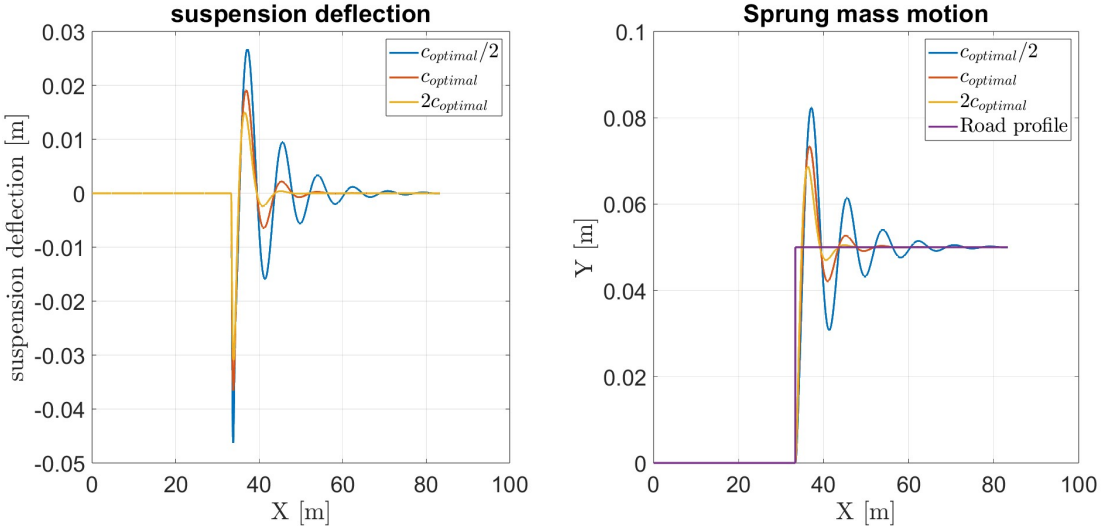

(a) (b)

Figure 30: Step analysis results: a) suspension deflection; b) Sprung mass position

5.2 The Hybrid control logic

In the current section the Hybrid control rationale is presented and tested. The design of the Hybrid control logic is based on the evaluation of the pre-existing controllers, considering their strengths and weaknesses. The *Hybrid* control logic, as the term suggests, is a composition of the controllers presented in section 3, with the scope of mastering both the handling and comfort. The reason why such a structure is adopted resides in the possibility of implementing a relatively simpler logic compared to the most sophisticated controllers presented in recent years but with the same overall performance, or even better. The controllers proposed in the literature review are now applied to the quarter-car model featured with the characteristics of table 3, and the results are compared and discussed. In figure 31 the Skyhook, the ADD and the Groundhook control logic are compared. It is visible that by applying the Skyhook and the ADD control logic to the quarter-car model considered, the results do not differ substantially from the graph shown in section 3. Moreover, the suspension transfer function equipped with the ADD rationale presents the optimal shape for comfort, except for the low-frequency region,

where the Skyhook outperforms the ADD logic. Therefore, to maximise the comfort property of the suspension, near the sprung mass natural frequency it is necessary to switch from the Skyhook control logic to the ADD. As a matter of fact, this result reflects the conclusion drawn in section 3.4, where it was pointed out the potentiality of a control strategy able to mix two different sub-optimal logics.

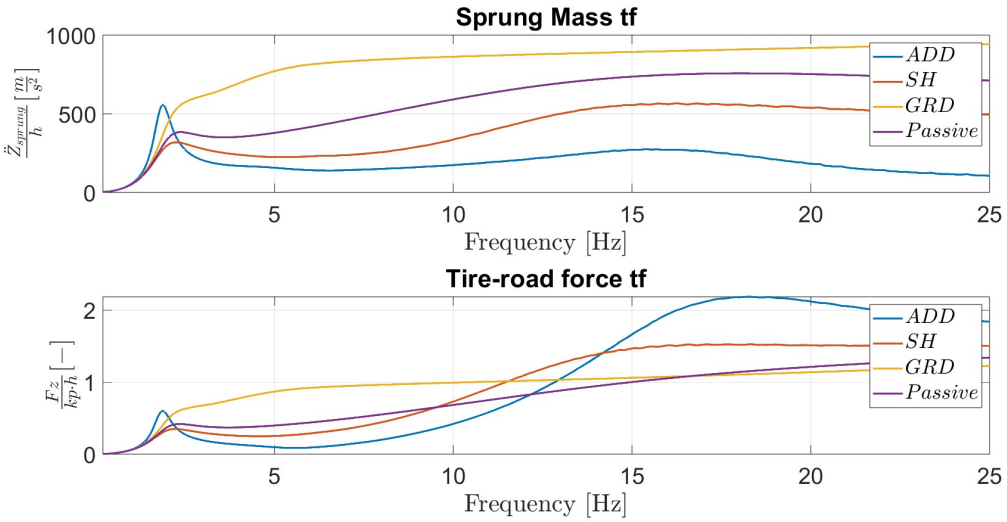

Figure 31: Comparison between the frequency response functions of different controllers

Adopting a quarter-car model with the features shown in table 3 presents a SH-ADD crossover frequency close to 2Hz. Regarding the road-holding, the conclusions differ substantially. As previously shown in section 2.3, also in this analysis it is visible the contraposition between handling and comfort. The comfort-optimal string of controllers in frequency domain does not fit the ideal solution regarding the road holding. From figure 31 it is also visible the tyre-road vertical forces transfer function; which is the principal key factor concerning the handling property of the vehicle. It is possible to state that the SH-ADD mix do not involve the optimal ground forces since in the vicinity of the unsprung mass natural frequency there is a massive force variability, which induces a decrement in the handling efficiency of the controller. As discussed in previous chapters, the ADD and skyhook are particularly indicted to absorb the oscillation close to the natural frequency of the sprung mass, but on the other hand, they are almost ineffective at higher frequencies. It is evident the necessity of implementing a different rationale. From this statement a second parallel string of control logics is studied. From figure 31, thus from the characterisation of the suspension in frequency domain, it is possible to come to the same conclusion

shown in chapter 3.2, where it was pointed out the efficiency of the Groundhook control logic to damp out the unsprung mass oscillation, specifically at high frequency. Therefore, the handling-oriented control strategy design is based on the rationales that diminish the variability of the tyre-ground forces along the entyre frequency window: the ADD logic at lower frequencies, and the Groundhook at higher frequencies. The current suspension model shows a handling cross-over frequency at 12 Hz. It was also possible to anticipate the ADD logic with the SH at very low frequencies, anyway, for sake of simplicity it was avoided.
However, a critical aspect arises when considering the switching across the crossover frequencies. In fact, it is necessary to know the frequency of the road input, to properly switch rationale when it is required. A possible solution is to record the vehicle speed and link the input frequency to the vehicle velocity based on statistical assumptions. Such a solution anyway, requires the implementation of the full vehicle model, therefore it is not implemented in the quarter-car simulations for obvious reasons. To estimate the frequency of the input signal, a frequency estimation function is implemented. Such a mathematical function consists of analysing the frequency spectra of the road signal and estimating the predominant frequency on the basis of the maximum amplitude perceived through the application in real-time of a Fast Fourier Transform (FFT) over an acquired input road signal. To implement an FFT live, a *rolling vector* is exploited. This solution consists of storing the input signal in an array of length N, and once N samples of the road signal are memorised into the vector thus saturating it, every value will be shifted by one position, and the following input sample will be overwritten in the first position. At each time instant the controller's logic performs an FFT evaluating the principal frequency components of the incoming road signal. This process shows good performance whenever it is applied in a controlled environment, where there is a limited amount of frequency components and therefore it is possible to observe a predominant frequency. In real conditions this hypothesis is not always ensured, and more predominant frequency components are not visible. Therefore once the frequency components are estimated, a weighted average is performed on the first 'n' frequencies disposed in order of magnitude. The averaging is performed as shown in equation 22, where 'n' is the number of frequencies taken into account and the P_n terms are the respective amplitude of the frequencies f_n.

$$freq = \frac{P_1^4 \cdot f_1 + P_2^4 \cdot f_2 + ... + P_n^4 \cdot f_n}{P_1^4 + P_2^4 + ... + P_n^4} \tag{22}$$

The adopted formula facilitates the incorporation of diverse frequency components. However, a significant limitation of this approach arises from its susceptibility to include noise components inherent in real-world applications during the selection of primary frequencies. Consequently, the parameter 'n' is set to 2, indicating that

the selection of the frequency carrier involves an amplitude-weighted averaging of the initial 2 frequency components identified through Fast Fourier Transform (FFT) analysis. The dimension of the rolling vector N is set equal to 500 in order to cover a time window of half a second and catch high-frequency dynamics. The frequency estimator is tested with a single-tone chirp signal. Since the input is a linearly increasing frequency sine wave signal from 0.2 to 25 Hz in 100 seconds, the expected results consist of a linear increasing trend of the estimated frequencies with respect to time. Figure 32 represents the resulting frequencies and the spectrogram of the input signal. It is evident that the frequency content of the sine wave exploited to test the frequency estimation function has the expected linear trend. The results of the frequency filter under test are brilliant since the estimated frequencies are perfectly overlapped with the major frequency contents of the input.

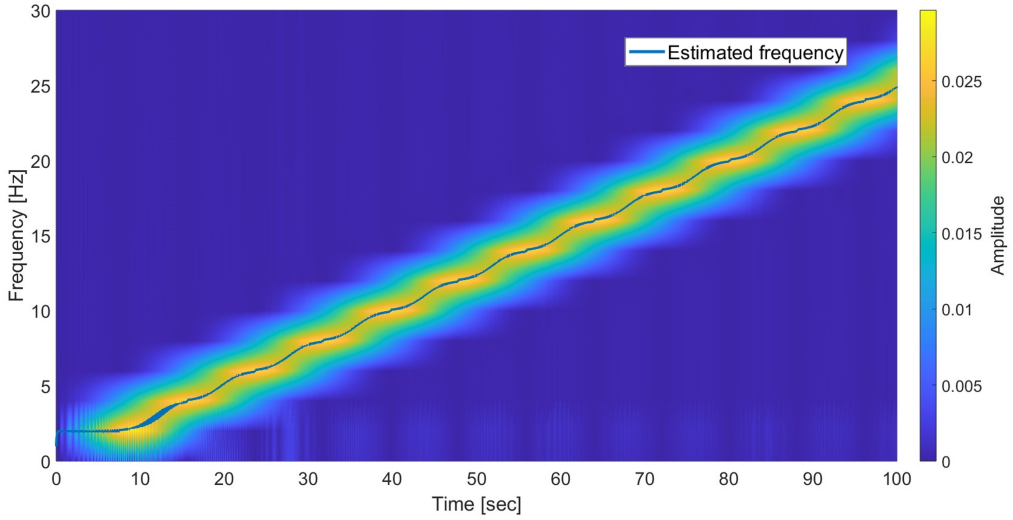

Figure 32: Estimated frequency compared to the single-tone input chirp signal spectrograph

The single-tone input does not reflect the complexity of the real road frequency contents. Therefore it is necessary to complete the test of the frequency estimator function with the Belgian block pavement input. In this case, the real road profile is fed to the frequency filter, and the results are reported in figure 33 where the estimated frequencies and the time-frequency analysis of the Belgian road pavement are compared. It is evident how the road profile adopted to test the controller represents a real road profile; the frequency content is substantially more complex with respect to figure 32. The main frequency carriers are the spots where the amplitude is more accentuated. As mentioned in equation 22, therefore, for each time

instant the estimated frequencies will position towards the *more yellow* frequencies observed.

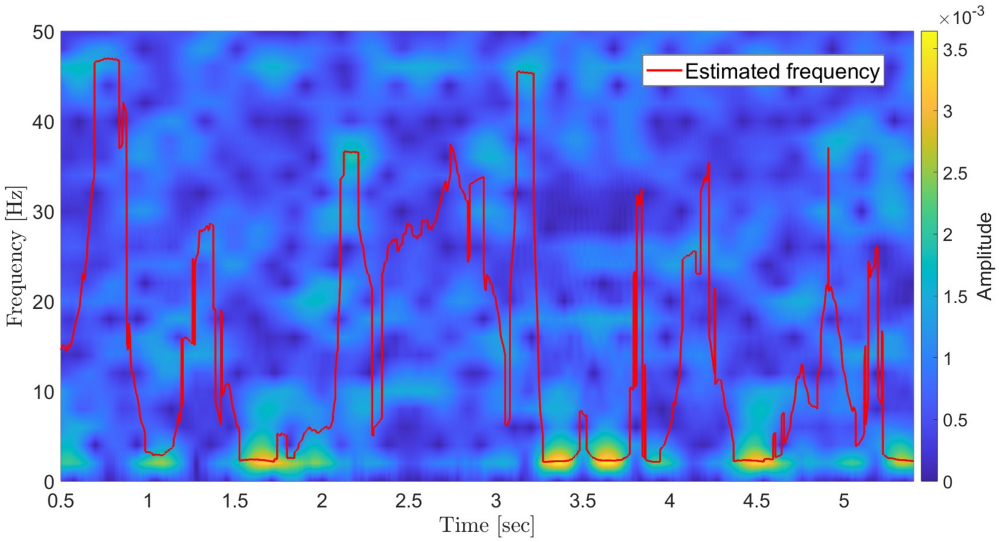

Figure 33: Estimated frequencies and spectrogram of the Belgian block road profile

As previously discussed, the strength of this suspension control fashion lies in the possibility of uncoupling the handling and comfort-oriented rationales, and therefore implementing the optimal logic to master a single objective, without the necessity of introducing a trade-off. This is a possible solution to overcome the previously mentioned comfort-handling conflict. The control rationale, finally, will be able to switch from a comfort-oriented strategy to a handling-optimized rationale based on a weight parameter. Such an index will gradually move the orientation of the suspension control logic towards handling or comfort on the basis of the motorcycle attitude. Moreover, the state of the motorcycle will be defined as a consequence of the acceleration perceived by the motorcycle sensors: when limited longitudinal and lateral accelerations are sensed, the state function will select a cruising state of the vehicle, thus enhancing the comfort focus of the rationale. Differently, high longitudinal or lateral accelerations will result in a handling requirement. As imaginable, the weighting function was designed on the assumption that when cruising the main objective of the suspension control system has to be comfort, whereas when the riding is more dynamic it is more likely the rider is expecting demanding road-holding and good handling. Based on the specifications presented, the weight parameter η is computed as proposed in equation 23

$$\ddot{\eta} = \gamma(\frac{1}{g}|\ddot{x}| + \frac{1}{g}|\ddot{y}|) - \delta\dot{\eta} - \epsilon\eta \tag{23}$$

where γ, δ and ϵ are gain parameters to tune the response of the weighting parameter η. Given that the suspension controller leverages this parameter as a pivotal input, the vehicle's response is significantly influenced by it. Consequently, the feasibility of fine-tuning the controller's behaviour by adjusting the aforementioned gains was considered. In a practical implementation, the controller could feature a graphical interface, including a dedicated settings page. This page would allow users to adjust the controller's response based on the rider's preferences or riding style. Consequently, parameters can be modified according to the selected settings, providing a customizable experience tailored to the individual rider. The structure of the η function is inspired by the mass-damper-spring model forced response, therefore, it is possible to observe an analogy with the damping factor (δ) and the stiffness (ϵ) of an equivalent 1 D.O.F mass motion. To ensure a correct duality between handling and comfort orientation, the equation 23 once implemented in the suspension control unit is digitally saturated in order to not exceed the range [0;1]. Figure 34 presents the trend of the longitudinal and lateral acceleration of the motorbike as well as the trend of the weighting function η. This plot is retrieved using IPG MotorcycleMaker, which simulates a full motorcycle model travelling on a straight road followed by a U-turn. As visible, when a combination of the vehicle acceleration is perceived, meaning a more demanding road holding performance is required, the η value rapidly moves towards 1, thus enhancing handling. Differently, when the motorbike simply cruises on a straight path, the comfort is augmented by a lower η value. The resulting Hybrid rationale will therefore admit a gradually more comfort-oriented strategy when η is approaching zero, and a progressively enhanced handling property when η increases. A possible final structure is depicted in equation 24 [14].

$$C = (1 - \eta) \cdot C_{comfort} + \eta \cdot C_{handling} \tag{24}$$

where $C_{comfort}$ and $C_{handling}$ are the optimal damping factors of the comfort rationale and the handling control logic, as discussed in the previous paragraphs.
It is worth mentioning that the accelerations perceived are not always appropriate to feed the weighting function 23 and manage it as intended. Therefore it is necessary to consider a preconditioning process of the sensed signal before the weighting function computation. In line with the introductory remarks of this chapter, the Hybrid law represents a synthesis of two distinct control methodologies: one prioritising comfort, and the other emphasising handling. These approaches are further compounded by various control logics, collectively aimed at globally optimising the controller's response. To conclude, the Hybrid control law gives its name due to the hybridisation on two different layers in which consists the rationale.

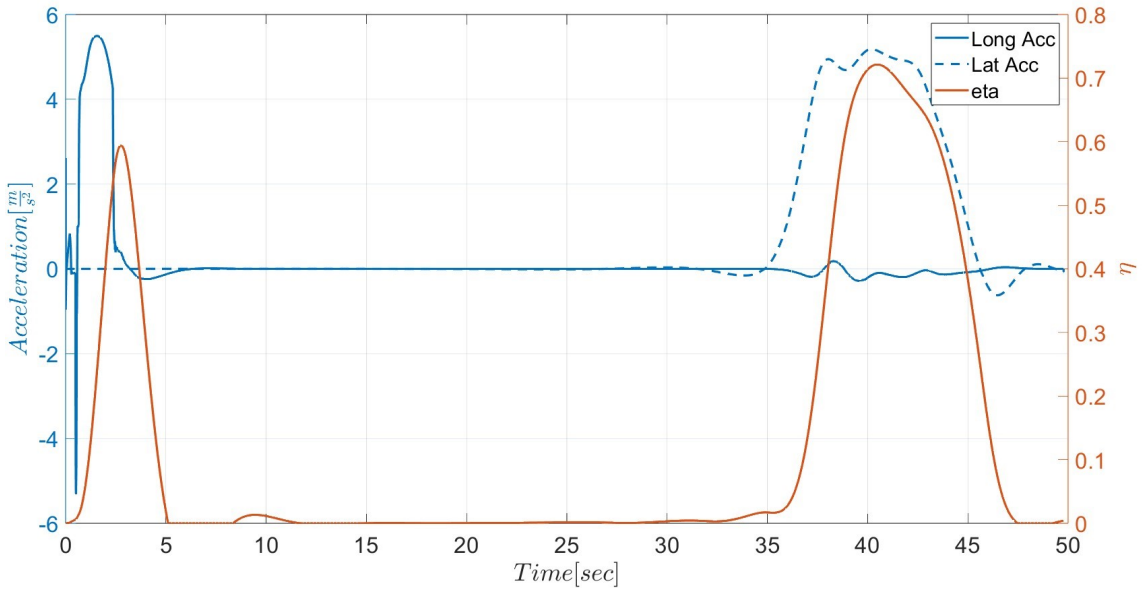

Figure 34: Longitudinal and lateral accelerations and weighting function η trend during a simple full-vehicle manoeuvre in IPG

Moreover, $C_{comfort}$ is selected following the SH before the 2Hz, and the ADD after such comfort crossover frequency. Differently, the complementary handling damping characteristic $C_{handling}$, will be defined following the ADD rule within 0 and 12 Hz, to switch for the Groundhook control logic after the handling crossover frequency. The resulting suspension setting rule can be summarised in equation 25 and 26

$$C_{comfort} \begin{cases} \begin{cases} C_{max,comf} & if \quad \dot{z}_s(\dot{z}_s - \dot{z}_u) > 0 \\ C_{min,comf} & if \quad \dot{z}_s(\dot{z}_s - \dot{z}_u) \leq 0 \end{cases} & if \quad fr \leq \alpha_{comfort} \\ \begin{cases} C_{max,comf} & if \quad \ddot{z}_s(\dot{z}_s - \dot{z}_u) > 0 \\ C_{min,comf} & if \quad \ddot{z}_s(\dot{z}_s - \dot{z}_u) \leq 0 \end{cases} & if \quad fr > \alpha_{comfort} \end{cases} \tag{25}$$

$$C_{handling} \begin{cases} \begin{cases} C_{max,han} & if \quad \ddot{z}_s(\dot{z}_s - \dot{z}_u) > 0 \\ C_{min,han} & if \quad \ddot{z}_s(\dot{z}_s - \dot{z}_u) \leq 0 \end{cases} & if \quad fr \leq \alpha_{handling} \\ \begin{cases} C_{max,han} & if \quad -\dot{z}_u(\dot{z}_s - \dot{z}_u) > 0 \\ C_{min,han} & if \quad -\dot{z}_u(\dot{z}_s - \dot{z}_u) \leq 0 \end{cases} & if \quad fr > \alpha_{handling} \end{cases} \tag{26}$$

Equation 25 and 26 represent the final version of the Hybrid controller, where $\alpha_{comfort}$ and $\alpha_{handling}$ are the comfort and handling crossover frequencies, respectively equal to 2 and 12 Hz. The maximum and minimum damping values have to be optimized accordingly to the vehicle properties. To conclude, as mentioned earlier, a brief description of the etymology of the controller is proposed. The term 'Hybrid' in the context of the control logic underscores its dual nature, amalgamating various elements: Primarily, it amalgamates pre-existing control logics, and additionally it exemplifies a fusion of comfort and handling priorities.

5.3 Quarter-car model simulation results

The maximum and minimum damping values, $C_{max,comf}$, $C_{max,han}$ and $C_{min,comf}$, $C_{min,han}$, among which the proposed Hybrid control logic switches are initially set arbitrarily to 2500 and 100 N*s/m respectively for the maximum and minimum damping for both the hybrid orientations, comfort and handling. The comfort and handling control strategy does not imply mandatorily the same damping setting, but such a hypothesis is assumed for sake of simplicity in a first characterisation of the Hybrid control logic. The transfer function of the hybrid-controlled semi-active suspension is retrieved and compared with the composing control strategies in figure 35. The simulation is conducted as proposed in section 4.1, therefore the quarter-car model is fed with a sinewave chirp signal, linearly increasing the frequency from 0.2 to 25 Hz. The frequency response function is estimated via the '*tfestimate*' Matlab command. The aim of the simulation is to identify the steady-state response of the Hybrid control logic in terms of acceleration isolation and tyre-ground force variability. In figure 35 a), the Hybrid control logic implements the SH control rationale up to 2Hz, corresponding to the comfort crossover frequency, before transitioning to the ADD control logic. Conversely, in part b), its road-holding-oriented strategy is apparent. Here, the Hybrid control logic employs the ADD logic up to the handling crossover frequency of 12Hz, shifting to the GRD logic thereafter.

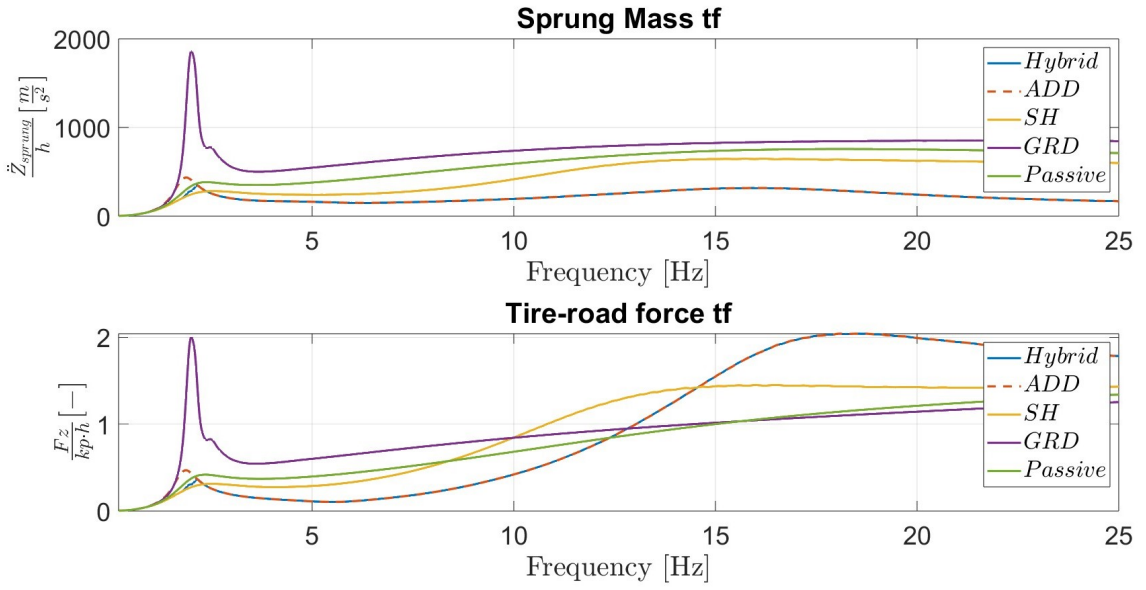

(a)

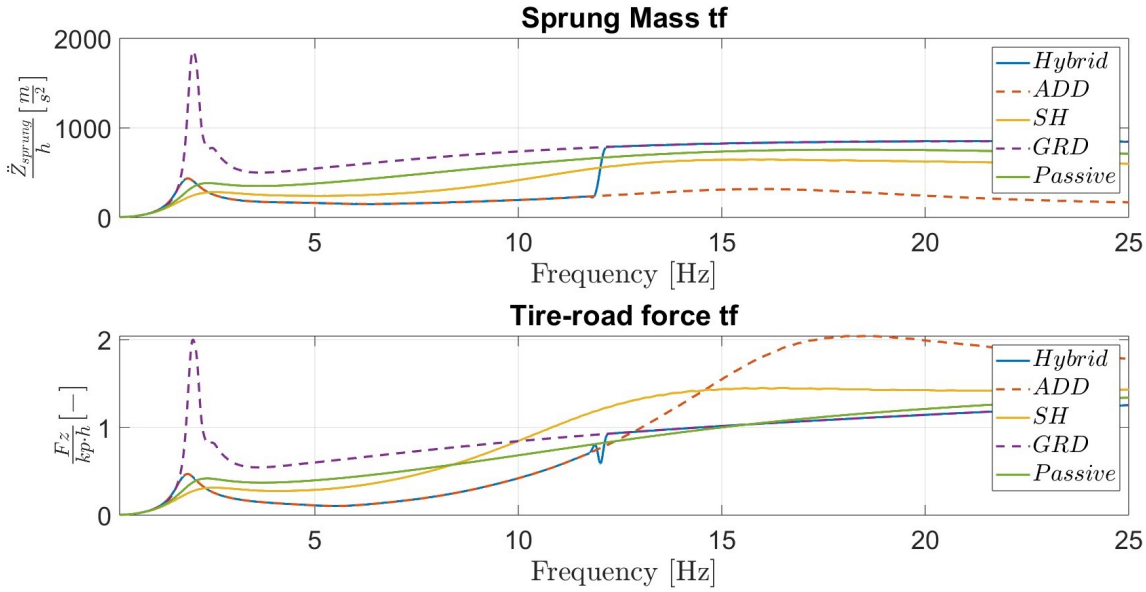

(b)

Figure 35: Frequency response function: a) comfort-oriented hybrid strategy, $\eta = 0$, b) handling-oriented hybrid control logic, $\eta = 1$

Both graphs distinctly demonstrate the transition between fundamental controllers within their respective frequency ranges. In addition, it is transparent how the hybrid control logic delineates the frequency response envelope characterized by the minimal magnitude of the transmitted accelerations when $\eta = 0$, which means the comfort-oriented strategy is enhanced, and of the variation of the tyre-ground vertical forces when $\eta = 1$ (i.e. the handling focus of the Hybrid logic is implemented), aimed at facilitating optimal comfort and handling control. As briefly mentioned in the previous paragraph, the maximum and minimum damping set of the comfort and handling-focused rationale can be defined independently, thus optimising their respective objective. Hence, Figure 36 presents the comfort and handling performance metrics of the controller, relative to the indices utilised to evaluate the controller's performance in the step analysis. The step road simulation is run repeatedly in a sensitivity analysis to quantify which are the optimal damping settings of the Hybrid controller, firstly when the comfort-oriented strategy is adopted, and successively when the handling-oriented controller is imposed.

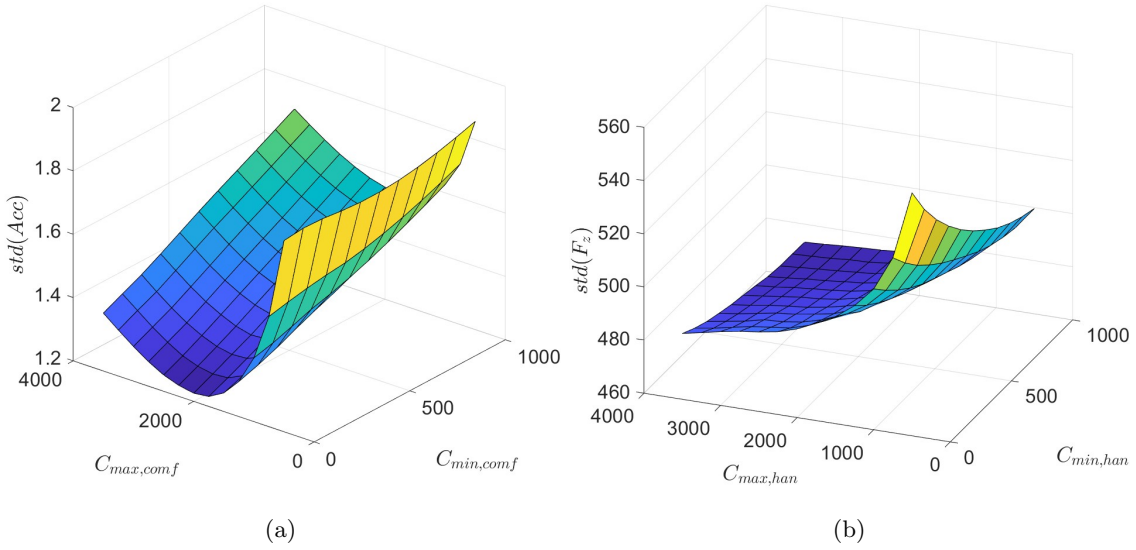

(a) (b)

Figure 36: Step road sensitivity analysis: a) comfort-oriented hybrid strategy, $\eta = 0$, b) handling-oriented hybrid strategy, $\eta = 1$

Therefore from figure 36 is evident that the optimal semi-active damper set that implies the minimization of the sprung mass acceleration does not meet the handling optimization properties. The Hybrid control logic facilitates the decoupling of damper settings. This approach enables the $\eta = 1$ strategy to adhere to the handling-optimized setting for its rationale, while the comfort controller implements

a combination of maximum and minimum damping setting that maximise the isolation of the sprung mass from road disturbances. Therefore, from the step road profile sensitivity analysis the proposed combination of parameters is suggested.

- $C_{max,comf} = 2000 \ \frac{N \cdot s}{m}$
- $C_{min,comf} = 0 \ \frac{N \cdot s}{m}$
- $C_{max,han} = 3500 \ \frac{N \cdot s}{m}$
- $C_{min,han} = 1000 \ \frac{N \cdot s}{m}$

Anyways, since the aim of the project is to guarantee the optimal behaviour of the motorcycle in a real operational condition, the same optimisation process is also applied to the Belgian block pavement road. From figure 37 the resulting performance grid for different combination of damping values is proposed.

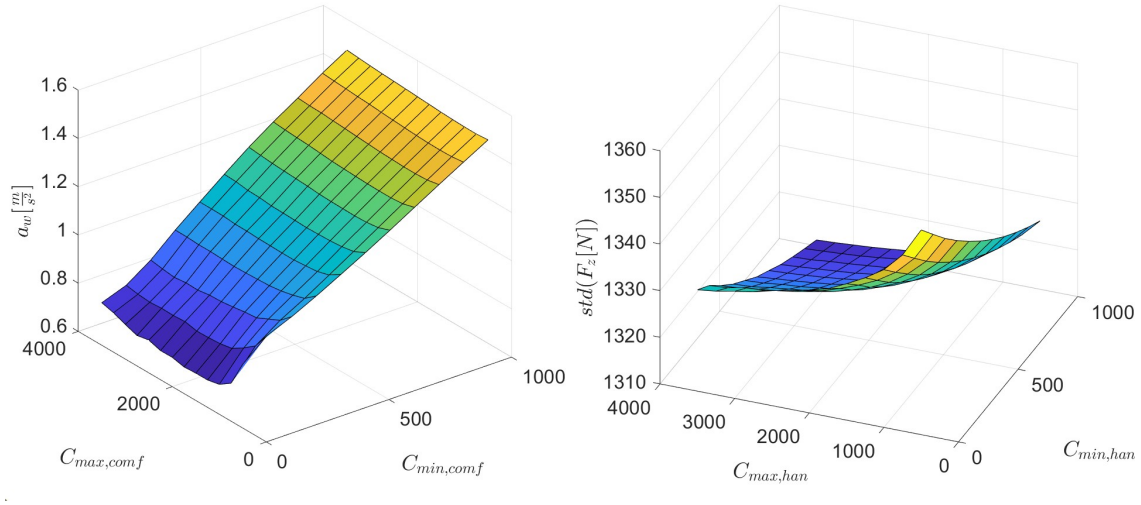

(a) (b)

Figure 37: Belgian block road sensitivity analysis: a) comfort-oriented hybrid strategy b) handling-oriented hybrid strategy

Therefore, from figure 36 it is possible to observe that the optimal damper setting regarding the comfort is again different from the optimal handling shock absorber. Consequently the parameters of the hybrid control logic that best fit the performances expected are reported below:

- $C_{max,comf} = 1500 \ \frac{N \cdot s}{m}$

- $C_{min,comf} = 0 \ \frac{N \cdot s}{m}$
- $C_{max,han} = 3500 \ \frac{N \cdot s}{m}$
- $C_{min,han} = 1000 \ \frac{N \cdot s}{m}$

Finally, it is possible to observe how the optimal parameters resulting from both sensitivity analyses are similar. More in detail, the minimum damping that best provides comfort properties is null, for both the orientation strategies of the suspension control unit. The same conclusion can be drawn when considering both the maximum and the minimum damping level of the handling-oriented control strategy, since from both the sensitivity analysis it is recommended to opt for a minimum damping of 1000 $\frac{N \cdot s}{m}$ and a maximum one of 3500 $\frac{N \cdot s}{m}$. The only compromise between the optimisation of the step response, and the Belgian block road performance, is the maximum damping of the comfort-oriented strategy. Therefore the following damper settings are chosen to simulate the performance of the hybrid-controlled semi-active suspension:

- $C_{max,comf} = 1750 \ \frac{N \cdot s}{m}$
- $C_{min,comf} = 0 \ \frac{N \cdot s}{m}$
- $C_{max,han} = 3500 \ \frac{N \cdot s}{m}$
- $C_{min,han} = 1000 \ \frac{N \cdot s}{m}$

5.3.1 Quarter-car model result: Step road

In the current subsection the step analysis results are investigated. The goal of the simulation is to retrieve an approximation of the suspension response when the motorcycle faces a step profile, for example a pothole, a road junction, or a steep bump. From a suspension point of view it is important to ensure proper isolation of the sprung masses and good road holding. It was largely discussed how those topics can represent a critical aspect and how the proposed control logic would be able to overcome this duality by the introduction of two separate rationales: one specifically implemented when comfort is necessary, and a second exploited whenever the handling must be ensured. In the following analysis process both orientations are examined and discussed. The Hybrid comfort rationale provides the results proposed in the bar plot of figure 38 a), whereas the Hybrid control logic focused on the handling provides the results of figure 38 b). In both figures, the Hybrid logic is compared with the competitive controllers on the basis of the performance indexes proposed in chapter 4.1. The standard deviation of the sprung mass oscillations is adopted to

provide a level of assessment of the isolation of the rider from the road, thus representing the level of comfort of the analysed controllers, and for the handling, the standard deviation of the tyre-road forces is applied. The aforementioned results are obtained by simulating the quart-car model presented in chapter5.1 equipped with the control logic proposed in equations 25 and 26. The step road as discussed in 4.1 consists of a steep rise of 0.05 m of the road profile.

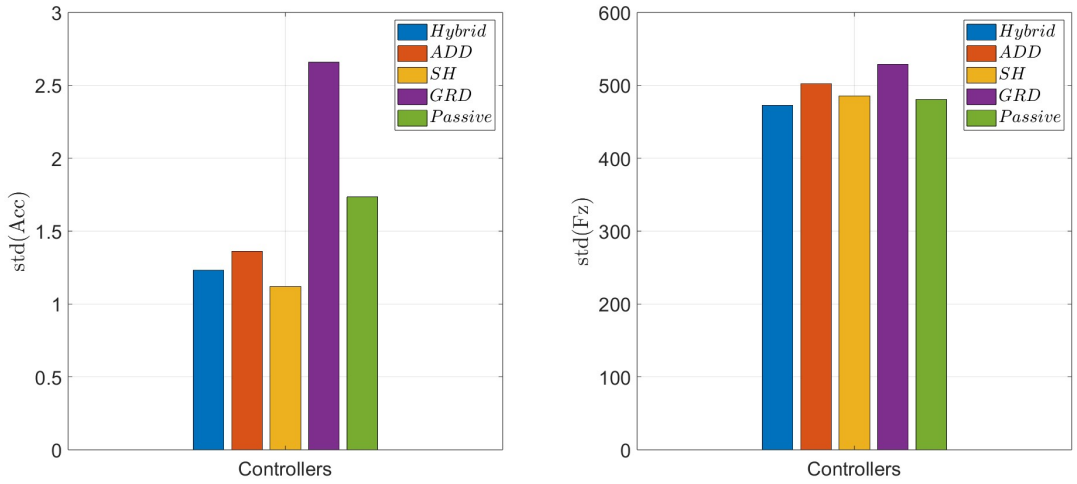

(a) (b)

Figure 38: Step road analysis and comparison: a) comfort; b) handling

It is possible to observe from figure 38 that the Hybrid control logic is indeed able to master both the handling and the comfort when compared to ADD, Groundhook and the passive system. Anyways, the Skyhook control logic provides slightly better performance in terms of comfort as visible from figure 38 a), due to the damping setting proposed in the previous paragraph. In fact, the optimal step road performance of the hybrid control logic can be observed for a slightly more damped controller, as happens when adopting the Skyhook controller. As mentioned, the key factor of the Hybrid controller lies in the possibility of focusing on a single objective and switching it when needed, thus avoiding the necessity of a trade-off. Such orientation is properly described in chapter 5.2, where it was presented the η function, a weighting function able to guide the controller gradually towards the handling or comfort on the basis of the accelerations perceived. Eventually, the performance of the controller over the step road is summarised in figure 39, where the overall performance of the Hybrid control logic is shown via a radar plot representing the handling through three parameters, the Road Holding coefficient, the Flying time and the standard

deviation of the tyre-ground vertical forces. The comfort is represented by the standard deviation of the sprung mass acceleration. To represent the fully-functional Hybrid controller performance applied to the quarter-car model the step analysis is run for different η values. Moreover from figure 39 it is possible to observe the gradual change in focus of the Hybrid controller from comfort to handling as the weighting function η moves gradually from 0 to 1.

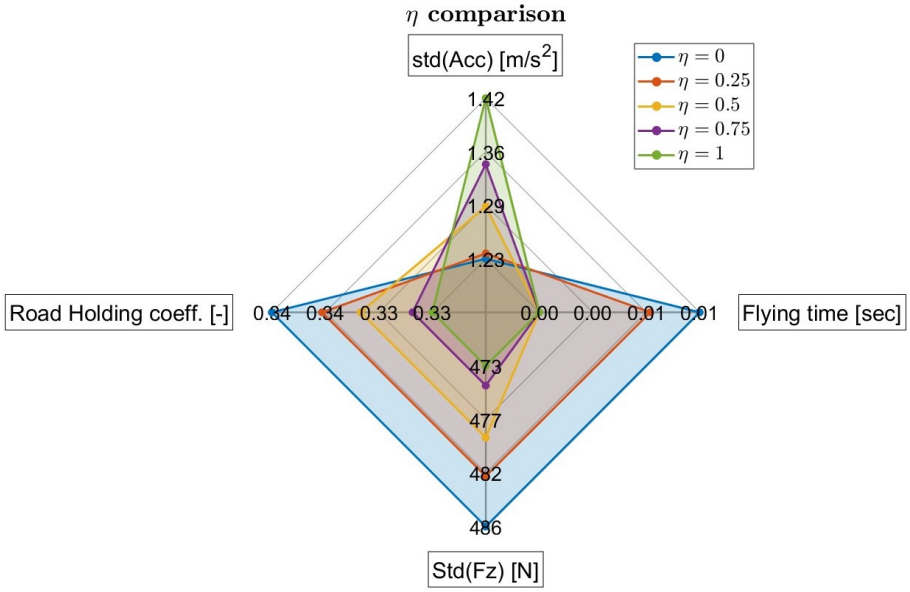

Figure 39: Hybrid control logic performance on a step profile for for different η values

Finally, to have a deeper analysis the resulting suspension deflection and the sprung mass position over the step are provided in figure 40. Coherently with the previous analyses the Skyhook, ADD and Groundhook controllers are compared to the passive system and the Hybrid control logic. Since the sprung mass position and suspension deflection are quantities mainly related to the comfort objective of the controller, the Hybrid comfort-oriented rationale (i.e. $\eta = 0$) is adopted in the graph. More in detail, figure 40 a) provides the suspension deflection with respect to the travelled space X [m], whereas the 40 b) provides the sprung mass oscillations. From 40 a) and b) is visible the sub-optimality of the Hybrid$_{\eta=0}$ controller since the Skyhook provides a slightly better reduction of the oscillation as a function of time, symptom of a less damped response. At lower frequencies the comfort-Hybrid rationale adopts the Skyhook logic, therefore the dissimilarities in performance observed

in figure 40 a) and b) are inevitably to be attributed to the ADD control logic which, even comes into operation to a limited extent, slightly impacts on the performance of the rationale implemented by the Hybrid control logic. The performances of the frequency estimator indeed degrade when a step input is faced, and the subsequent ADD control logic may be selected for a short period of time. Anyway, the overall performance of the controller is inspiring.

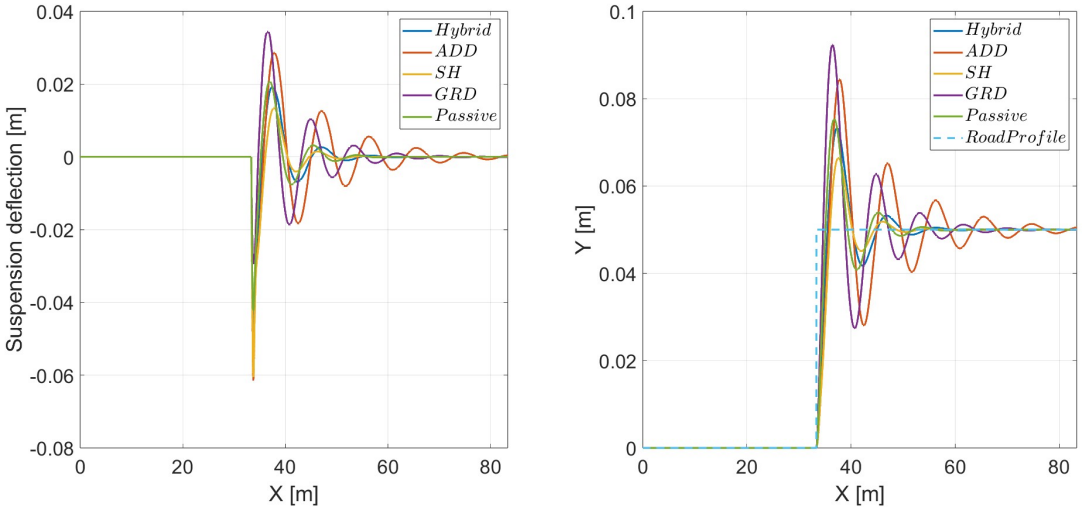

(a) (b)

Figure 40: a) Suspension deflection b) sprung mass oscillation

5.3.2 Quarter-car model result: Belgian block road

An approximation of the controller's performance in real operational conditions is provided by the *Belgian block* pavement analysis. In 4.1 the road profile is presented and it is discussed the reason why it can be considered a valid candidate to test the motorbike in real-exercise conditions. Therefore the results that are going to be presented in figure 41 and 42 are a pivotal aspect of the Hybrid suspension controller. The goal of the analysis is to take into consideration the different indexes that characterise the semi-active suspension layout, the weighted acceleration a_w, the Road-Holding coefficient, the flying time and the standard deviation of the tyre-ground vertical forces. Therefore a radar plot condensing such aspects is employed in the analysis. The road is run at different speeds to consider a fully extended scenario and different suspension working conditions. The speeds considered have to cover a wide range of uses of the 2-wheeled vehicle, therefore an urban speed of 30 Km/h is considered, a cruising speed of 60 Km/h is also taken into account, and

finally, an extra-urban speed of 90 Km/h is simulated. As mentioned the controller has to be tested in both orientations, i.e. it is necessary to analyse separately the comfort-oriented strategy of the Hybrid controller (Hybrid$_{\eta=0}$) and the handling one (Hybrid$_{\eta=1}$). The results in figure 41 present the comfort-oriented results of the Hybrid logic at 30 Km/h. The simulations performed at higher speeds perfectly resemble the graph in figure 41. Therefore the suspension control unit will implement the Skyhook or the ADD on the basis of the frequency estimated by the frequency selector function as shown in 5.2. It is visible how the frequencies read are within the ADD frequency region of action, since the performance of the Hybrid control and the ADD are overlapped over the four indexes. The estimated frequency of the Belgian block input signal proposed in figure 33 confirms such an assumption. Differently from the step analysis, the ADD outperforms the Skyhook control logic. This is an example of how hybridisation allows mastering the performance of the suspension control unit over a wide range of applications: switching the rationale implemented in the control unit allows choosing the optimal logic for every operational condition. To conclude, the Hybrid$_{\eta=0}$ follows the ADD and masters the comfort properties compared to the competitive controllers, but more importantly compared to the passive layout, for all the speed ranges considered.

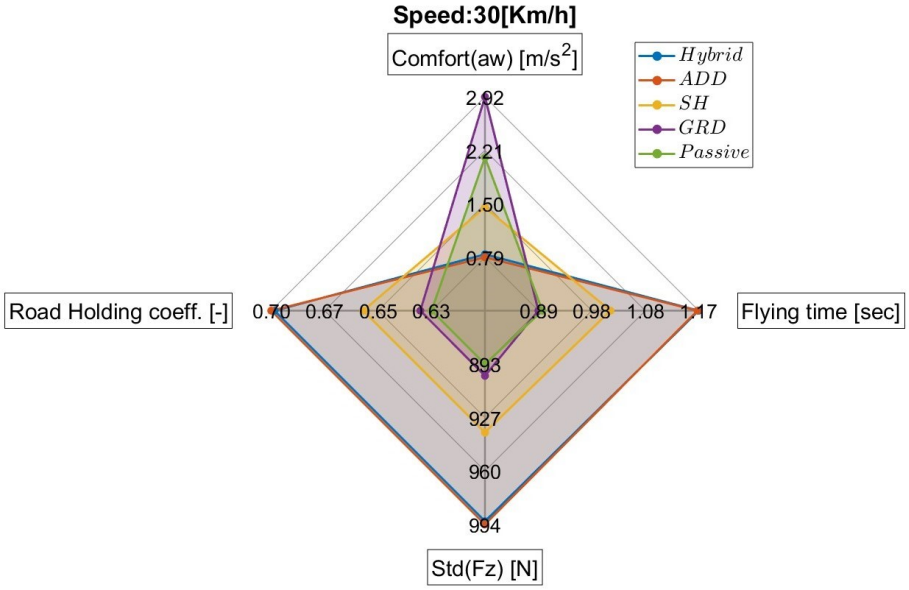

Figure 41: Belgian block road analysis of Hybrid$_{\eta=0}$ at 30 Km/h

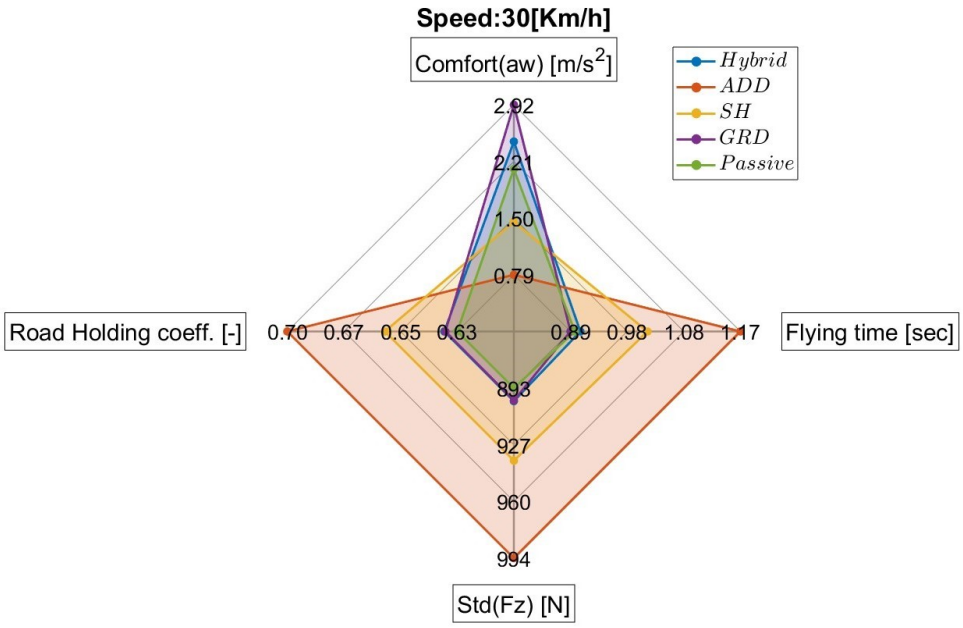
Speed:30[Km/h]
Comfort(aw) [m/s2]
2.92
2.21
1.50
0.79
Hybrid
ADD
SH
GRD
Passive
Road Holding coeff. [-]
0.70 0.67 0.65 0.63
0.89 0.98 1.08 1.17
Flying time [sec]
893
927
960
994
Std(Fz) [N]

(a)

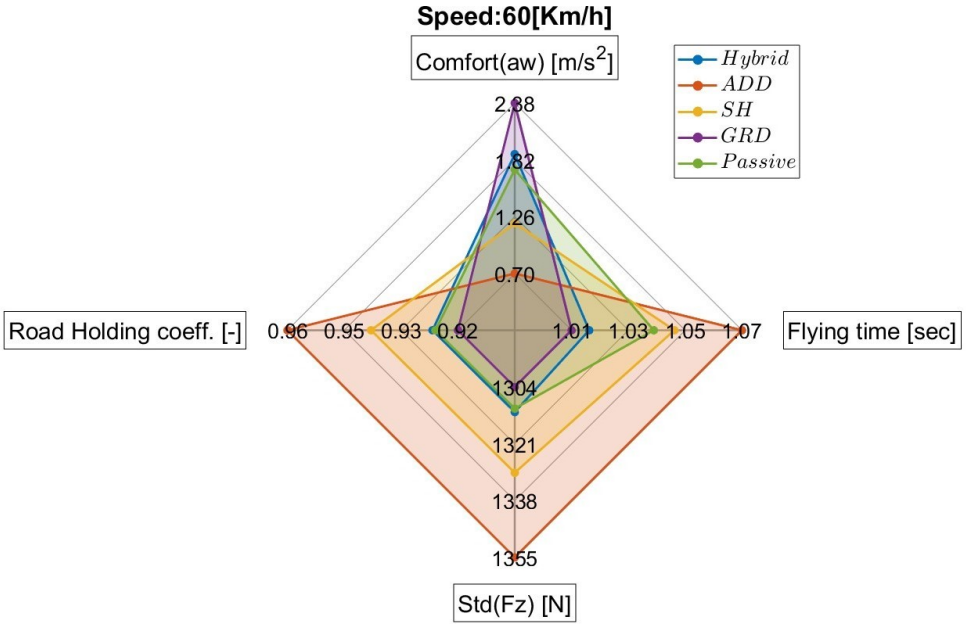
Speed:60[Km/h]
Comfort(aw) [m/s2]
2.38
1.82
1.26
0.70
Hybrid
ADD
SH
GRD
Passive
Road Holding coeff. [-]
0.96 0.95 0.93 0.92
1.01 1.03 1.05 1.07
Flying time [sec]
1304
1321
1338
1355
Std(Fz) [N]

(b)

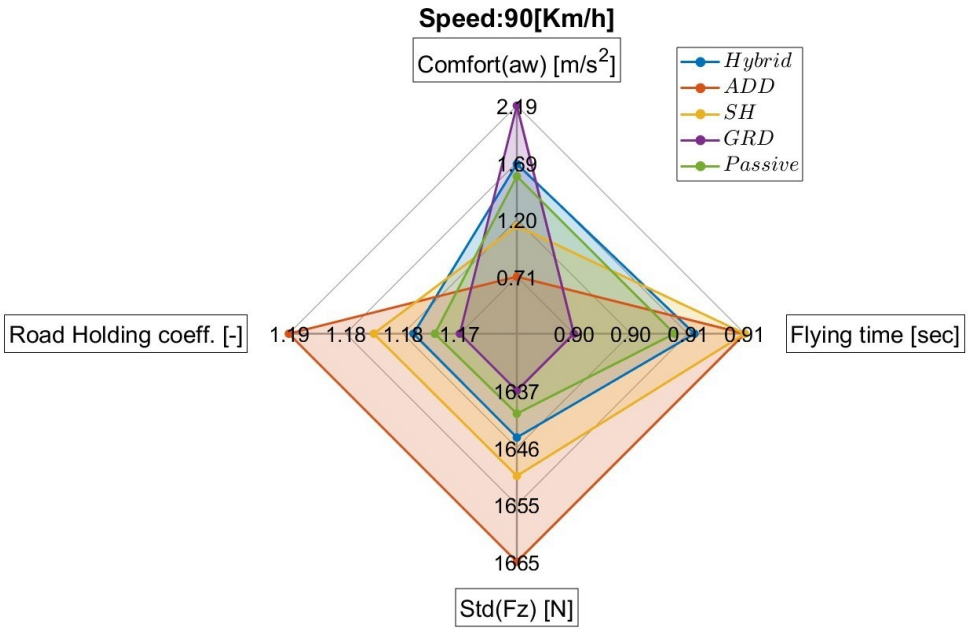

(c)

Figure 42: Belgian block road analysis of Hybrid$_{\eta=1}$. a) 30 Km/h b) 60 Km/h c) 90 Km/h

Figure 42 provides sub-optimal results since the Hybrid$_{\eta=1}$ control logic masters the handling only at low and medium speeds. When the vehicle reaches higher speeds and encounters a deteriorated road or a broad-band frequency-content road like the Belgian block pavement, the Hybrid controller performance degrades. The non-optimality of the control law is linked to the frequency selector function, which at higher speeds induces the Hybrid controller to switch for the ADD control rationale. This transition persists for a duration that adversely impacts performance. To have a deeper insight into the simulation results, the Hybrid controller response over the Belgian block pavement for different weighting function η values is presented in figure 43. In this manner it is possible to have an approximation of the overall behaviour of the control logic, when gradually moves from Hybrid$_{\eta=0}$ to Hybrid$_{\eta=1}$. Lastly, the analysis of the results is concluded with the presentation of the tyre-ground contact forces with respect to time. It is evident the demanding road conditions and the high oscillations of the contact forces.

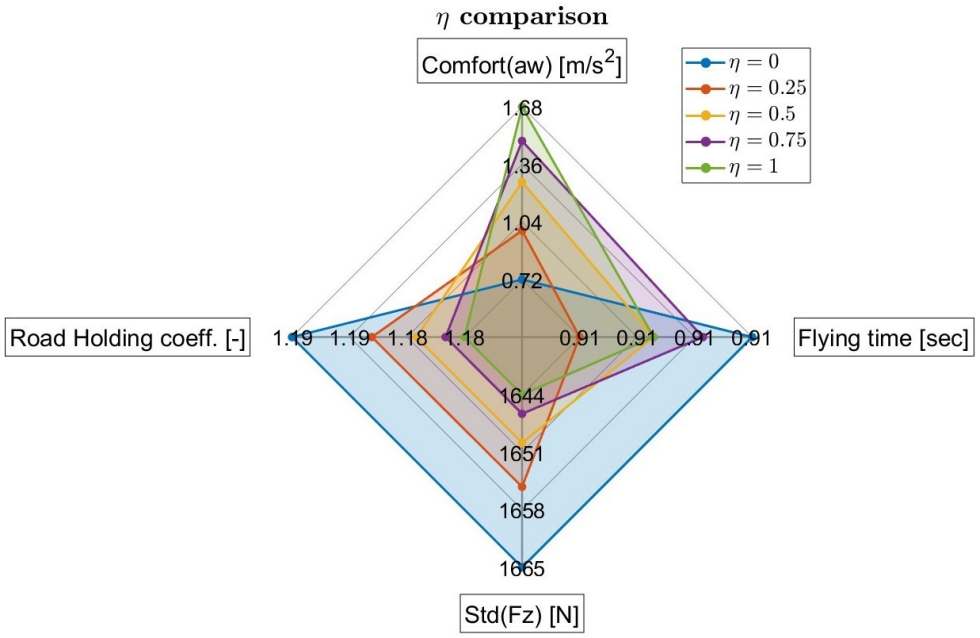

Figure 43: Performance of the hybrid control logic when moves gradually from comfort ($\eta = 0$) to handling($\eta = 1$)

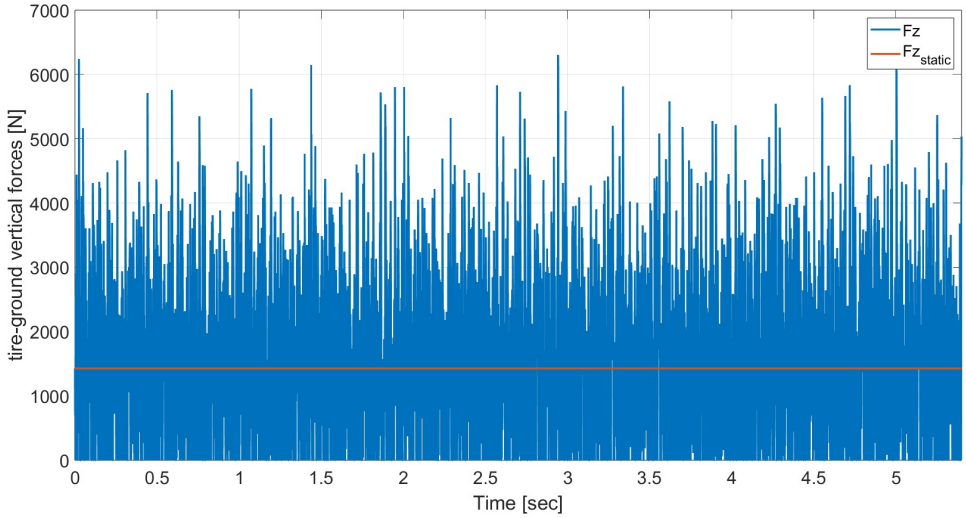

Figure 44: tyre-road vertical contact forces

6 Hybrid control logic: 4DOF model

6.1 4DOF Model description and parameters

The Hybrid control logic has been applied to a suspension model, the quarter-car model, and some interesting conclusions have been drawn. Nevertheless, it is imperative to evaluate the efficacy of the Hybrid control logic and compare its outcomes against those of competing controllers in the context of implementing the suspension control unit within a comprehensive vehicle model. Therefore the 4DOF vehicle model proposed in figure 45 is analysed in the current chapter. The full motorcycle is modelled in order to investigate the ride dynamics and the vibration of the masses of the vehicle. Such a vehicle scheme is also referred to as '*half-car model*' since it is possible to observe that the system is an in-plane representation of both axes of the vehicle. Moreover, it differs from the *quarter-car model* since it considers at the same time the front and rear suspension and how such elements affect the sprung body pitch oscillation. It is also possible to imagine to the current vehicle model as a *lateral view* of a 4-wheels vehicle. For the 2-wheeler considered in the current project, it is no longer correct to refer to the model as a 'half-car' model since it can represent the full-vehicle in-plane dynamics. Therefore the 4DOF motorcycle model visible in figure 45 will be composed of the following elements:

- Sprung mass: all the masses supported by both the front and rear suspension systems. Differently from the 2DOF model presented in chapter 5.1 the sprung body has two different degrees of freedom: a rotation around its centre of mass and a vertical motion. The sprung mass can be regarded as the sum of all the bodies that are attached to the suspended structure over the suspension such as the motorcycle frame, the engine and gearbox, the upper section of the suspension and obviously the rider.

- Unsprung masses: a major difference with the quarter-car model is the presence of two unsprung masses relative to both the front and rear bodies underneath the suspensions: the rims, tyres, braking systems, swingarm, part of the transmission system and the lower section of the suspension. Each unsprung mass is free to vertically translate.

- two suspension systems: in this vehicle model, there are two simplified linear suspension systems, which constitute the core of the design. As expected, these suspensions are situated at both the front and rear ends of the motorcycle configuration. Each suspension system is structured with a parallel arrangement consisting of a spring and a damper. Notably, it is crucial to emphasise that the damper utilised is a semi-active controllable element as visible from figure

45.

- two tyres: the model incorporates two tyres—front and rear—each modelled with a spring and a damper in a parallel scheme situated between the road disturbance and the unsprung masses. Furthermore, within the context of this vibration-oriented vehicle model, there is no need to conceptualise the tyres differently from the scheme presented. It is indeed important to model solely the radial stiffness and damping properties of the tyres.

It is immediate to verify that the sprung mass presented two degrees of freedom of its centre of mass, a vertical translation and a pitch rotation, whereas the unsprung masses provide one single vertical translation degree of freedom each. Therefore, it is evident that the nomenclature "4DOF model" is aptly descriptive, as the presence of the model's four degrees of freedom previously outlined. In this model, the road input signal is fed to the tyres' spring and damper lower end as a vertical translation. To consider the wheelbase filtering effect on the pitch oscillation and the system vibration, the road elevation profile is fed to the front tyre model, to be successively delayed by an amount of time to simulate the passage of the vehicle over the road disturbance before being fed to the rear tyre.

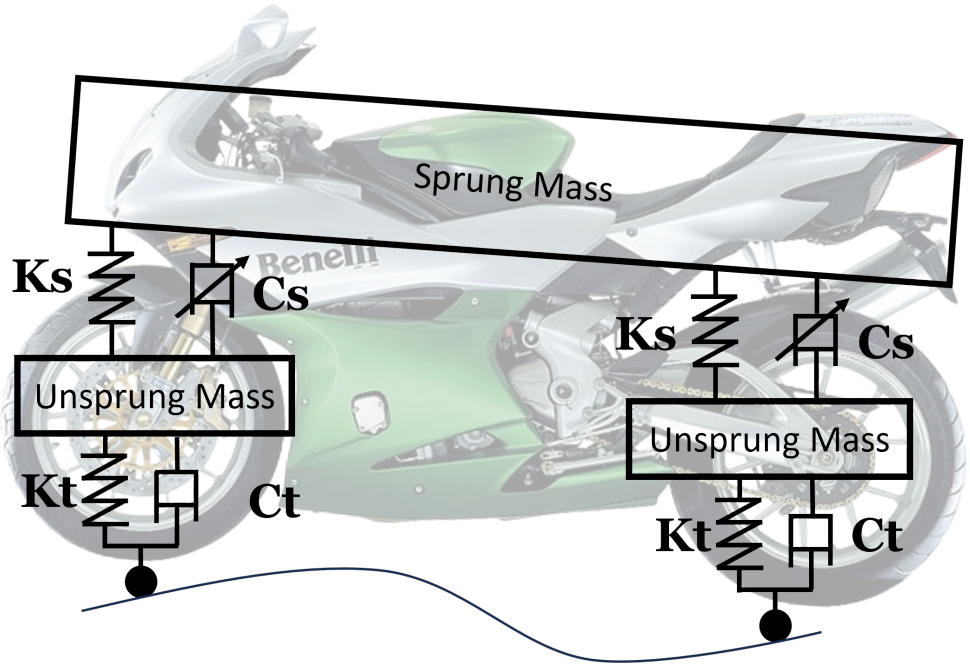

Figure 45: 4DOF motorcycle model

The importance of considering such a complicated model is rewarded by a more accurate description of the vibration perceived by the rider, and also to take into consideration the motion sickness induced by the pitch oscillation of the sprung masses. Finally, it is worth mentioning that, as conducted in the first analysis adopting the 2DOF quarter-car scheme, also in this context the model is simulated in Matlab-Simulink. The parameters that characterise the model are particularly significant since they affect directly the motorbike's response to a road disturbance. The analyses shown in this thesis aim to present and compare the behaviour of the vehicle equipped with a suspension control logic purposely designed to fit the motorcycle's needs. Therefore the standard vehicle characteristics proposed in 4.1 are directly applied to the 4DOF model, and reported in table 1 for sake of clarity.

Body mass	265	Kg
Front unsprung mass	12	Kg
Rear unsprung mass	14	Kg
Polar moment of inertia	82	$Kg \cdot m^2$
Wheelbase	1.4850	m
Front-semi-wheelbase	0.81	m
Rear-semi-wheelbase	0.6750	m
Front suspension stiffness	20e3	$\frac{N}{m}$
Rear suspension stiffness	30e3	$\frac{N}{m}$
Front tyre radial stiffness	100e3	$\frac{N}{m}$
Rear tyre radial stiffness	150e3	$\frac{N}{m}$
Front suspension damping	1218	$\frac{N \cdot s}{m}$
Rear suspension damping	1827	$\frac{N \cdot s}{m}$
Front tyre radial damping	500	$\frac{N \cdot s}{m}$
Rear tyre radial damping	600	$\frac{N \cdot s}{m}$

Table 4: 4DOF model characteristics

It is important to underline that small differences in simulation settings are introduced when analysing the 4DOF model with respect to the 2DOF quarter-car. More in detail, the step analysis road adopted in the following analyses is a more sophisticated double-step road: a steep rise in road profile followed by a plateau and a rapid descent. To present coherent results with the previous analyses, a full characterisation of the vehicle is proposed in the following passages. Firstly, it is

possible to retrieve a rough characterisation of the vehicle by considering the mode shapes. As a matter of fact, the 4DOF model allows to inspect the first 4 natural frequencies of the vehicle and analyse their estimated mode shapes.

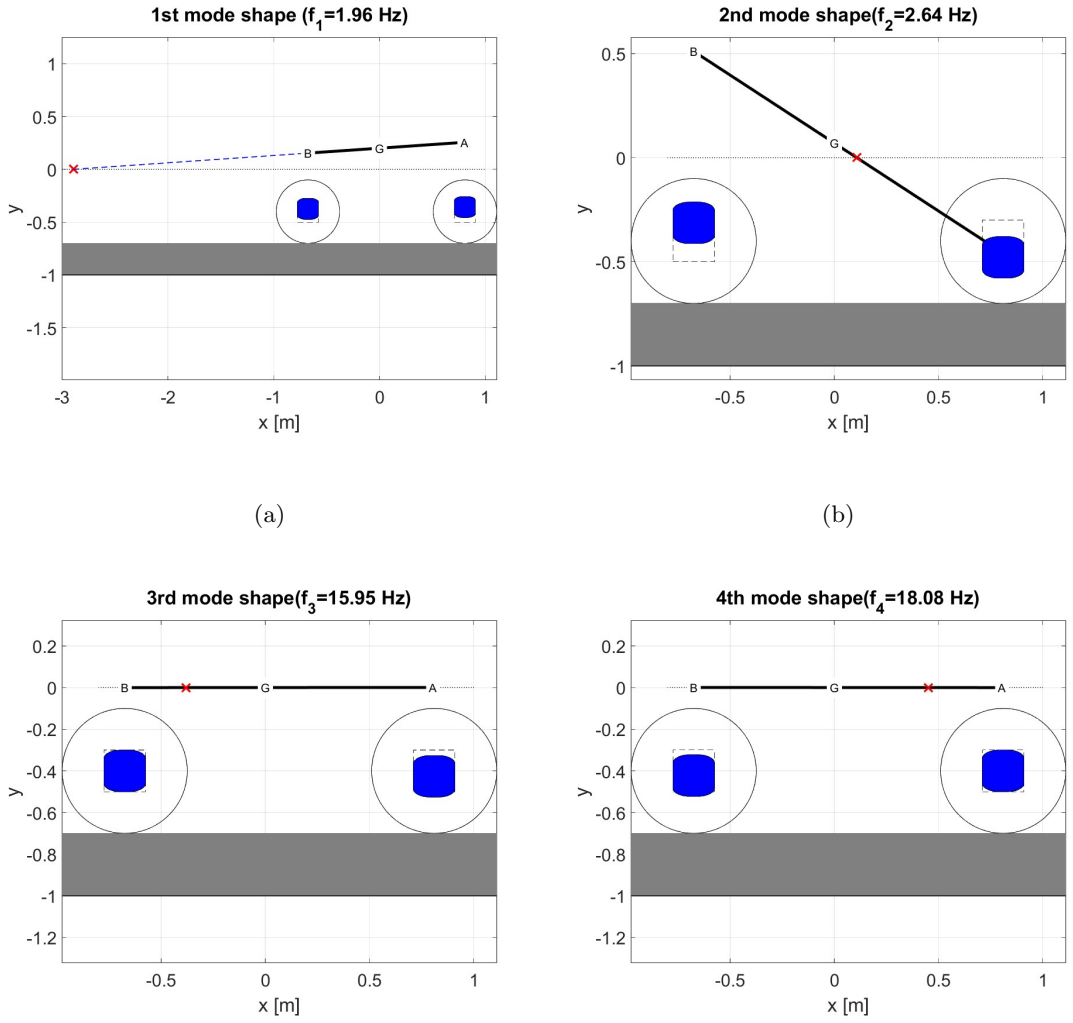

(a) (b)

(c) (d)

Figure 46: First 4 mode shapes of the 4DOF motorcycle model: a) Bounce-1.96 Hz b) Pitch-2.64 Hz c) Front wheel-15.95 Hz d) Rear wheel-18.08 Hz natural frequencies and mode shapes

In figure 46 the first 4 mode shapes and the frequencies at which they undergo

are presented. In such figures it is also provided the centre of pitch rotation of the sprung body of the motorcycle, which returns the type of motion observed.

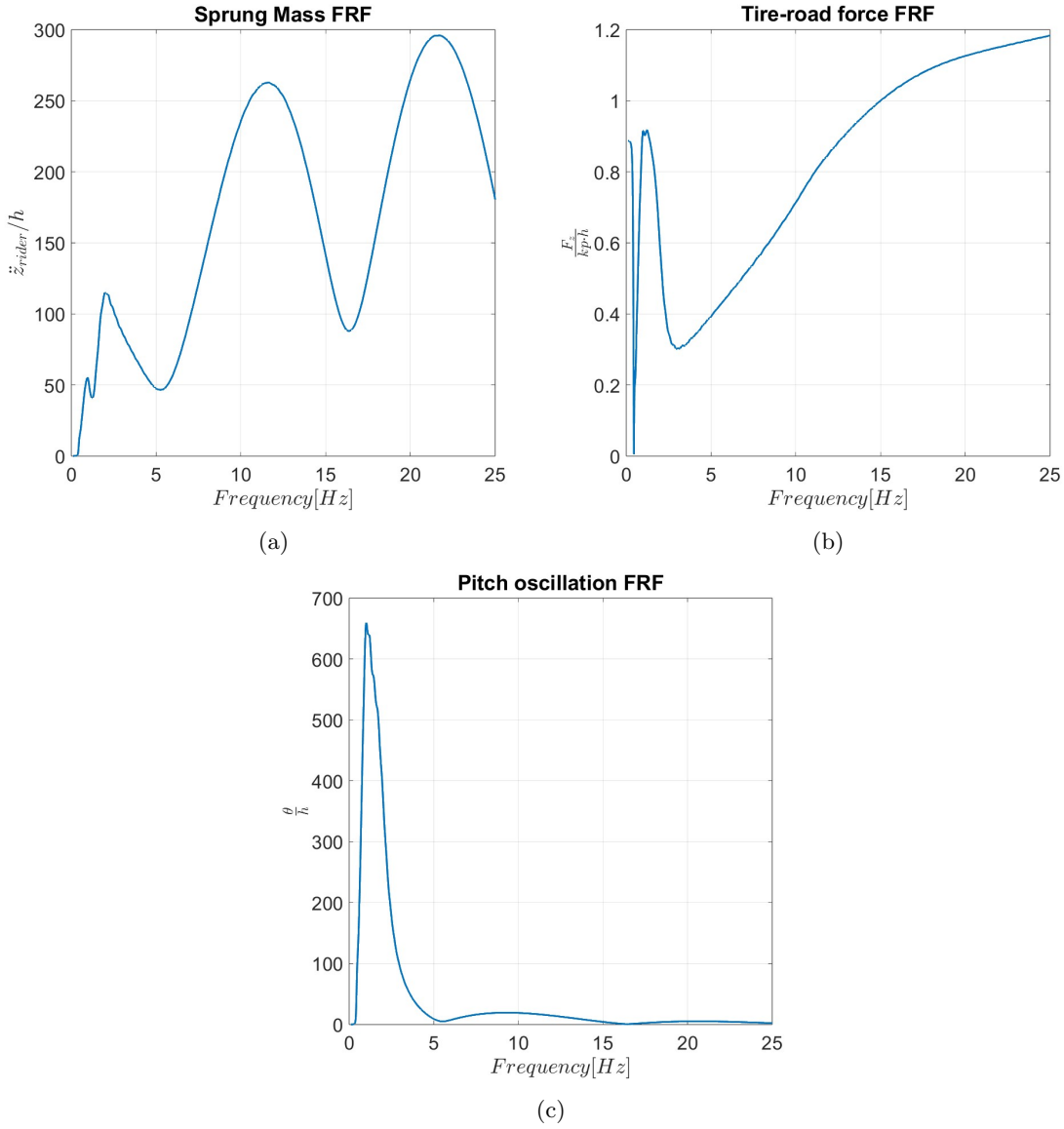

Figure 47: Frequency response function of the 4DOF model: a) From road to rider acceleration b) From road profile to tire-ground vertical reaction forces c) From road to pitch oscillation

It is possible to affirm that a pure-pitch motion considers a centre of pitch rotation in the exact position of the sprung mass centre of mass, as it is a pure rotation of the

suspended masses. Differently, a pure-bounce motion consists of a centre of rotation at an infinite distance from the centre of mass, since it is a simple translation. In reality, the motion of the motorcycle body is always a mix of bounce and pitch, but it is possible to state that the first natural frequency observed at 1.96 Hz is predominantly exciting the bouncing motion of the vehicle, since the centre of rotation is relatively far from the sprung centre of mass. Oppositely the second natural frequencies of 2.64 Hz correspond to a pseudo-pitch mode shape since the centre of rotation of the body is extremely close to the centre of mass. Therefore it is imaginable the motorcycle to undergo such types of motion when the input road frequency matches those of the mode shapes, but a second important aspect is mentionable: the natural frequency of pitch oscillations is higher than that of bounce, thus ensuring a proper comfort property of the motorbike [7]. It is also possible to compare the first and second natural frequencies with the reduced bounce and pitch pulsation estimated in table 2. To conclude the analysis of the motorcycle, the third and fourth mode shapes relative to the front and rear unsprung mass resonance frequencies are also provided in figure 46.

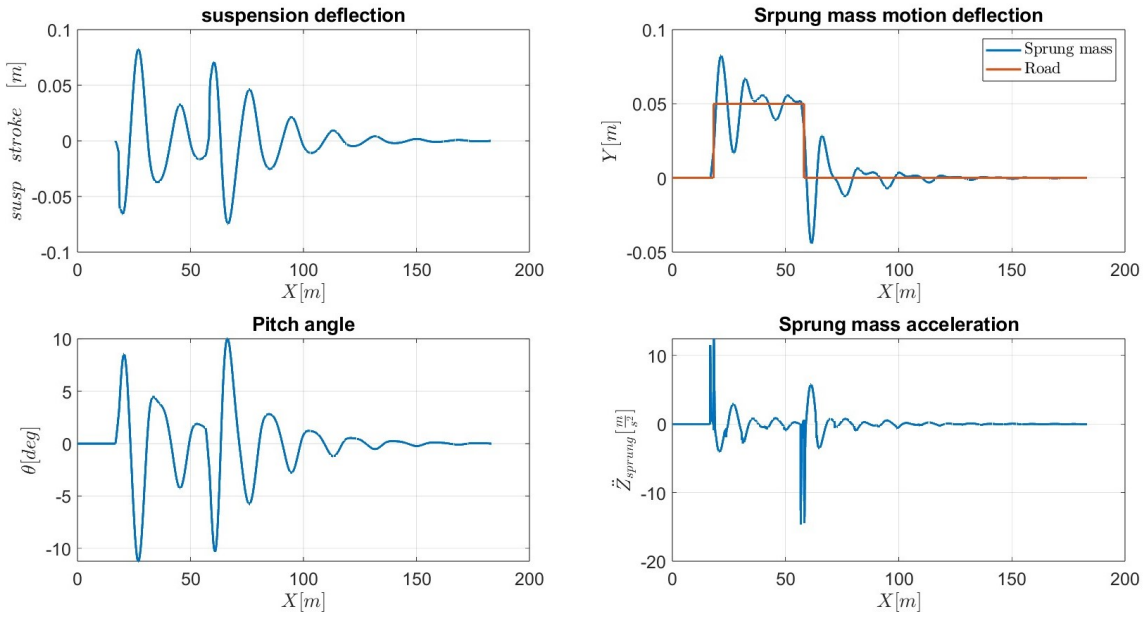

Figure 48: 4DOF model step analysis results

In figure 47 the frequency response function of the rider-perceived acceleration, the rear tire-ground vertical forces and the body pitch oscillations are reported. The simulation is conducted as proposed in 4.1, therefore through the adoption

of a numerical Matlab tool able to extract the estimated transfer function of the mentioned signals. The simulation consists of a chirp sinewave signal directly fed to the tyres as imposed vertical translations. From figure 47 a) is visible that the acceleration perceived by the rider are result of the combination of pitch and bounce motion of the motorbike sprung mass. Differently, figure 47 b) shows that the tyre ground forces variability tends to increase as the frequency of the road signal in input increases. Finally, with a more sophisticated model like the 4DOF motorcycle model adopted in the current analysis, the pitch oscillation effect on comfort can be considered. It is clearly visible from figure 47 c) the pitch oscillation peaks and in particular the pitch resonance frequency. It is also useful to provide a step analysis response to frame the vehicle ride and handling properties. In figure 48 the suspension stroke, pitch oscillations, sprung mass motion and acceleration are plotted. The graph provides an acceptable suspension deflection and a moderate pitch oscillation, indicating the passive suspensions of the vehicle are correctly tailored to the vehicle considered. Noticeable is the more sophisticated step road adopted to simulate this working condition in comparison with the quarter-car model analysis.

6.2 4DOF model simulation results

The 4DOF model differs substantially from the 2DOF quarter-car, in detail, the Hybrid control logic is applied to both the front and rear semi-active suspensions in two independent rationales. In this application, adherence to the quarter-car model control principle necessitates the replication of its framework. This is achieved by considering the signals of the equivalent front and rear sprung masses as the quantities measured -or estimated- by hypothetical sensors mounted on the steering plate and on the rear suspension shock absorber body mount; therefore the front and rear sprung mass-related quantities will be retrieved as the accelerations, speeds and motions of the upper suspension mounts of the respective sections. The quantities related to the unsprung masses are more straightforward to imagine. Those accelerations and velocities correspond to the front and rear wheel centre of mass. On the other hand in 6.1 it was mentioned that the unsprung masses of the 4DOF model represent all the bodies underneath the suspensions, therefore their centre of mass may not exactly correspond to the wheel centre, and its definition may represent a crucial aspect. Anyway, such details are real implementation issues that would be discussed successively and not considered in this framework.

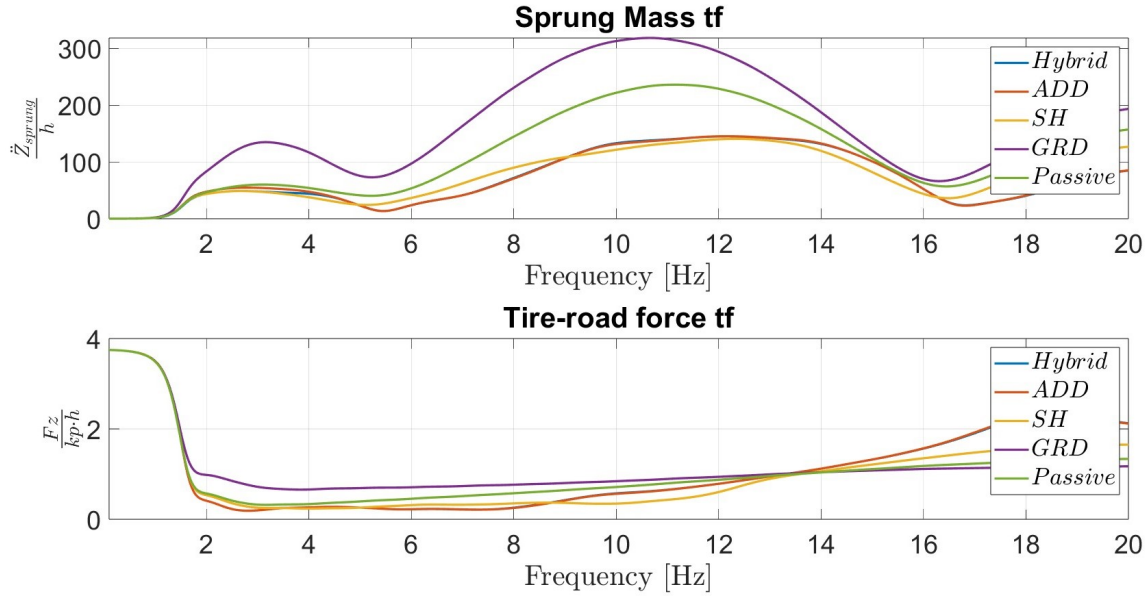

(a)

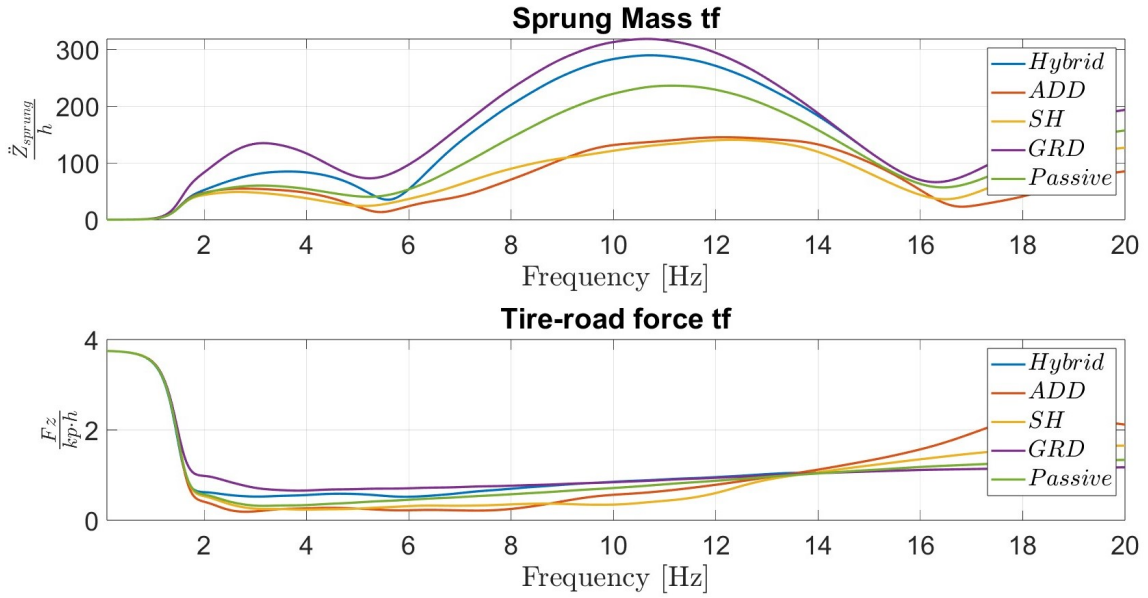

(b)

Figure 49: 4DOF Frequency response function of the hybrid control logic. Transfer functions from road to rider-perceived accelerations and tyre-road forces with: a) Hybrid$_{\eta=0}$. b) Hybrid$_{\eta=1}$

To implement a pseudo-prediction feature in the control logic, the frequency estimated from the selector function in the front suspension control logic will be directly fed to the rear suspension Hybrid controller. In this manner, it is possible to optimise the response of the rear suspension, the most significant regarding the comfort of the rider. The response of the 4DOF model to a chirp sinewave road sweeping frequency from 0 to 25Hz is investigated to unveil the controller's key features and presented in figure 49. It is visible that the outcomes of the semi-active suspensions controlled by the Hybrid rationale and the competitive logics are remarkably in proximity to each other. It is not particularly evident that the optimal comfort-oriented control logic is represented by the Skyhook before 2Hz and successively by the ADD rationale. Anyway, it is possible to observe that the Hybrid control logic will switch from the Skyhook logic to the ADD once the comfort crossover frequency is faced. It is more evident that the ADD masters the handling properties at lower frequencies since the tire-ground forces variability in figure 49 b) are minimized by it. The Groundhook as expected outperforms the ADD when the 14 Hz handling crossover frequency condition is met. Once again the Hybrid logic satisfactorily changes logic to implement the optimal force oscillation-reducing control rationale, based on the frequency perceived.

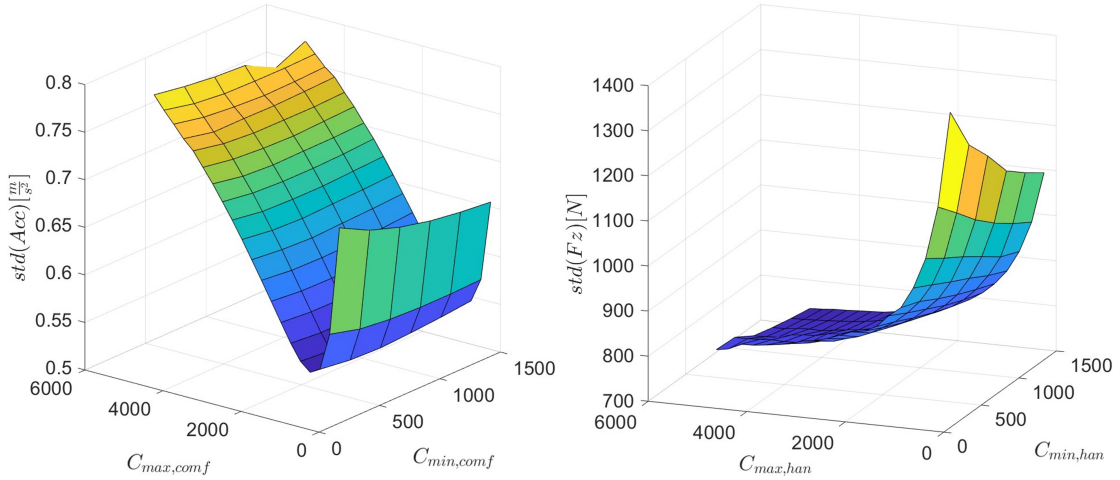

(a) (b)

Figure 50: Step simulation sensitivity analysis. a) comfort-oriented Hybrid rationale optimisation, b) handling-oriented Hybrid control optimisation

Also in this framework the controller is tuned via a *grid search* process: the operational conditions are simulated in a loop changing the controller properties and

the results are plotted in the surface graph of figure 50 and 51. This sensitivity analysis, therefore, consists of varying the maximum and minimum damping of the Hybrid control logic to investigate for the optimal combination of parameters that maximise the comfort when hybrid$_{\eta=0}$ is active, and minimises the tire-ground forces variation when the handling logic hybrid$_{\eta=1}$ is imposed. Initially, the step simulation is considered, and the step road profile is adopted in the sensitivity analysis to retrieve which are the best control parameters that optimise the behaviour of the Hybrid controller. In 50 a) the standard deviation of the sprung mass accelerations measured in the rider seat are reported for multiple damping combinations when the Hybrid comfort-oriented controller is imposed, whereas in 50 b) the hybrid$_{\eta=1}$ is adopted and the resulting variation of the tire-ground contact forces are represented for any plausible combination of damping. The optimal damper setting is reported below.

- $C_{max,comf} = 1000 \ \frac{N \cdot s}{m}$
- $C_{min,comf} = 250 \ \frac{N \cdot s}{m}$
- $C_{max,han} = 5000 \ \frac{N \cdot s}{m}$
- $C_{min,han} = 1500 \ \frac{N \cdot s}{m}$

Successively in figure 51 the sensitivity analysis is concluded taking into consideration the Belgian block.

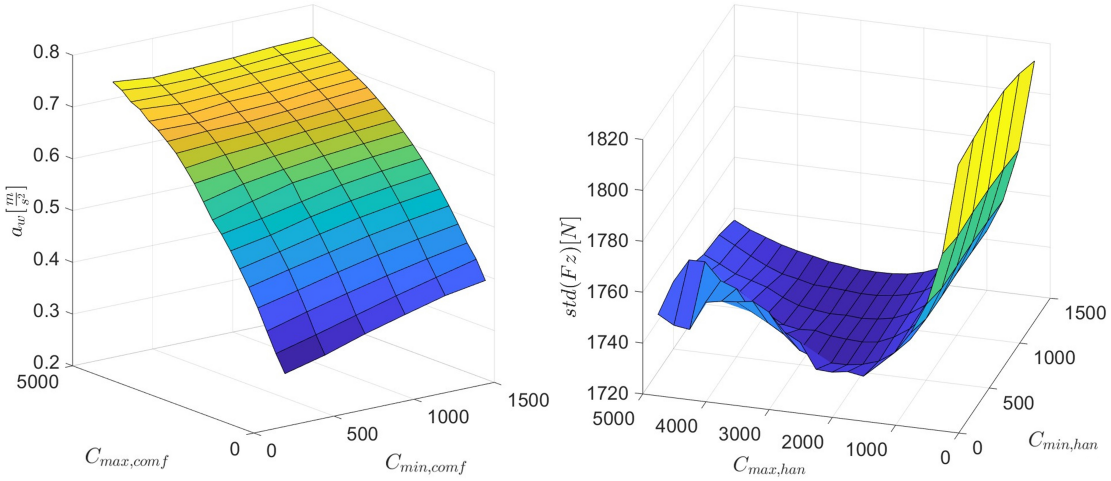

(a) (b)

Figure 51: Belgian road simulation sensitivity analysis. a) effects of damping on comfort, b) effects of damping on handling

As mentioned, the final objective is to guarantee an optimal performance over both operational grounds. In figure 51 the hybrid$_{\eta=0}$, figure a), and hybrid$_{\eta=1}$ in figure b), are shown. The goal is to represent through the sensitivity analysis which is the optimal comfort and handling-oriented parameters of the Hybrid control logic. Coherently with the focus of the Hybrid controller, the index considered in figure 51 a) is the weighted rider acceleration, and the index adopt to quantify the quality of the handling-oriented control in figure 51 b) is the tire-road contact force standard deviation. From the analysis of the sensitivity results it is possible to conclude that the optimal Hybrid controller setting is the one proposed below.

- $C_{max,comf} = 1000\ \frac{N \cdot s}{m}$
- $C_{min,comf} = 0\ \frac{N \cdot s}{m}$
- $C_{max,han} = 3000\ \frac{N \cdot s}{m}$
- $C_{min,han} = 1250\ \frac{N \cdot s}{m}$

From this assumption it is evident how the comfort setting of step and Belgian block analyses almost match, and therefore a significant compromise is not necessary. It is not possible to come to the same conclusion considering the handling properties, since the two optimal settings differ substantially. Here the necessity to come to a trade-off when defining the damping setting of the hybrid$_{\eta=1}$ controller. It was considered the Belgian block as the most demanding proving ground, and as a consequence the choice of the final set of handling-oriented damping values fell over the optimal handling parameters over the Belgian road profile. Consequently, the final characterisation of the Hybrid control law results as shown:

- $C_{max,comf} = 1000\ \frac{N \cdot s}{m}$
- $C_{min,comf} = 250\ \frac{N \cdot s}{m}$
- $C_{max,han} = 3000\ \frac{N \cdot s}{m}$
- $C_{min,han} = 1250\ \frac{N \cdot s}{m}$

6.2.1 4DOF model results: step road

In comparison with the quarter-car the road profile adopted in this simulation, as mentioned, is slightly different. As a matter of fact, the full step was considered in the analysis. The goal of the simulation is to retrieve a comparison of the performance of the Hybrid control logic designed in this thesis project with the competitive control logics. The controller parameters adopted are the damping values suggested in the

previous chapter, and are applied to all the control logics proposed. The main idea supporting this premise is the coherence of the control rationales analysed, in fact it is important to observe the same amount of damping provided by all the control laws to have comparable results. The results are compared following the methodology proposed in 4.1, and thus both the orientation of the Hybrid rationale are analysed separately and compared with Skyhook, ADD, Groundhook and the passive system equipped with the optimal damping set. In figure 52 the handling and comfort indexes, produced by the respective Hybrid setting, are compared to the performance of the competitive controllers. Therefore, for sake of clarity, in 52 a) the Hybrid control logic is focused on comfort and confronted with the competitors, while in figure 52 b) the Hybrid logic is implemented with a η value equal to 1, therefore its handling-oriented logic is now juxtaposed to the contender controllers. In the aforementioned figure the speed of the vehicle is set equal to 30 Km/h. It is evident that the Hybrid control law is providing brilliant results in terms of handling since the Hybrid$_{\eta=1}$ logic outperforms the competitors. It is particularly outstanding since the Hybrid logic can, by implementing the two sub-rationales hybrid$_{\eta=0}$ and hybrid$_{\eta=1}$, master the handling without sacrificing the comfort. From 52 a) in fact, the resulting comfort comparison shows that the Hybrid$_{\eta=1}$ control law can guarantee comfort whenever it is needed by keeping stable sprung masses accelerations.

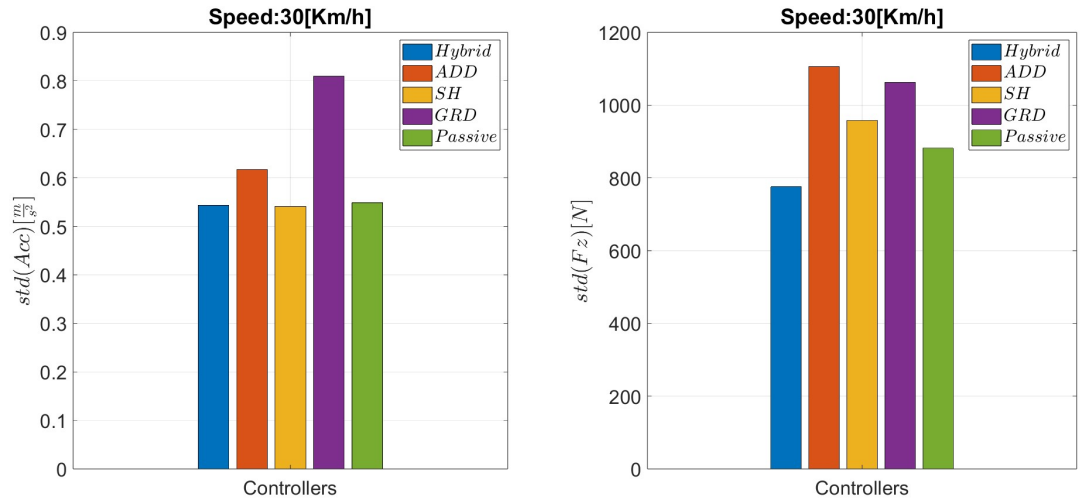

(a) (b)

Figure 52: Step road simulation at 30 Km/h: a) Comfort analysis b) Handling analysis

Such a more sophisticated model of motorcycle and step road allows to consider the performance of the vehicle in different speed conditions. It is important to take

into consideration a variety of working conditions to state that the hybrid controller proposed is a valid option against the traditional controllers of semi-active dampers. As conducted in figure 52, the comfort and handling properties of the Hybrid control logic are investigated with the rival rules at higher speeds. The results show rather analogous conclusions to the outcomes of the 30 Km/h analysis. It is always important to comment that in such Hybrid control logic, handling and comfort-oriented strategies are not implementable at the same time, the suspension control unit is able to switch to a more suitable control law rather than the opposite one whenever the riding conditions necessitate it. To conclude the step analysis the suspension stroke and the sprung mass motion over the road disturbance are provided in figure 53. The analysis represented is conducted at 30 km/h and with the hybrid control law set on the handling strategy in figure a), and on the comfort rule in figure b).

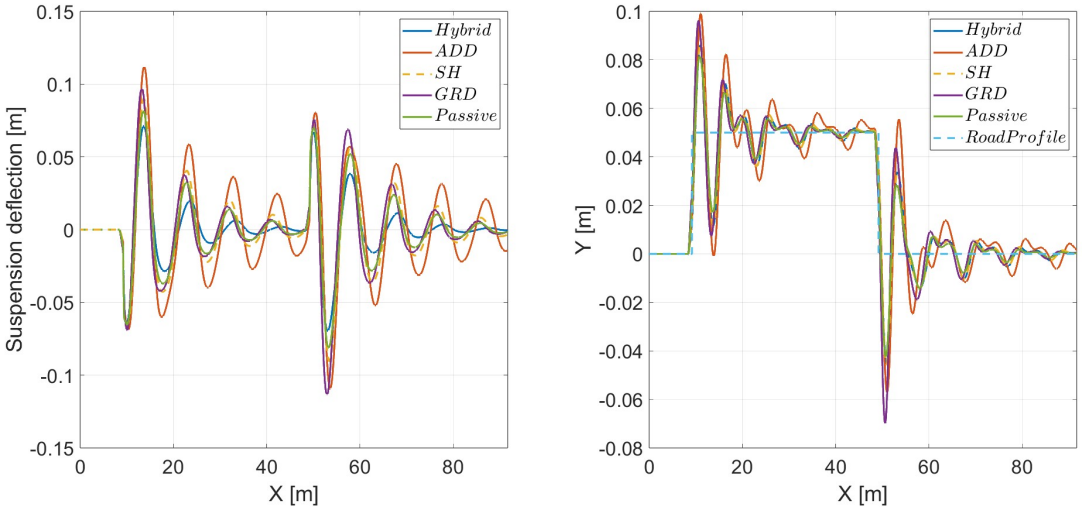

(a) (b)

Figure 53: Step road simulation at 30 Km/h: a) Suspension stroke b) sprung mass oscillations

Considering also figure 53 it is possible to draw the same conclusion reported in the previous paragraph. The Hybrid-controlled semi-active suspension system is able to master the handling, as visible from figure 53 a) where the suspension stroke oscillations are minimised by the proposed controller. The sprung mass oscillation analysis also confirms the conclusions regarding the body isolation capability stated in the previous section. In fact, the sprung mass oscillations from figure 53 b) are strongly reduced with the adoption of the aforementioned controller. It is worth mentioning that the Hybrid logic is fully replicating the Skyhook rationale in Figure b), thus showing the optimality of such a control rule regarding the overcoming of

steps. It is important to verify that not only the two extreme opposite orientation strategies of the controller are able to master their respective focuses, Hybrid$_{\eta=0}$ and Hybrid$_{\eta=1}$, but it is also mandatory to ensure that the performance indexes are capable of gradually following the Hybrid logic focus for all the intermediate η values. Therefore in figure 54 three different intermediate values of the weighting function are considered and their respective performances are reported.

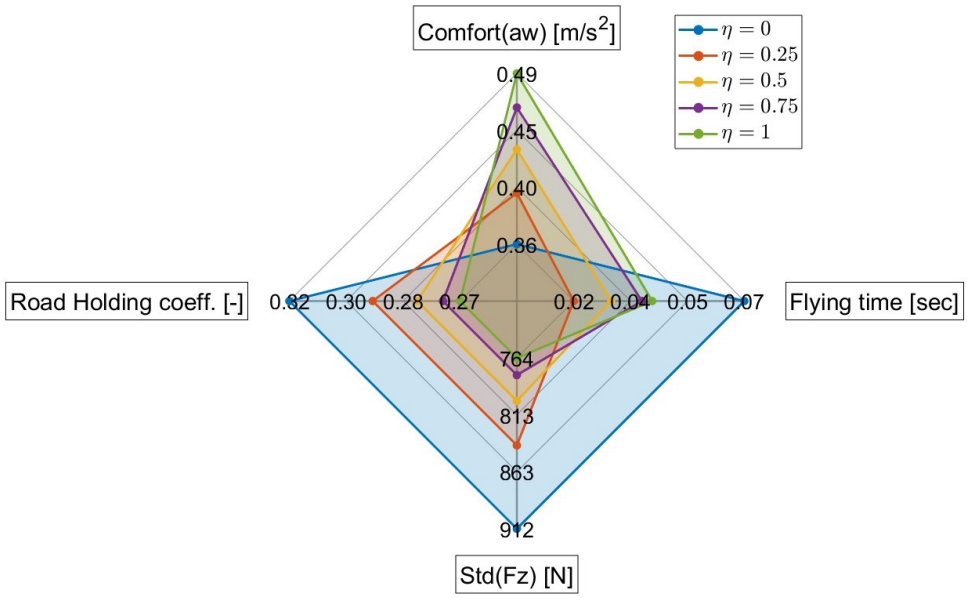

Figure 54: Performance of the Hybrid control law for different η values in the step road simulation

As expected, the controller's performance gradually moves towards better handling as the weighting function η increases. Such a result is brilliant, showing that the monotone behaviour of the controller is ensured. Therefore in real conditions the optimality of the proposed semi-active solutions is demonstrated.

6.2.2 4DOF model results: Belgian block road

In the current section of the essay the second principal working condition is investigated. The Belgian block pavement is fed to the motorcycle model and the simulation is repeated for different speeds, in order to cover a large variety of environments that the control law can face. Figure 55 and 56 represent the comparison of the perfor-

mance indexes between the Hybrid logic and its rivals in a radar plot. Coherently with the step analysis, also in this context the simulation is performed at three different speeds, 30, 60 and 90 Km/h. Anyway, the resulting graphs are similar at each speed considered, and consequently, only the 60 Km/h simulation is reported. Figure 55 is retrieved by employing the Hybrid$_{\eta=0}$ control strategy whereas figure 56 presents the performances of its complementary rationale, the hybrid$_{\eta=1}$. The radar plot is adopted in order to keep track of the different indexes adopted to measure the performance of the vehicle at the same time.

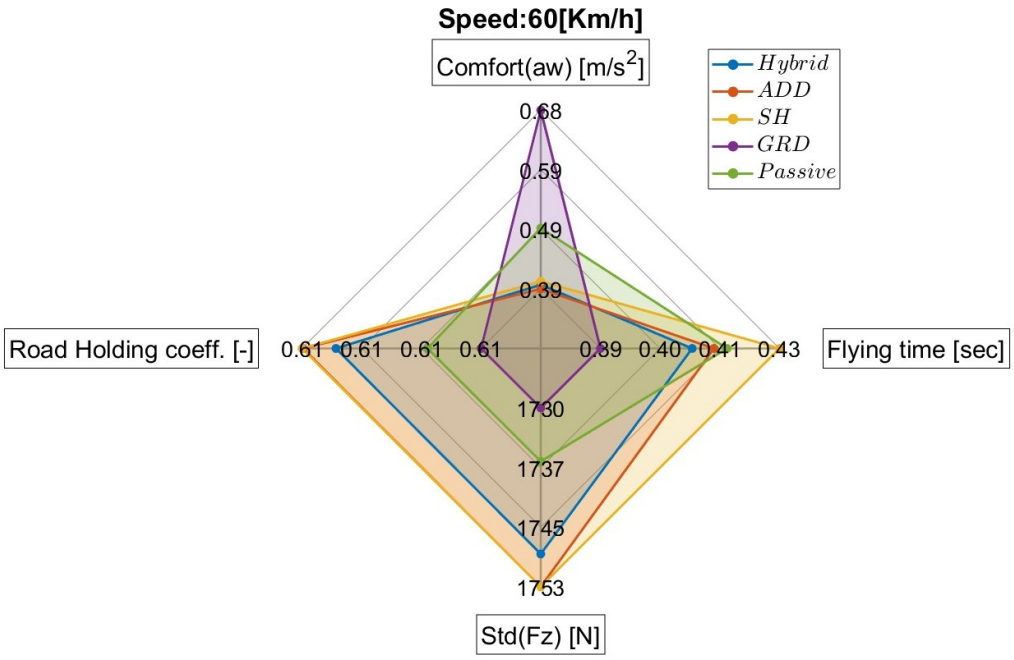

Figure 55: 4DOF model over Belgian block road: comparison between Hybrid$_{\eta=0}$ and preexisting controllers at 60 Km/h

The Belgian block road is considered a meaningful pavement since it can replicate a real-road-like broadband-frequency signal. The results shown are definitely inspiring. It is worth mentioning that the Hybrid controller is replicating the ADD logic since, as it was shown previously, it is the optimal control law to face such a road in the range of motorcycle velocities adopted. In figure 56 the graphs proposed the comparison of the handling-oriented control law with the competitors. It is straightforward how the proposed strategy is the optimal control law in terms of tire-ground

force variability. Considering the flaying time, instead, the efficiency of the controller decreases in comparison with the competition, but the differences are minimal and not particularly significant. It is possible to conclude that the Hybrid logic guarantees optimal performance in terms of handling, whenever the weighting function is set to 1, i.e. the vehicle is riding in a demanding adherence state. The suspension control unit is capable of providing optimal comfort index as well when the weighting function is equal to 0, and a cruising state is enhanced. The comparison with other controllers shows that regarding the comfort the Hybrid control strategy is at least comparable with the optimal ADD rationale, or even superior in specific cases.

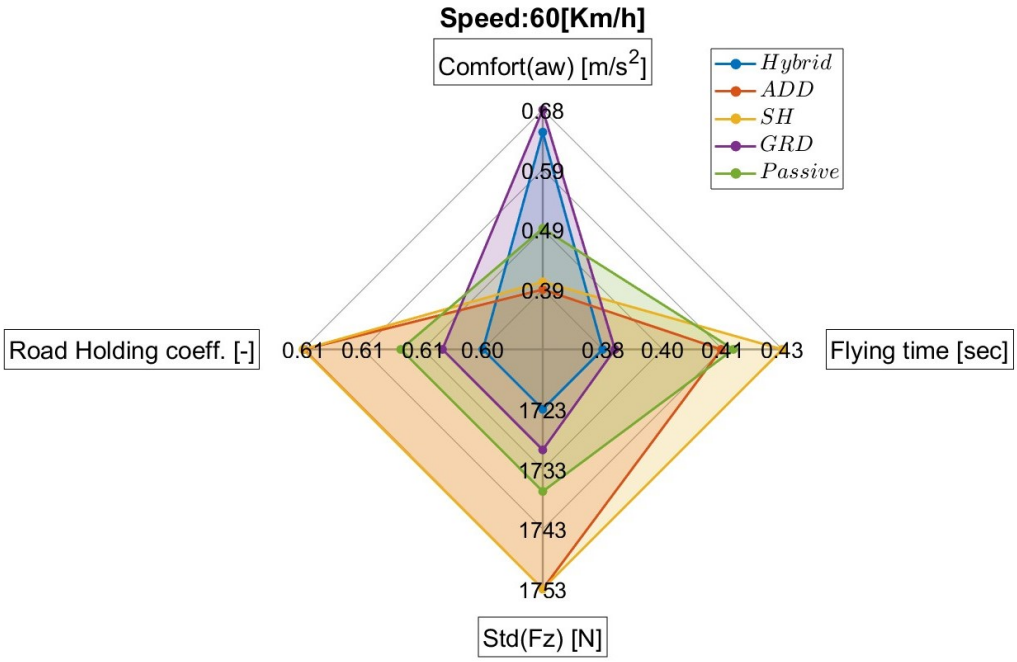

Figure 56: 4DOF model, Belgian block road: comparison between Hybrid$_{\eta=1}$ and competitors at 60 Km/h

To ensure the correctness of the proposed hybrid control logic, the consistency of the hybrid performance for different η values is investigated. As performed in figure 54, also over the Belgian pavement is important to guarantee the correct controller transition from optimising comfort indexes to master handling as the weighting function η moves from 0 to 1. The test provided brilliant results, and the obtained performance graph perfectly replicates the step road outcomes. Finally, a brief insight

into the tyre-ground force trend over the Belgian road is proposed for sake of completeness. The graph in figure 57 shows a comparison between the Hybrid controller and the passive system in terms of tyre-ground force.

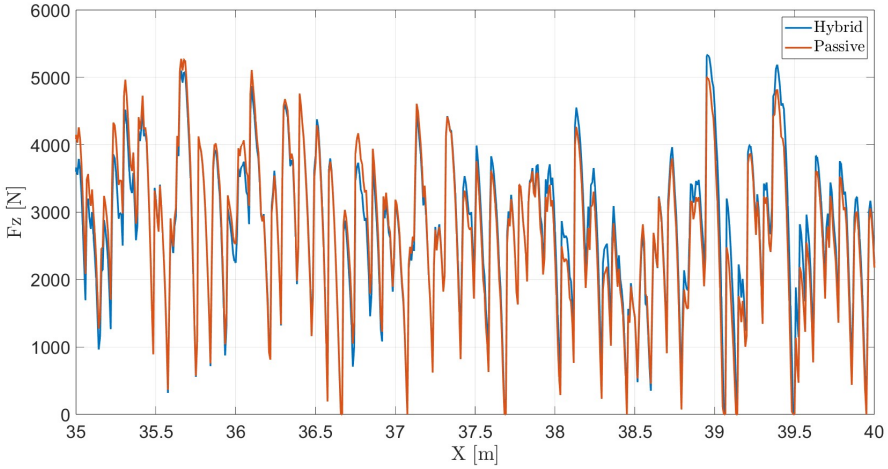

Figure 57: Tyre-ground vertical forces over the Belgian block.

7 IPG - MotorcycleMaker model

The current section endeavours to conduct a comprehensive analysis of the findings delineated in the preceding chapters. It is important to examine whether the findings presented in the previous graphs are supported when using a more sophisticated vehicle model. The motivations underlying the decision to consider a more complicated motorcycle simulator stem from its distinguished level of simulation accuracy, facilitating the evaluation of the controller's performance under conditions mirroring practical scenarios. As a matter of fact, the ultimate objective is to conclusively demonstrate its efficacy in real-world exercises. The simulation is no more conducted in a Matlab-Simulink environment, it is instead necessary to adopt a specific tool able to take into consideration the whole motorcycle and implement the out-of-plane motorbike dynamics. The *MotorcycleMaker* software distributed by the IPG company facilitated a significant advancement and elevated the quality of results to a higher level.

7.1 The virtual vehicle environment

A virtual vehicle refers to a computer-generated replica of a real vehicle, designed to mimic its behaviour accurately. In MotorcycleMaker, this virtual representation is constructed using mathematical models incorporating equations of motion, kinematics, and other relevant formulas defining the vehicle's dynamics. The model is then customized with data directly corresponding to the specific vehicle under analysis. This methodology enables the testing of various vehicles using validated parameter sets, with the flexibility to switch between different virtual vehicles simply by adjusting the parameter data within the model. The virtual vehicle encompasses all components of a real vehicle, including the powertrain, tyres, chassis, brakes, and more. The integration of automotive controllers (in this case the Suspension Control Unit-SCU) or software-modelled controllers into the virtual vehicle is facilitated through hardware or software in the loop. Complementary elements are modelled to simulate the vehicle in an real-environment-like scenario. Therefore, a virtual road refers to a digital or computer-generated representation of a real road, track, or course. To complete the simulation a virtual rider is included, which is actually able to perform all the control actions a real rider would execute. To have a deeper understanding of the simulations, it is worth briefly presenting the motorcycle model's structure. The vehicle model is no longer simplified to consider a limited amount of degrees of freedom to facilitate the simulations. Still, an approach to analysing the motorcycle comprehensively is taken into account. For this purpose, the 2-wheeler is based on a multi-body system, composed of the main structure that completes the motorcycle such as a main frame, front and rear suspension subsystems, and a

rider. The main frame is a single rigid body that represents all the elements that the chassis enclosures, for instance the engine, any additional element of the powertrain, the tank and the motorcycle frame itself are considered as single entities rigidly coupled to the *main frame* and thus composing a single rigid body. The suspensions are rigidly coupled with the main frame and connected to the wheels through a compliance element. The mentioned components represent the suspension spring and damper interaction with the suspended and unsprung masses. The rider is represented as a single point-mass directable by the virtual rider algorithm to control the motorcycle in a representative manner. In figure 58 the multi-body layout composing the motorcycle is proposed.

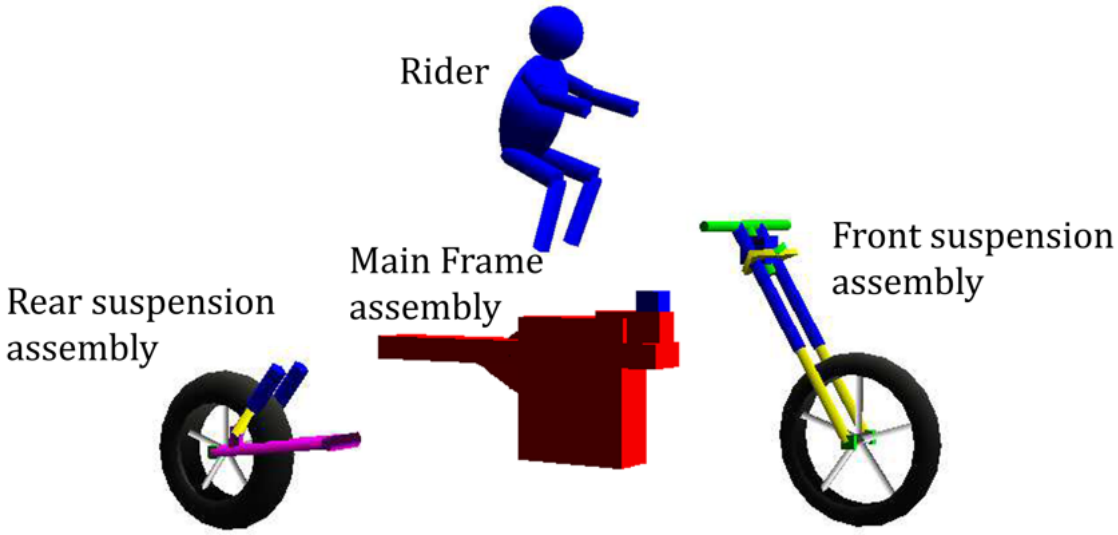

Figure 58: IPG motorcycle model scheme

7.2 Motorcycle model characteristics

As mentioned in 4.1 the vehicle taken into account for the design and development of the suspension control unit is a standard motorcycle belonging to the so-called *naked* motorbike class, a middle-class motorcycle inclined towards sport utilisation and middle-long range riding tours. A second class that can potentially represent the target vehicle is the middle-class gran-tourer motorcycles segment. Moreover, the vehicle characterisation is a critical point of the analysis, and therefore the features of the bike model are defined as conducted in the previous chapters. Such a sophisticated model allows the implementation of a rear swingarm and an inclined front telescopic fork, the most common arrangement observed in the motorcycle seg-

ment taken into consideration, as previously discussed in 2.2 and implemented in 59 b). Anyway, an intermediate vehicle model is worth considering in this context: in figure 59 a) is reported a multi-body motorcycle model with the same linear simplified damper-spring system chosen in chapter 6.1. In this manner, it is possible to apply the standards adopted in the 4DOF and 2DOF models to the current IPG bike layout. More in detail, the specifications reported in table 1 and 2 are replicated on the simplified IPG vehicle model of Figure a), to ensure coherent development of the bike simulations.

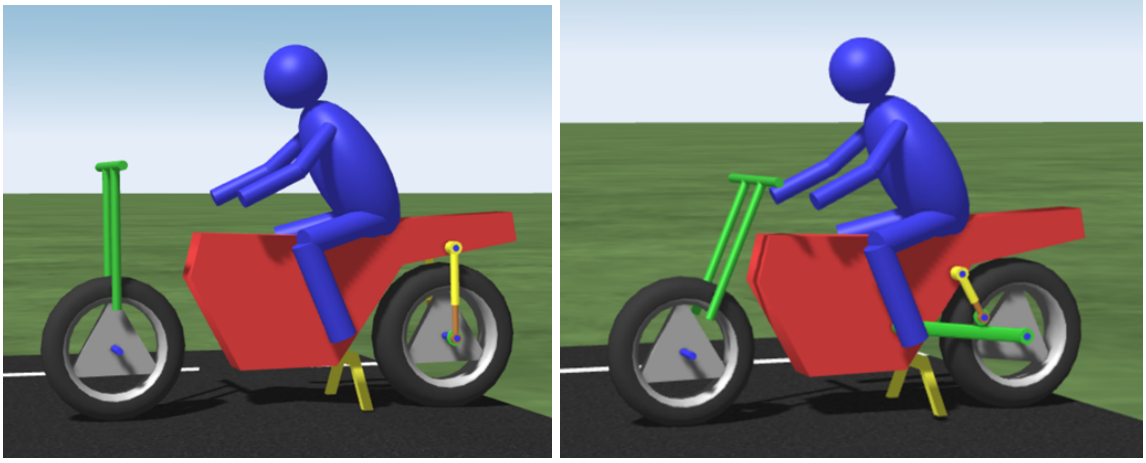

(a) (b)

Figure 59: IPG bike models: a) simplified b) real

Finally, once the very same vehicle model considered up to now is implemented in the IPG environment, a further step consists of applying an equivalent stiffness and damping coefficient to the inclined front telescopic suspension and the rear swingarm of the final real-vehicle model of figure 59 b). To perform this task, it is necessary to analyse the front and rear suspension layouts and develop a mathematical formalisation of them.

7.2.1 Definition of the equivalent suspension characteristics

In the present paragraph the mathematical formalisation of the equivalent stiffness is investigated. The goal of the analysis is to describe the equivalent simplified vertical stiffness of the suspension (figure 60-a) from the rear swingarm scheme(figure 60-b). Moreover, it is possible to define the *equivalent stiffness* of the swingarm's layout as the property of a spring such that when incorporated into a simplified

vertical suspension, it generates an equivalent vertical force for the same magnitude of wheel displacement in both considered schemes. Based on this consideration, it becomes feasible to ascertain the ultimate objective: identify the properties of the final swingarm of figure 60 b) to create an equivalent version of the rear simplified suspension of figure 60 a) adopted in the previous chapter, ensuring identical dynamic characteristics. As imaginable, to accomplish this final task it is enough to adopt the inverse formula of the equivalent stiffness just defined.

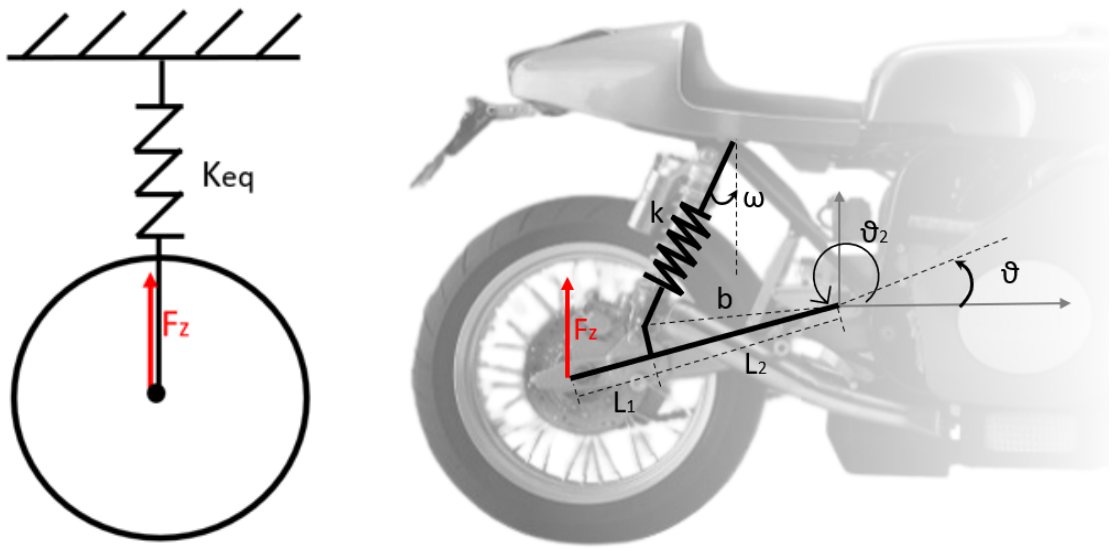

(a) (b)

Figure 60: Simplified rear vertical suspension a) and Swingarm version b)

The swingarm is now taken into account and the free-body diagram is considered. From the analysis of the operating conditions of the swingarm, it can be observed that the forces distribute as shown in figure 61. From a simple torque balance it is possible to retrieve the interaction that holds between the wheel displacement and the resulting force from the spring deformation.

$$F_z cos(\theta)(L_1 + L_2) = F_{s,y} \cdot x_b + F_{s,x} \cdot y_b \tag{27}$$

From the analysis of the kinematic properties of the swingarm it is easy to retrieve the position of the swingarm-spring mount as a function of θ_2 as:

$$\begin{aligned} x_b &= b \cdot cos(\theta_2) \\ y_b &= b \cdot sin(\theta_2) \end{aligned} \tag{28}$$

where b and θ_2 are the polar coordinates of the swingarm-spring mount point with respect to the reference system positioned in the swingarm pivot.

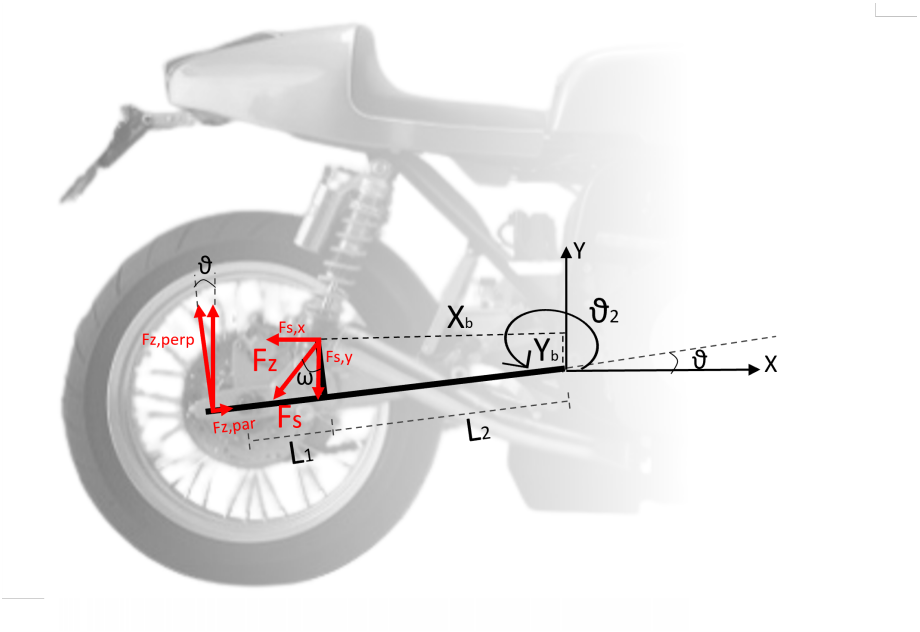

Figure 61: Rear swingarm free-body diagram

The 28 then becomes:

$$F_z cos(\theta)(L_1 + L_2) = F_{s,y} \cdot b \cdot cos(\theta_2) + F_{s,x} \cdot b \cdot sin(\theta_2) \tag{29}$$

It is also immediate to notice that the components of the spring force can be rewritten as follows:

$$\begin{aligned} F_{s,y} &= F_s \cdot cos(\omega) \\ F_{s,x} &= F_s \cdot sin(\omega) \end{aligned} \tag{30}$$

where the term ω is the spring force inclination with respect to the reference frame adopted. It is necessary to maintain only one single unknown in the equation, such as the swingarm inclination angle θ. Therefore it is investigated the spring geometry in order to link the term ω with θ. From figure 62 it is visible the relationship between the spring point B and the swingarm oscillation angle.

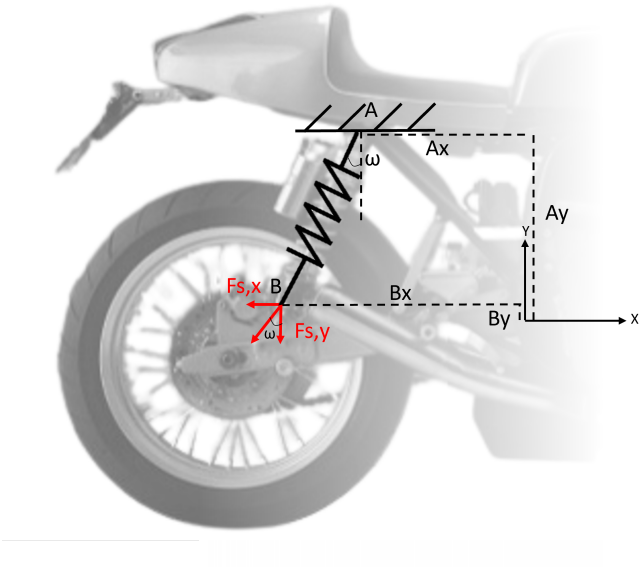

Figure 62: Spring geometry analysis

Therefore it follows that the force inclination angle ω is equal to:

$$\omega = \tan^{-1} \frac{A_x - B_x}{A_y - B_y} = \tan^{-1} \frac{A_x - b \cdot cos(\theta_2)}{A_y - b \cdot sin(\theta_2)} \tag{31}$$

It is important to underline that the terms A_x and A_y are the swingarm-body mount coordinates and in the analysis considered it is a good hypothesis to assume it as a constant term since it is a geometric property of the swingarm assembly. In addition, it is evident that also the term θ_2 is a variable parameter and not an unknown, since it is a linear combination of the swingarm oscillation θ. In fact, the following equation holds due to the geometric properties of the swingarm.

$$\theta_2 = \theta + \theta_{2,0} \tag{32}$$

where $\theta_{2,0}$ is a constant term and it is equal to the initial angle between point B and the reference X axis proposed in figure 62. As mentioned, such a parameter results as a function of the geometric construction of the rear suspension, and therefore the only unknown is still the term θ. For sake of clarity, the mathematical description of the constant term $\theta_{2,0}$ is provided as follows

$$\theta_{2,0} = \tan^{-1} \frac{B_{y,0}}{B_{x,0}} - \theta_0 \tag{33}$$

where $B_{y,0}$ and $B_{x,0}$ are the initial position coordinates of point B, the swingarm-spring attachment point, and θ_0 is the initial swingarm inclination angle with the X

axis. Finally, if the equation 30 is substituted into 29, it further develops in:

$$F_z cos(\theta)(L_1 + L_2) = F_s cos(\omega) \cdot bcos(\theta_2) + F_s sin(\omega) \cdot bsin(\theta_2) \tag{34}$$

It is possible to explicit the spring force term F_s from 34.

$$F_s = \frac{F_z cos(\theta)(L_1 + L_2)}{cos(\omega) \cdot bcos(\theta_2) + sin(\omega) \cdot bsin(\theta_2)} \tag{35}$$

At this point, it is possible to derive the spring deformation as reported in the following equation

$$\Delta z = \frac{F_s}{K} cos(\omega) \tag{36}$$

and by substituting the 35 in 36 the on-swingarm-mounted spring displacement will result as shown in 37:

$$\Delta z = \frac{F_z cos(\theta)(L_1 + L_2)}{(cos(\omega) \cdot bcos(\theta_2) + sin(\omega) \cdot bsin(\theta_2)) \cdot k} cos(\omega) \tag{37}$$

From the definition of the equivalent stiffness reported at the beginning of the chapter, it is straightforward to conclude that the equivalent vertical stiffness K_{eq} given a swingarm spring characteristic K is:

$$K_{eq} = \frac{cos(\omega) \cdot bcos(\theta_2) + sin(\omega) \cdot bsin(\theta_2)}{cos(\theta)(L_1 + L_2) \cdot cos(\omega)} \cdot K \tag{38}$$

The same procedure can be applied to the equivalent damping coefficient since the damper and the coil spring are coaxial in the rear swingarm scheme. Therefore the equation 37 can also be applied to define the vertical simplified shock absorber characteristics. As mentioned earlier in the paragraph, the final goal is to define the swingarm's spring stiffness starting from the vertical spring characteristics of the simplified suspensions adopted in the 4DOF model, which were demonstrated to fit the features of a *standard* motorbike. Therefore, to obtain the swingarm's spring characterisation it is enough to reverse the equation 38 to retrieve the term K from the known K_{eq}. In this manner, it was possible to obtain a *real vehicle* equivalent to the 4DOF motorbike model adopted in previous chapters and thus continue the simulations in IPG with a coherent vehicle. In 2.2, it was shown that the front standard suspension layout for the segment of motorcycles considered in this framework is an inclined telescopic fork. Moreover it is necessary to analyse the front-end motorcycle structure to investigate the relationship between the equivalent simplified vertical spring characteristics of figure 63 a) and the inclined telescopic fork adopted in the IPG vehicle model 63 b).

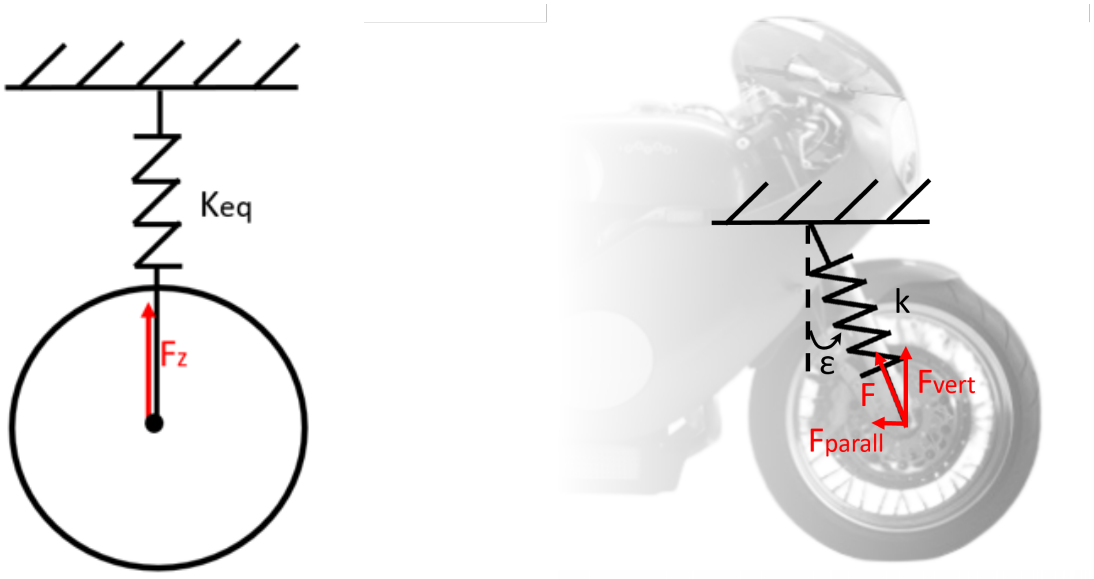

(a) (b)

Figure 63: Simplified front vertical suspension a) and telescopic version b)

From a simple consideration of the force schemes presented in figure 63, the following equation is straightforward

$$K_{eq} = \frac{K}{cos^2(\epsilon)} \tag{39}$$

where ϵ is the steering plate inclination angle. Also in this case, the construction of the suspension assembly implies that the spring and the damper are mounted coaxially, as shown in 2.2. Consequently to identify the vertical damper characterisation is possible to exploit the same relation shown in 39. It is worth noticing that the final objective is to define the inclined spring stiffness and damper coefficients, therefore once the front simplified suspension adopted in the previous models is available, it is possible to obtain the real front suspension description by reversing the 39. The resulting layout perfectly replicates the real motorcycle structure proposed in 2.2 and reflects the dynamic properties of table 2, thus ensuring a coherent vehicle with the previous analysis. Finally, the resulting characteristics of the non-simplified vehicle equipped with standard vehicle structures are reported in the following table 5. The vehicle model is equipped with an MF-Swift tyre model in its standard configuration, thus implementing the Pacejka tyre magic formula. It is worth mentioning that the IPG software allows mounting sensors' scheme on the vehicle, and therefore it is possible to implement the suspension control unit in a specific ECU.

Front wheel mass	12	Kg
Rear wheel mass	14	Kg
Body mass	162	Kg
Roll moment of inertia	29	$Kg \cdot m^2$
Pitch moment of inertia	82	$Kg \cdot m^2$
Yaw moment of inertia	76	$Kg \cdot m^2$
Rider weight	80	Kg
Engine weight	15	Kg
Wheelbase	1.4850	m
Estimated front-semi-wheelbase	0.8150	m
Estimated rear-semi-wheelbase	0.6750	m
Front suspension stiffness	16.5e3	$\frac{N}{m}$
Rear suspension stiffness	48.2e3	$\frac{N}{m}$
Front tyre radial stiffness	170e3	$\frac{N}{m}$
Rear tyre radial stiffness	170e3	$\frac{N}{m}$
Front passive suspension damping	976	$\frac{N \cdot s}{m}$
Rear passive suspension damping	2855	$\frac{N \cdot s}{m}$
Front tyre radial damping	50	$\frac{N \cdot s}{m}$
Rear tyre radial damping	60	$\frac{N \cdot s}{m}$
Front suspension assembly weight	5	Kg
Rear suspension assembly weight	10	Kg
Steering head angle	23.5	deg

Table 5: IPG model characteristics

To conclude the introduction to the IPG simulations, a first analysis to compare the simplified vehicle equipped with the specifications reported in table 1, and thus replicating the 4DOF model, and the real-vehicle system adopted in this chapter is presented. Both vehicles are simulated in step analysis, therefore the two motorcycles are run over the step road profile presented in 4.1 but in an IPG environment, and the front and rear sprung mass positions with respect to the space travelled are reported in figure 64.

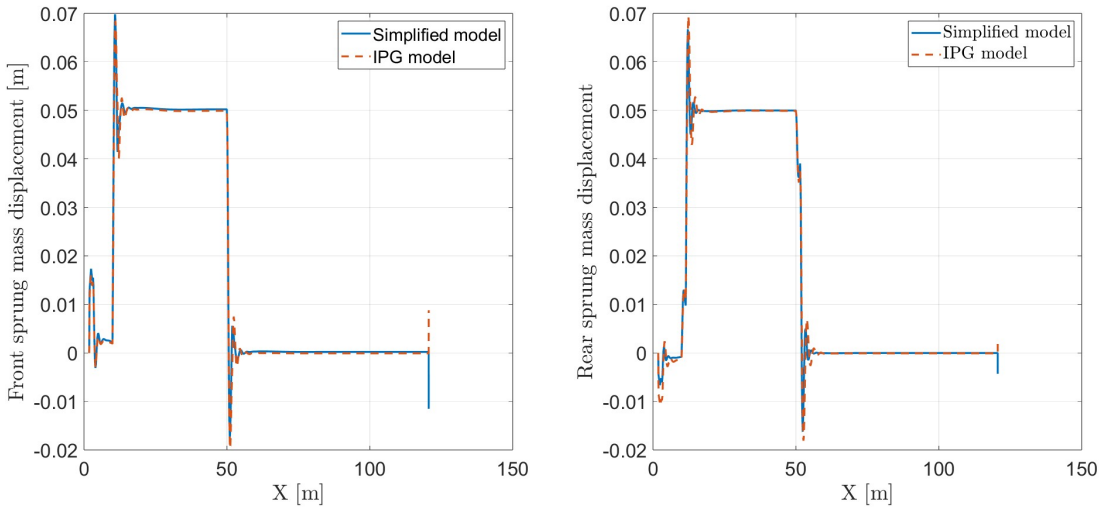

Figure 64: Simplified-real vehicle position comparison: a)Front sprung mass b)Rear sprung mass

It is visible from figure 64 that the responses of the two models are perfectly overlapped, meaning that the suspension definition process described in the current chapter is optimal. As expected, when the vehicle is equipped with the real suspension layout and the simplified scheme, the same sprung mass oscillation is perceived for the same road profile displacement. Finally, an important mention regards the front and rear stiffness values observed in table 5. In fact, the proposed spring stiffness is retrieved by applying the inverse formula represented in equations 38 and 39 imposing a simplified vertical suspension stiffness equal to 19600 and 31300 N/m respectively to the front and rear layouts. Such values are not defined arbitrarily but are chosen to obtain a reduced natural frequency of the front and rear suspensions equal to 2.0 and 2.3 Hz, the resonance frequencies imposed in the 4DOF model. The standard passive damping is defined by applying equation 15 to the present motorcycle model, and then a proportional damping is assessed to the front and rear suspension assemblies as shown in 16. To summarise the characterisation process of the IPG model it is possible to assert that the vehicle is defined on the bases of the previous simplified models to ensure a correct continuity, and thus the same ride properties. However, an equivalent more realistic suspension layout is fitted to the motorcycle model to correctly represent a real standard vehicle in the multi-body simulations performed in this framework.

7.3 MotorcycleMaker simulations results

The motorcycle model described in 7.2 is now loaded into the IPG-MotorcycleMaker simulator, and the road profiles shown in 4.1 are adopted. More in detail, the simulations employ the step of figure 65 a), which features a height of 0.05 meters and a plateau length of 25 meters. In this section is still implemented the Belgian block pavement, more specifically, the road presented in figure 65 b) replicates meticulously a real road profile previously measured and provided by the IPG software house.

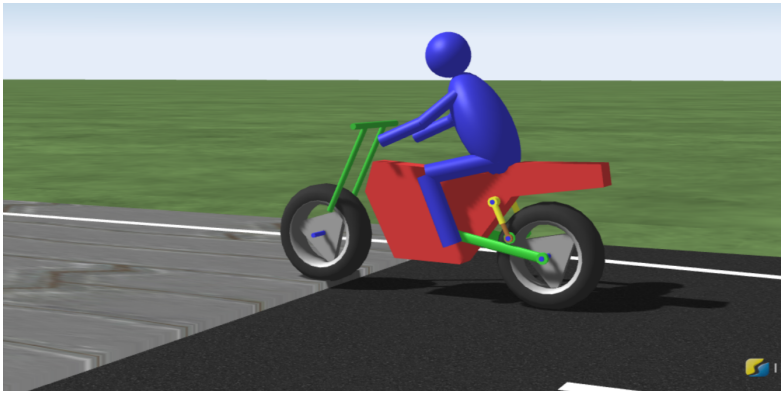

(a)

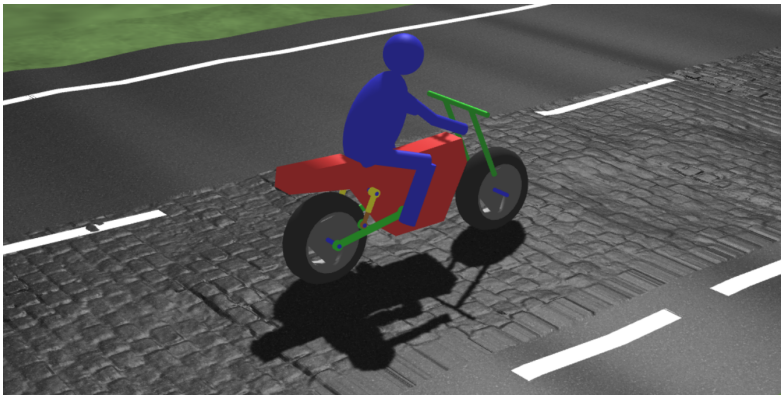

(b)

Figure 65: Step road and Belgian block road profile adopted in the IPG simulations

Regarding the indexes to assess the performance of the vehicle, the current simulations rely on the mathematical formulas present in chapter 4.1. The frequency estimator is maintained in these simulations to ensure the same framework, but such an aspect will be discussed in future chapters.

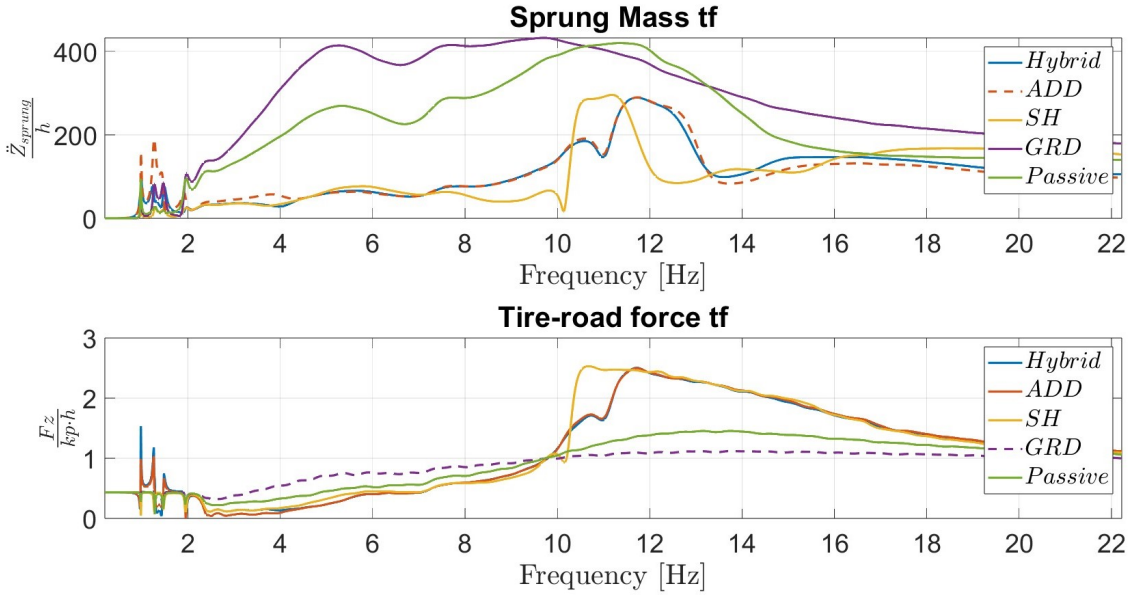

(a)

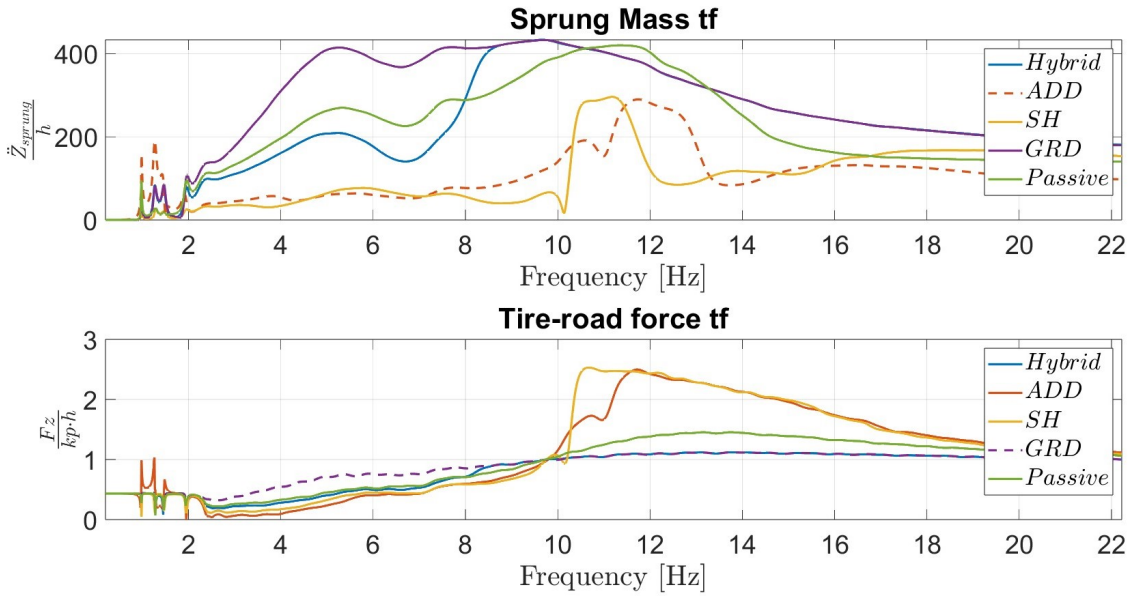

(b)

Figure 66: Comparison between the FRF obtained via different controllers. a) Hybrid-comfort b) Hybrid-handling

The Hybrid control logic relies on the front suspension road sensor, which defines the input frequency and directly feeds the rear SCU with the expected incoming frequency bandwidth, thus providing a rudimental wheelbase-based preview system. The identification of the dynamic properties of a vehicle, in particular regarding the ride characterisation or the NVH features of the bike, is retrievable from the suspension transfer function. As conducted in the previous analysis, the frequency response function from the road to the sprung mass acceleration is adopted to assess the level of comfort of the occupants. Differently, a metric to measure handling is the analysis of the magnitude and variability of the tire-ground forces for different frequencies. In figure 66 a comparison between the aforementioned transfer functions is proposed. It is important to note that the gear-changing process induces the spikes at lower frequencies, and such an aspect is only an example of how the results may differ from the previous analysis due to the introduction of non-idealities. As a matter of fact, such graphs were obtained by letting the vehicle run over a sinusoidal road for a linearly slow-increasing vehicle speed. Such a process is a replication of a real-road experiment to retrieve the suspension transfer functions. It is imaginable how different hypotheses that were present in the previous analyses are not more valid in this context, such as the consideration of the pure in-plane dynamics, the perfectly linear speed increasing, the effect of longitudinal dynamics, the more sophisticated tyres model, the non-uniform weight distribution, the action of the rider and other minor aspects.

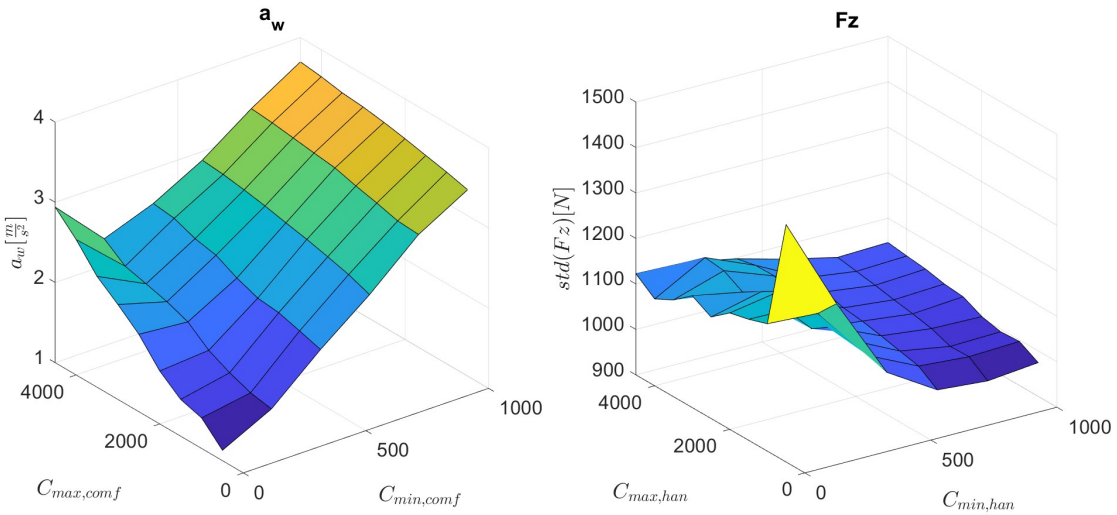

(a) (b)

Figure 67: Optimisation process on Belgian road, for different focus: a) comfort b) handling

Those considerations have driven different results in comparison with the 4DOF model simulation, but the main aspects are still valid: the peak succession is present and more importantly, the main sprung mass oscillation peak around 12 Hz is visible. On the other hand, the different tyre models adopted provided substantially different results, particularly when adopting the ADD or the SH strategy. To conclude the FRF analysis, it is worth mentioning that such results were obtained once the control Hybrid law was finely tuned over the Belgian and step road profile. This process is investigated in figure 67, where the Belgian block pavement is run multiple times with different combinations of damping values between which the controller can switch. The orientations of the Hybrid law are tuned separately, indeed, from figure 67 a) is visible the resulting comfort index when the comfort-oriented strategy is imposed, and the 67 b) provides the handling level by adopting the handling-oriented law of the Hybrid rationale. The step road is also taken into consideration in the optimisation process, but the results are definitely similar and therefore are omitted in this work. Nevertheless, the set of the comfort and handling-focused controller is a matter of compromise to master the passage over the city centre pavement or the step, and finally the following damping values were considered as optimal and therefore considered in the simulation:

- $C_{max,comf} = 1000 \ \frac{N \cdot s}{m}$
- $C_{min,comf} = 0 \ \frac{N \cdot s}{m}$
- $C_{max,han} = 1750 \ \frac{N \cdot s}{m}$
- $C_{min,han} = 800 \ \frac{N \cdot s}{m}$

7.3.1 MotorcycleMaker-Step analysis

The first simulation is centred on the step road behaviour of the motorbike. The Motorcycle is run at different speeds over the step road shown in figure 65 a), notice the fact that in the figure only a small segment of the step is represented, and at the end of the plateau a descending step is present in order to investigate also the counterpart of the sudden spring compression scene depicted in the figure. Such a comprehensive analysis permits the retrieval of information regarding the expected behaviour a real motorcycle would show when adopting the Hybrid controller in a real environment. In fact, it is not a rare condition to face sudden disturbances on the road, such as potholes or grooves. In figure 68 the bar plot represents a comparison between the Hybrid control law and the competitive rationales considered in the work.

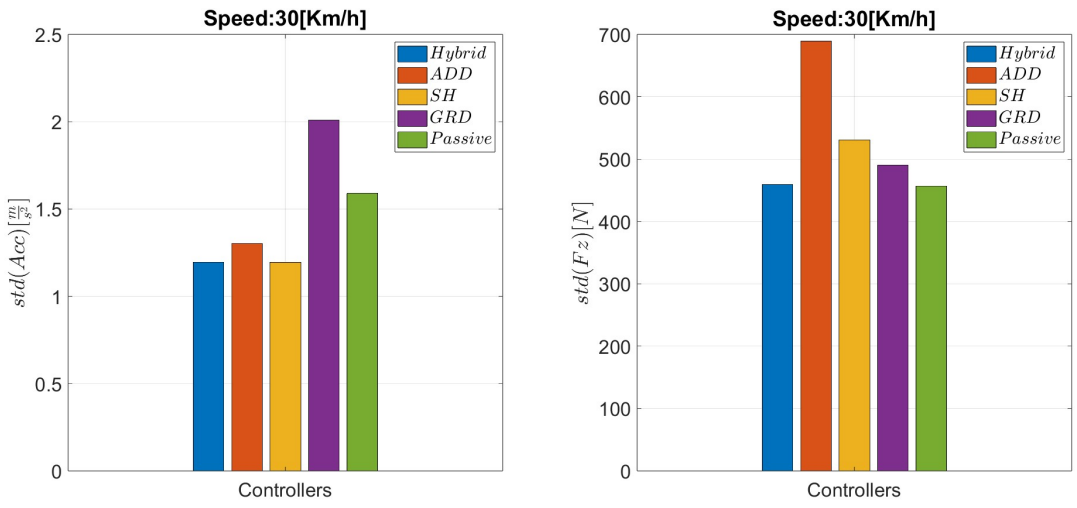

(a) (b)

Figure 68: Step road at 30Km/h: a) comfort b) Handling

The results proposed are retrieved from a run performed at 30 Km/h, both adopting the comfort orientation of the Hybrid logic, named for simplicity Hybrid$_{\eta=0}$, and the handling side of the controller, the Hybrid$_{\eta=1}$. The final results show that the proposed logic is the most competitive rationale in the semi-active controlled suspension controller segment. Indeed, both the comfort metric and the handling index are minimized -or at least not magnified- by the proposed Hybrid logic. The simulation is repeated at different velocities, but the outcomes confirm the findings outlined in this paragraph. More in detail, the speed range covers the most common riding conditions, from the urban 30 km/h condition, to the high fast-flowing road velocity of 60 km/h and up to highway speed of 90 Km/h. The control law is finally tested in order to demonstrate its coherence with the assumption, such as sweeping the weighting function η from 0 up to 1 gradually, thus adapting the control law to the riding conditions, the outcomes of the step simulations gradually moves from comfort towards the handling optimisation. The graph in figure 69 testify such an attribute. It is worth underlining that the handling performance is quickly improved as the weighting function moves towards 1, but on the other hand the performance saturates as quickly when η equals 0.5. It is important to take into account such an aspect when the controller's performance is verified in the final tests replicating real operating conditions on a proving ground. The results shown in figure 70 present a comparison of the different control law performances in terms of suspension stroke and sprung mass position during the simulation.

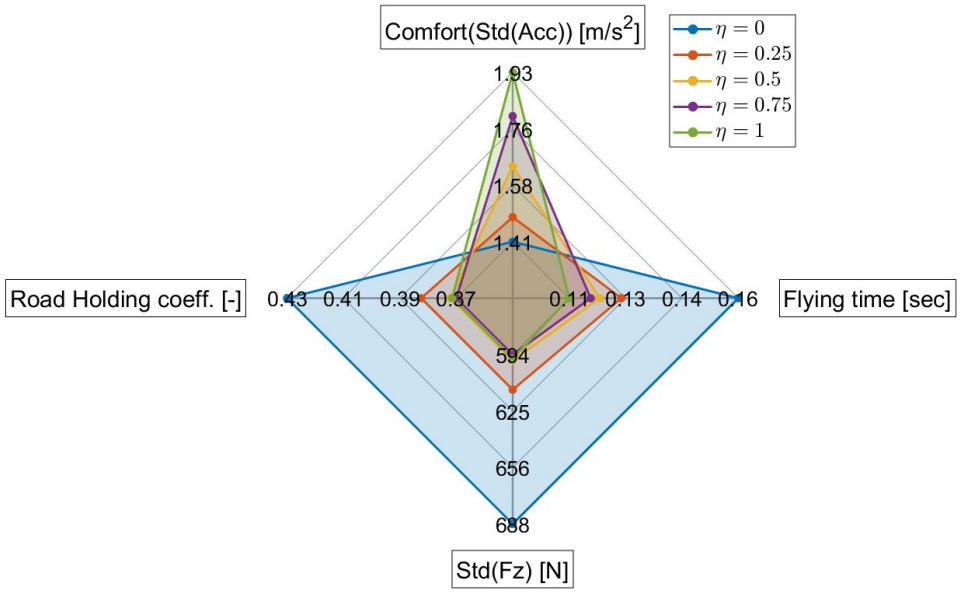

Figure 69: Performance of Hybrid control law for different η orientations

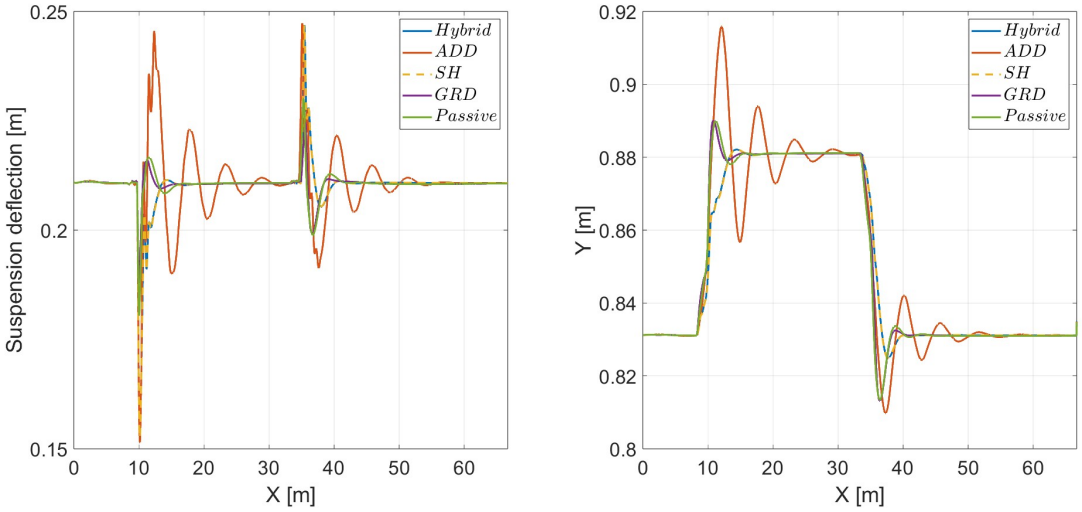

(a) (b)

Figure 70: Comparison of the suspension stroke a) and sprung mass position b) over a step

Figure 70 allows to consider in depth the behaviour of the controller when applied to the real vehicle simulator. The trend of the oscillations perceived perfectly replicates the Skyhook control logic since the Hybrid law is set on the comfort orientation ($\eta = 0$), and the step road implies a low-bandwidth frequency input, thus determining a perfect replica of the Skyhook. Such a controller, in fact, provides the most damped response, once again demonstrating its outstanding performance.

7.3.2 MotorcycleMaker-Belgian block analysis

The analysis of the results continues with the Belgian block road, a real road profile measured by the IPG software house that distributes the MotorcycleMaker simulator. Therefore the simplest method to quantify the performance of the vehicle equipped with the controller and to compare its results with the competitor logics consists of adopting such a road profile, which is normally spread in a vast number of city centres. Hence, as mentioned in previous chapters, such a simulation can represent a valid metric to assess the behaviour of the controlled suspension in real working conditions. The road is run at different speeds, 30, 60 and 90 km/h to replicate the different exercises the controller would face. To stick to the analyses performed previously, the Hybrid controller is investigated both considering the handling and the comfort-enhanced focus.

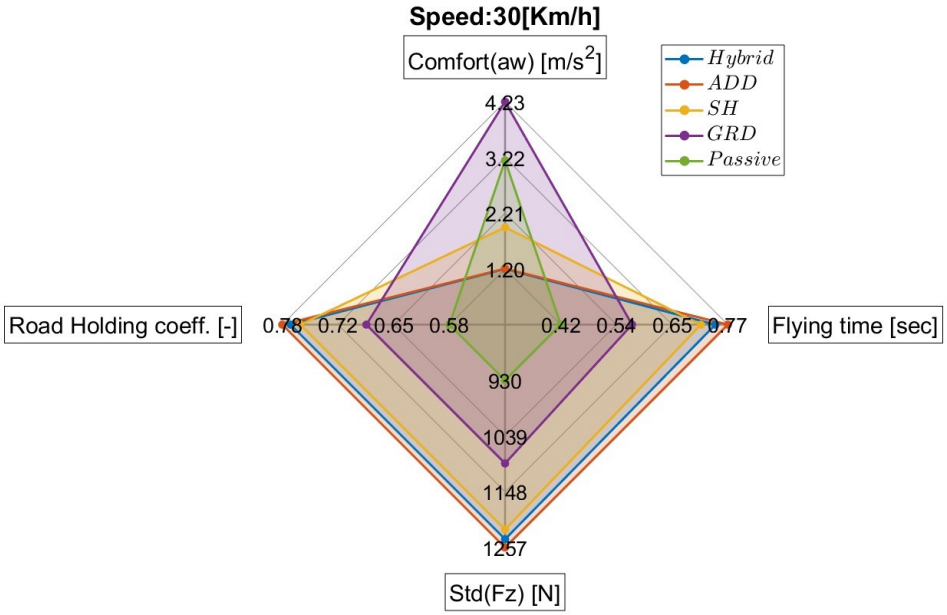

Figure 71: Belgian road performance comparison, at 30 Km/h. Hybrid logic set on comfort.

In figure 71 the comfort-oriented rationale of the hybrid control law is imposed and the city centre pavement is run at 30Km/h. The results are brilliant since the Hybrid logic is one of the most outstanding comfort controllers able to master the minimisation of the rider-received accelerations. As expected the Hybrid$_{\eta=0}$ perfectly overlaps the ADD behaviour, since the frequencies perceived are within the range of frequencies where such a logic provides superior performances. The tests conducted at different speeds, 60 and 90 Km/h, are tested on the same road profile but since they do not append any other information regarding the controllers and simply confirm the drawn conclusions, they are not included in this paragraph. The analysis continues focusing on the handling-oriented rationale, taking into consideration two opposite speeds, 30 and 90 Km/h. When the Belgian block is run at urban speeds the frequency selector function implements in the SCU the ADD logic with the optimal set of handling-oriented damping values, thus producing the results shown in figure 72 a). For sake of clarity, the Hybrid controller's performance does not cover the ADD area since the last rationale is implemented in the *comfort* version, adopting the optimal comfort damper set. It is visible the superior handling performance of the Hybrid rationale, which minimises both the flying time and the variations of the tire-ground forces. Anyway, at limited speeds it is possible to observe that handling optimisation is a far harder task compared with comfort, since the passive system provides a competitive functioning. Differently, at higher speeds, the frequency selector suggests switching for the Groundhook logic, indeed the Hybrid adopts the second handling-oriented strategy suitable for higher frequencies inputs. In figure 72 b) coherently the Groundhook and the hybrid$_{\eta=1}$ provide similar outcomes, since they are adopting the same damping set. The efficiency of the passive system in reducing the tire-ground force variation decreases at higher speeds and the Hybrid$_{\eta=1}$ control low outperforms the target suspension layout. At medium speeds, such as 60 Km/h the outcomes are intermediate results of the findings proposed in 72 a) and 72 b). Such an aspect suggests that the performance of the Hybrid handling-oriented law magnifies its superior performance compared with the passive suspension layout as the speed increases. Therefore it is plausible to expect that at very low speeds the semi-active hybrid vehicle may not outperform the traditional motorcycle scheme, but once faced the crossover speed (imminently, at reduced speeds) the proposed control law masters the handling metrics. Additionally, the test regarding the correct functionality of the Hybrid logic when the weighting function is gradually moving from 0 to 1 is outlined on the city centre road as well. Anyway, the results are very similar to the outcomes of figure 69, and therefore it is avoided to show the findings in this framework.

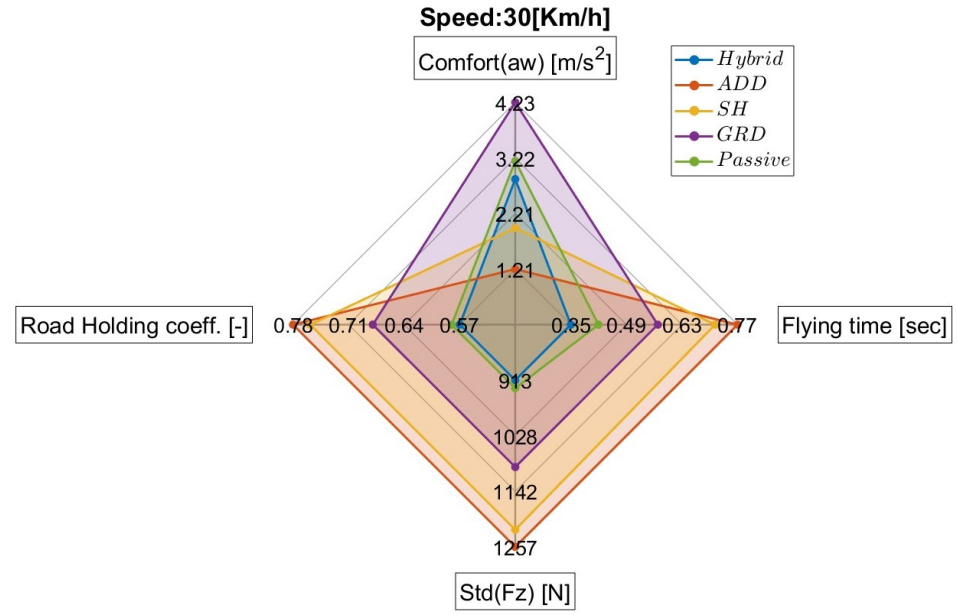

(a)

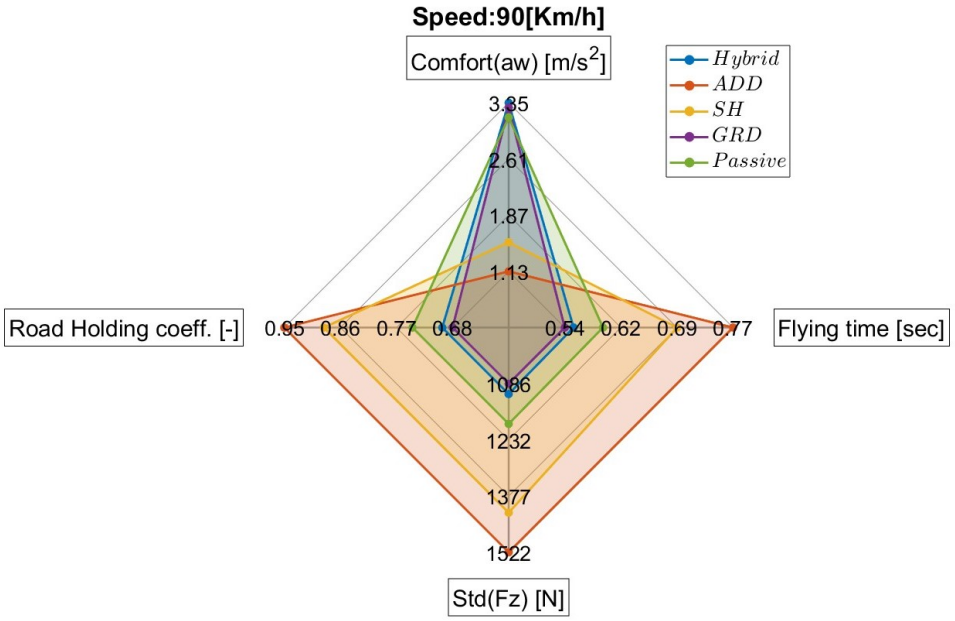

(b)

Figure 72: Controllers comparison over the Belgian block. Hybrid logic enhancing handling. a) 30 Km/h, b) 90 Km/h

7.3.3 MotorcycleMaker-Test on a proving ground

In this section the Hybrid controller is tested and compared to the competitive control strategies on a real proving ground simulation. Therefore the section's introduction is based on the description of a standard proving ground and the statement of the goals. The objective of the simulation is to validate the hypotheses proposed at the outset of the project, specifically regarding the ability of the controller to accurately perceive and interpret the state of the motorcycle, and subsequently adjust the control logic to align the performance with the objectives of each situation. Consequently, the anticipated outcomes should demonstrate that during straight cruising, the controller enhances comfort properties and optimises the corresponding indexes, whereas during cornering manoeuvres, the controller adopts a handling-oriented strategy from the hybrid law, thereby optimising handling metrics. The test track adopted for the simulations is purposely developed to stress both the cruising and the sporty riding. Therefore, the proving ground represented in figure 73 is adopted in the analysis. As visible, the track is composed of three different segments:

- Low-speed zone: a straight traversed at 30 Km/h equipped with a Belgian block pavement. This section is representative of an urban road, and the focus of the analysis is to highlight the low-speed comfort properties of the controller
- High-speed zone: a straight crossed at 65 Km/h, where the Belgian block road is faced a second time to evaluate the comfort performance at highway speeds.
- Medium-speed zone: a U-turn covered at 50 Km/h featured with the Belgian block in the middle of the corner. The goal is to excite the handling properties and evaluate the efficiency of the control law in ensuring handling, safety and avoiding crashes.

The speed signs proposed in figure 73 are not intended as a speed limit, instead they are the speed imposed to the motorcycle virtual rider. Moreover, the vehicle starts the manoeuvre at 30 Km/h and travels across the first low-speed road disturbance, across the first and second segments the rider accelerates rapidly up to 65 Km/h and performs the high-speed test. In such a region it is likely to observe an increase in the weighting function η, due to the quick rise in speed and rapid gear changing. In the last part, the most handling-stressing manoeuvre, the speed is limited to 50 Km/h and the rider quickly turns the motorcycle into the bend and the lateral accelerations will quickly rise up the η value to 1, thus enforcing the ADD-Groundhook handling-oriented strategy of the control law.

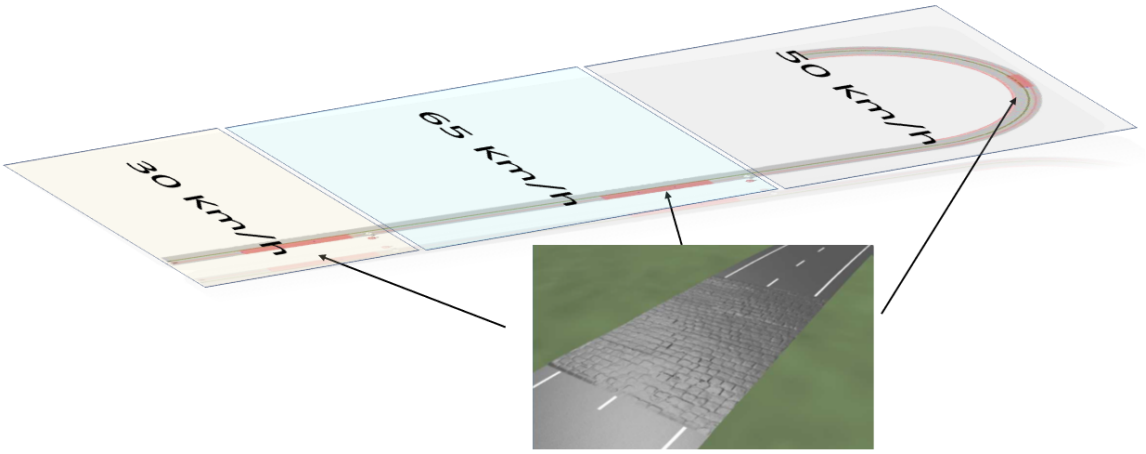

Figure 73: Proving ground representation.

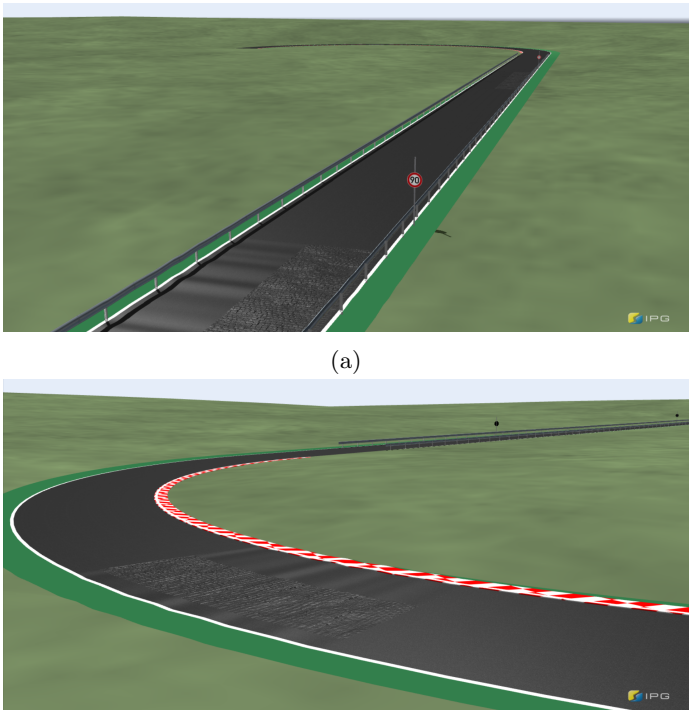

(a)

(b)

Figure 74: Proving ground virtual environment

The results proposed in figure 75 show the trend of the longitudinal and lateral

accelerations during the manoeuvre. The road profile inevitably induces acceleration spikes, particularly in the longitudinal sensor, thus unintentionally moving the η function up to higher values. A plausible solution is to filter the received longitudinal accelerations, however, such a method implies a substantial delay in the response of the weighting function and finally, the filtering process showed undesired results. Therefore, the frequency selector function is applied to the incoming signals to estimate the frequency of the accelerations sensed. A threshold was set, and any frequency value exceeding a specific target is disregarded. Such a solution is designed on the hypothesis that the meaningful signals to be considered in the weighting function η are accelerations resulting from the rider's actions, and therefore are limited to the low-frequency bandwidth signals. Figure 75 shows the raw longitudinal and lateral acceleration perceived during the test. The accelerations undergo preconditioning to appropriately input into the weighting function η, facilitating its intended functionality. This is especially crucial for lateral accelerations, which, in comparison to longitudinal ones, are sensibly reduced. However, as mentioned figure 75 shows the raw lateral and longitudinal accelerations for sake of clarity.

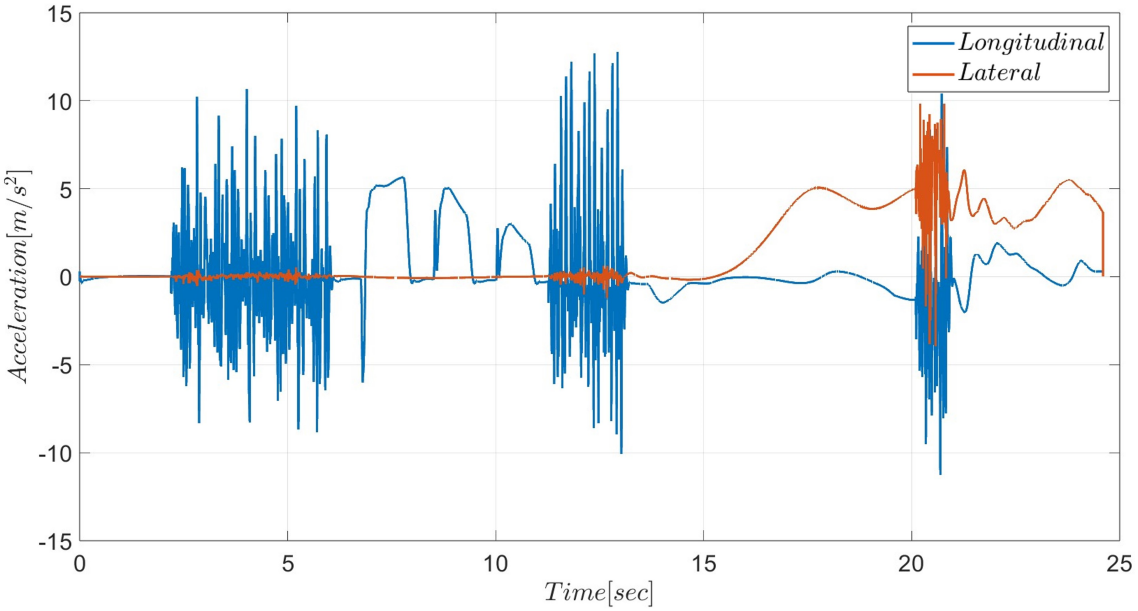

Figure 75: Accelerations perceived during the dynamic test

As expected in the first part of the test the comfort orientation is enhanced by the weighting function, which is limited to lower values. In fact, it is clearly visible from 76 that the trend of the η value is initially close to 0, thus focusing the objective of the control law completely on comfort. Anyway, as mentioned previously the road

disturbance generates a small deflection on the weighting function up to 0.05. The accelerations that follow the first segment induce a rapid increase in the orientation function that reaches values around 0.25, thus forcing the controller to take into consideration also the handling in such a phase. Once the transient phase is terminated the comfort properties are once again highlighted by a small η value. As expected, the high-speed sprung-mass isolation test over the Belgian pavement is conducted with the Hybrid$_{\eta=0}$ control law. Finally, the turn, as mentioned, induces a quick increment of η and the handling becomes the principal objective of the suspension control strategy.

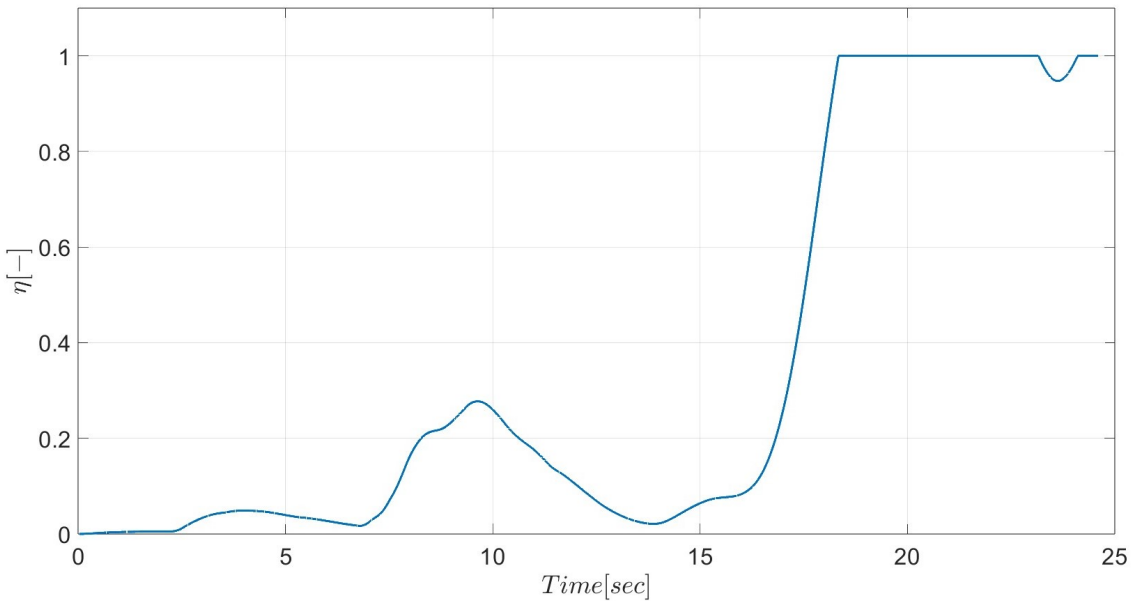

Figure 76: weighting function trend during the dynamic test

In figure 77 is reported an overview of the simulation results. Specifically 77 a) and 77 b) show the performance metrics relative to the straight (the first and second segments) and the curve (the third segment) respectively. the results are brilliant since they perfectly reflect the expected results: as long as the motorcycle is going in a cruising state, i.e. in a steady condition and low-varying velocity, the hybrid logic implements correctly the hybrid$_{\eta=0}$ thus minimizing the sprung mass oscillations and the rider-received accelerations. Differently, when the turn is faced the suspension control unit implements the Hybrid$_{\eta=1}$ logic and the tire-ground forces are effectively reduced. It is worth noticing that the results are coherent with graphs 71 and 72.

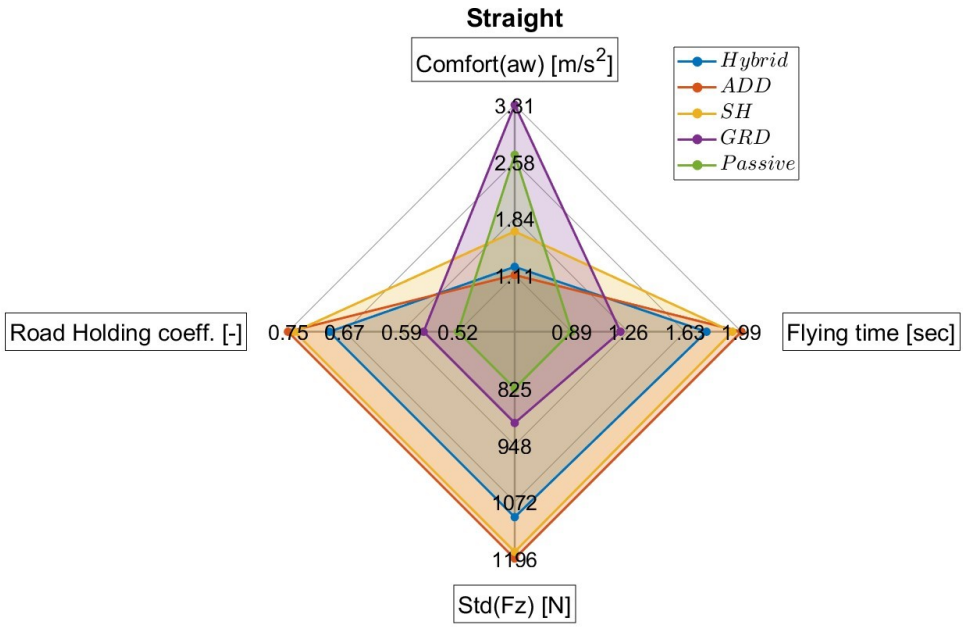

(a)

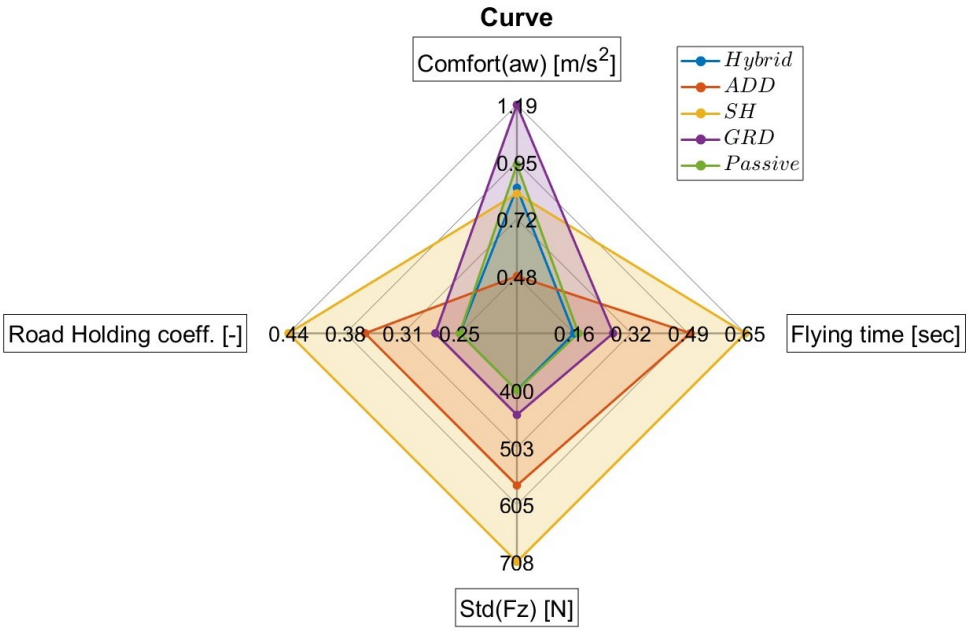

(b)

Figure 77: dynamic test result: a) on the straight b) during the turn manoeuvre

Further considerations regarding the graphs of figure 77 are stated in the current paragraph. The comfort-oriented control strategies may underestimate the importance of limiting the tyre-ground force variability, more specifically, in figure 72 is shown that ADD and Skyhook magnify considerably the possibility of reaching hazardous low tyre vertical forces when the corner speed is increased. The corner manoeuvre represents a critical situation since a reduced vertical ground force may induce an accident or an undesired handling feeling. As expected, the dynamic test proved that the aforementioned controllers optimise the acceleration isolation, however, they are not acceptable in corner events since the manoeuvre resulted in a crash, as shown in figure 78.

Figure 78: ADD and Skyhook resulted in crash

The Hybrid controller reduces the rider-perceived accelerations in the straight sections, providing a competitive solution to the ADD. On the other hand, the proposed controller guarantees acceptable handling properties limiting the tyre-ground forces variability or even minimising it. Moreover, considering the two main focuses of a suspension system separately, it is possible to state that the Hybrid law is able to master both handling and comfort, ensuring overall optimal performances. On the other hand, if the performances are measured only in the time domain, it is no longer possible to observe such superior outputs and the behaviour of the controller appears as a simple trade-off of the proposed competitive rationale. Anyway, the strength of the Hybrid-controlled semi-active suspensions lies in the possibility of adapting the controller to the context actively. Therefore it is legit to measure the performance in two separate moments, the first one when the cruising state is considered and comfort-enhanced properties are expected, and the second focused on the handling

capability during demanding manoeuvres, such as the U-turn in figure 74 b). Finally, to represent the motorcycle behaviour on a pothole in the middle of the corner, a very critical situation for a rider, the Belgian block pavement is substituted with a negative step of 0.05 m. The remaining aspects of the simulation are left unchanged, and the handling and comfort metrics are investigated. Figure 79 reports the handling indexes resulting from the simulation. The efficiency of the Hybrid control law during this exercise undergoes a small deterioration. In fact, the Hybrid logic is no longer the best handling-oriented strategy, since the frequency selector can not impose the Groundhook strategy in such a limited available time, and the Hybrid law is only able to approximate the Groundhook performances. Anyway, the hybrid strategy presents inspiring results and is definitely a competitive handling-focused controller for the passive and Groundhook systems.

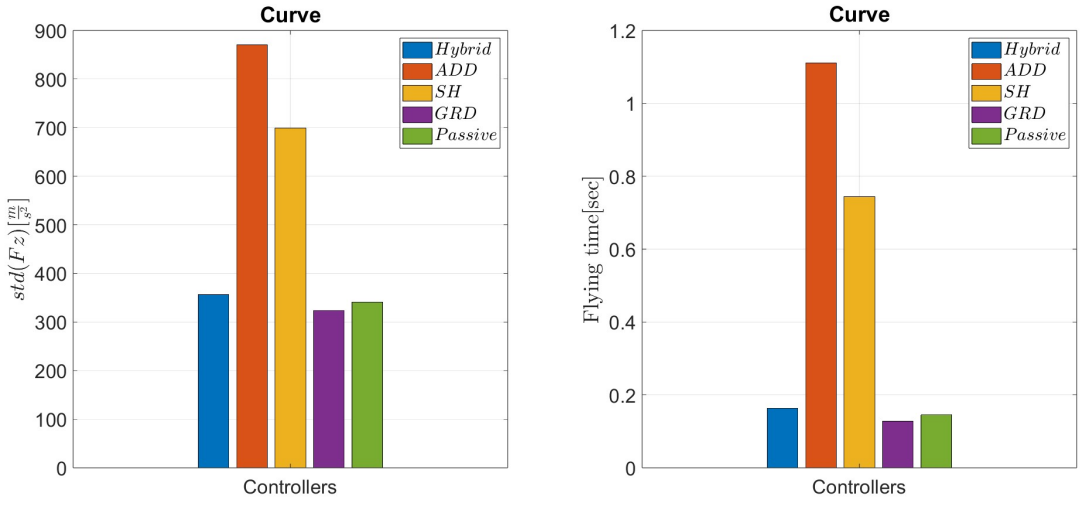

(a) (b)

Figure 79: a) Tire-ground force variability b) Flying time over a pothole

To have a complete overview of the Hybrid controller performance and behaviour over different disturbances in the most demanding condition as the centre of the corner, a positive step is finally simulated. Anyway, the results resemble the step analysis performed previously and reported in figure 68.

8 Manufacturing considerations and feasibility

The production of the Hybrid control logic presents numerous technical challenges, particularly when transitioning from theoretical design to prototyping, due to various practical implications. As deeply discussed in the previous passages the Hybrid control law is based on equation 26, therefore it is necessary to measure and estimate important quantities such as front and rear vertical accelerations and velocities of the vehicle body, and front and rear unsprung mass' kinematics. The sprung mass accelerations do not represent a critical point since absolute accelerations are relatively simple to determine. Indeed, the front and rear suspended mass accelerations are the only quantities which can be directly measured via accelerometers, positioned in meaningful motorcycle locations.

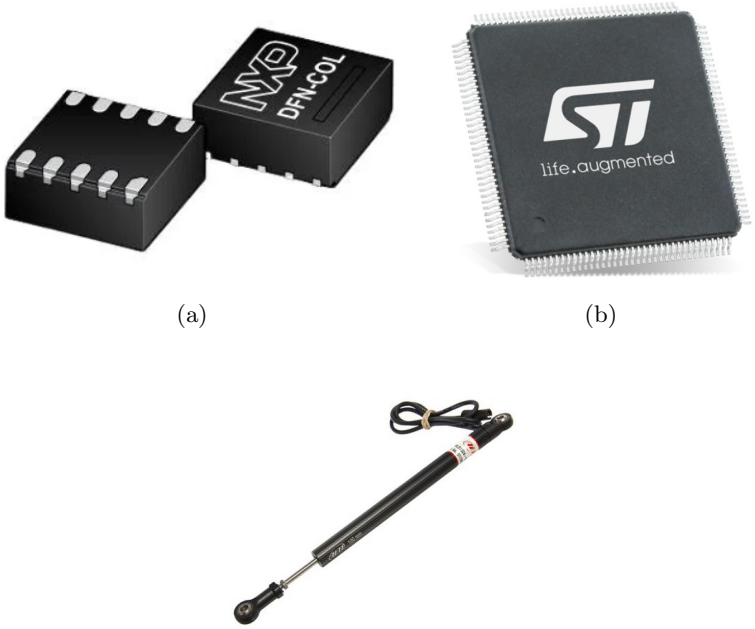

(a) (b)

(c)

Figure 80: Possible hardware requirement a) NPX triaxial accelerometer b) MCU STM32 series Micro-controller c) AIM potentiometer

To feed the suspension control unit with the front sprung mass acceleration signal it is possible to locate an accelerometer in the vicinity of the steering plate. Simi-

larly the rear sprung mass accelerations can be evaluated on the basis of the recorded signals from an accelerometer located nearby the rear suspension body mount. As imaginable, when the vehicle dynamic is limited to the vehicle in-plane it is enough to measure the vertical accelerations, however, when the motorcycle is proceeding into a turn it is necessary to correct the direction of the rider-perceived accelerations. To perform such an objective a gyroscope can be adopted to estimate the motorcycle tilt angle via a filtered integration of the rolling rate signal. Figure 80 a) represents a possible accelerometer which would fit the plant requirement since it is a triaxial accelerometer, equipped with an SPI or I2C interface and low working voltage requirement. Regarding the I/O requirements, the computation capability and the clock frequency necessary to perform the equations presented previously in real-time, the micro-controller unit proposed in figure 80 b) can be selected. It is impossible to directly measure the speeds of the sprung mass consequently, it is mandatory to estimate it through the integration of the perceived accelerations.

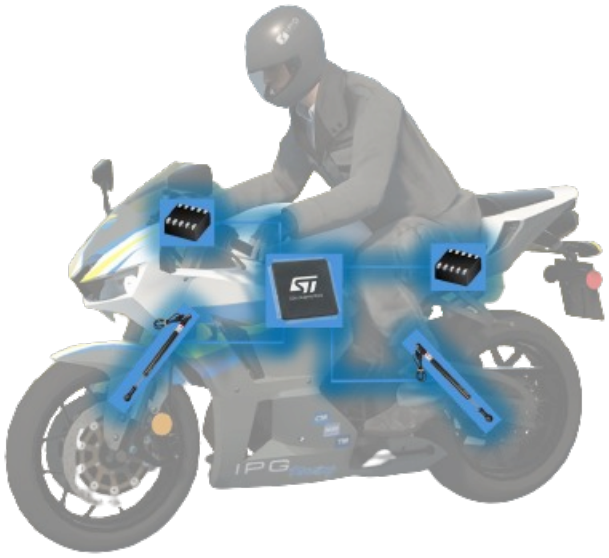

Figure 81: Vehicle data network scheme

Eventually, it is possible to apply a filtering process in advance to avoid the noise affecting the estimation quality. The unsprung mass velocity definition is a lesser trivial task. One of the simplest methodologies consists of retrieving the aforementioned quantity both at the front and rear suspension via a simple analysis based on the relative velocity estimated between the sprung and unsprung masses. Such

information is retrievable by the derivation of the filtered linear potentiometer signal. Indeed, the third important element in the hardware scheme of the suspension control unit is the linear position transducer shown in figure 80 c). Such a sensor measures the suspension stroke, and with good approximation, it is possible to state that it is equivalent to the sprung and unsprung mass relative position. By deriving such a quantity an estimation of the relative speed of the two masses is given. Anyway, the Hybrid control logic requires the absolute speeds of the cited bodies, therefore it is possible to estimate it by simply applying the relative motion laws to the sprung mass absolute speed and the sprung-unsprung mass relative velocity. The final configuration of the vehicle data network is represented in figure 81. The second point of this paragraph regards the semi-active damper system. As mentioned in 2.2 there are multiple solutions to implement a varying damping suspension, however, the simpler layout is constituted from a solenoid-controlled valve. Therefore the model of the controlled damper is represented by the following equation 40 and integrated into the vehicle Simulink scheme.

$$\dot{c}_{out}(t) = -\beta \cdot c_{out}(t) + \beta \cdot c_{in}(t) \tag{40}$$

The equation adopted is proposed by Savaresi in [18], where c_{out} is the actual damping value and the term c_{in} is the requested one imposed by the suspension control unit. The term β is the actuator's bandwidth and represents the semi-active suspension's rapidity to change the setting. It is worth mentioning that if the c_{in} value is confined between the minimum and the maximum damping, the c_{out} will be bounded as well, thus ensuring the passivity constrain [18]. The final consideration regards the frequency selector function. The main drawback of the proposed controller lies in the feasibility of retrieving the frequency of the input road profile. In literature multiple articles take into consideration a camera posed in front of the suspension pointed towards the road at a certain distance,e to provide a road preview. However, the strength of the Hybrid control law lies in its simplicity and relatively low-cost characteristics. Consequently, it is not recommended to adopt an expensive road preview system. A second possibility consists of estimating the road profile from the response of the front suspension and feeding such information to the rear axle [28]. An evident implication that limits the performance of the controller is the non-controllability of the front suspension, therefore only the rear damper has to ensure the target behaviour. A final resolution is simply based on the possibility of linking the vehicle speed to the expected input road frequency: if the road wavelength is known, it is possible to define the road frequency by simply dividing the vehicle speed in m/s by the road wavelength. It is straightforward to imagine the limitations of such a solution. Firstly, it is not always possible to observe a single specific wavelength, and large bandwidth signals are common in real road scenarios. In addition, it isn't easy to establish the wavelength of all the possible road ahead. Such a system can

be useful in circumstances in which the road characteristics are not varying largely or even rough information regarding the road is available, for instance in the case of connected vehicles. Possibly a resolution for the frequency estimation problem can be a hybrid of the proposed solutions.

9 Conclusions and future developments

The thesis project reported in this essay explores various avenues for addressing the suspension control of 2-wheeled vehicles. As discussed, the motorcycle panorama considers electronic suspension to a limited extent, due to the issues reported in the previous chapters, first among all the limited space available, the strict weight distribution limits and the energy harvesting. Such conditions drove semi-active suspension layouts to flourish in a limited manner to the premium motorcycle class, where a higher cost of the chassis technologies can be justified. The work presented aims to study the pre-existing suspension control rationale and evaluate alternative laws. More sophisticated competitor strategies are investigated nowadays, but for simplicity, the work focuses on simpler control logics. The idea is to retrieve a possible cheaper alternative based on simple logics, and possibly, hardware architecture. A second and as much important target is providing a controller capable of mastering both handling and comfort, two countertrend properties and a limiting factor of the traditional suspensions. The proposed suspension control strategy is a cutting-edge hybridisation of the literature rationales on two different plans: a first layer consists of two different control logics, one focused on mastering the comfort objective, and a second oriented towards the optimisation of handling indexes. The resulting controller is an adaptive logic able to switch for the optimal control law on the basis of the vehicle attitude. Along with a gradually increasing perceived acceleration, a weighting function gradually selects the handling strategy instead of the comfort law. Indeed, it is possible to assess that the control rationale is a hybridisation of comfort and handling-oriented controllers. A second level of hybridisation lies in the algorithms adopted to implement the aforementioned control logics: the comfort-oriented control strategy is a blend of Skyhook and Acceleration Driven Damper (ADD), more specifically the Suspension control logic (SCU) imposes the Skyhook at lower frequencies, whereas over a particular crossover frequency the ADD logic is adopted. Similarly, the adherence strategy is composed of a hybridisation of the ADD, the low-frequency handling optimal control law, and the best-handling-operating controller at higher frequencies, the Groundhook logic. Therefore to implement the proposed hybrid controller it is necessary to estimate the frequency of the incoming road signal. Such an aspect is the most critical point of the project since the road sensor adopted in the simulations is expensive and difficult to implement in real conditions. The proposed hybrid controller is designed and tested with different vehicle models. Once the parameters of the control logic are tailored to the motorcycle adopted in the simulations, the performance of the 2-wheeler is assessed via multiple simulations over different real road-like pavements, such as a Belgian block and a step road. The final results show that the proposed logic is

effective in enhancing comfort when the vehicle is cruising, thus riding in-plane with reduced accelerations perceived. On the other hand, when the vehicle turns the objective is no longer the comfort, and the safety of the rider becomes the major concern. Consequently, the SCU implements the handling-oriented control strategy to limit the possibility of experiencing a crash. To summarise, it is possible to state that if the performance of the controller is measured in time domain it is impossible to perceive an effective improvement in adopting the proposed control law with respect to the competitors or even the passive vehicle. However, if the performance is measured considering the level of comfort whenever comfort is the major objective, the Hybrid control law can effectively master such a metric. Similarly when the most important factor is adherence, the proposed solution is able to provide competitive or even superior results in minimizing tire-ground force variability and flying time. From this point of view, it is possible to assert that the Hybrid law is optimal in maximising comfort, without increasing the possibility of facing a crash or the degradation of the rider's feeling.

Possible future developments may focus on further reducing the perceived acceleration by including the pitch oscillation reduction. The mix-pitch algorithm proposed by Savaresi and reported in section 3 can represent an important starting point. Additional research may focus on the estimation of the crossover frequencies of the rationales proposed, and investigate the possibility of adopting a wheelbase preview system, based on Wiener filter theory or a cheap road sensor to estimate the frequency of the road input signal. A third possible field of development for frequency estimation consists of linking the vehicle speed to the road wavelength. The proposed work focuses on the design of the suspension control strategy on a target vehicle (and rider) with specific features. On the other hand, future works can focus on the possibility of adapting the rationale to a varied group of vehicles and riders, thus ensuring optimal responses to different working conditions. Even if briefly described in section 8, prototyping and testing a semi-active controlled suspension still represents an opportunity to further develop the work proposed, facing industrial and manufacturing-related challenges. Finally, a newsworthy development of the proposed controller lies in the implementation of a preview system, which may serve not only to assess road frequencies but also to investigate the potential advantages it offers to the project at hand.

A Appendix

The models and principal equations adopted in the simulations are shown in the current section. In order to have a deeper analysis into the presented results, it is important to explicit the methodology adopted to retrieve them. As mentioned in 4.1 the mathematical description of the models is composed of differential equation systems implemented in Matlab-Simulink, except for the last chapter, where the simulations were implemented exploiting the IPG-MotorcycleMaker software.

A.1 Quarter-car model

To simulate the behavior of the suspension the so-called quarter-car vehicle model is adopted. The 2 DOF system is represented by as many differential equations represented in 41, where the two statements refer to the sprung and unsprung mass respectively.

$$\begin{cases} m_s\ddot{z}_s = +c_s(t)(\dot{z}_u - \dot{z}_s) + k_s(z_u - z_s) \\ m_u\ddot{z}_u = c_t(\dot{h} - \dot{z}_u) + k_t(h - z_u) - c_s(t)(\dot{z}_u - \dot{z}_s) - k_s(z_u - z_s) \end{cases} \tag{41}$$

The terms h and $\dot{h}$ are the road profile and road speed profile, whereas $c_s(t)$, and k_s represent the suspension damping and stiffness properties. Differently, c_t and k_t are referred to the tyre vertical damping and stiffness value. $c_s(t)$ is the controlled damping value, consequently it is imposed in any time step by the suspension ECU, while the remaining symbols are constant parameters, thus imposed in the pre-processing phase of the simulation. Figure 82 reports the Simulink model where 41 is implemented. More specifically, the sprung mass and unsprung mass equations of motion are divided for the sake of clarity into two different subsystems. The unsprung equation of motion is fed with the road input (i.e. h and $\dot{h}$) defined in a specific blok as well. The controlled-suspension damper set $c_s(t)$ is also computed in a separate set of equations, and fed to both the subsystems presented. Referring to the masses' motion equation 41, the sum of forces is divided by the respective mass term thus isolating the acceleration term, and their velocity and position values are mathematically computed through an integration process. The simulation's setting is paramount, since it may induce computational errors or unexpected results. To properly catch the system dynamics, the simulation's solver step is a *fixed step* of an amplitude of 1 ms, furthermore, to simplify the numerical burden the solver type is chosen as *Automatic*, to avoid any possible simulation set mistake.

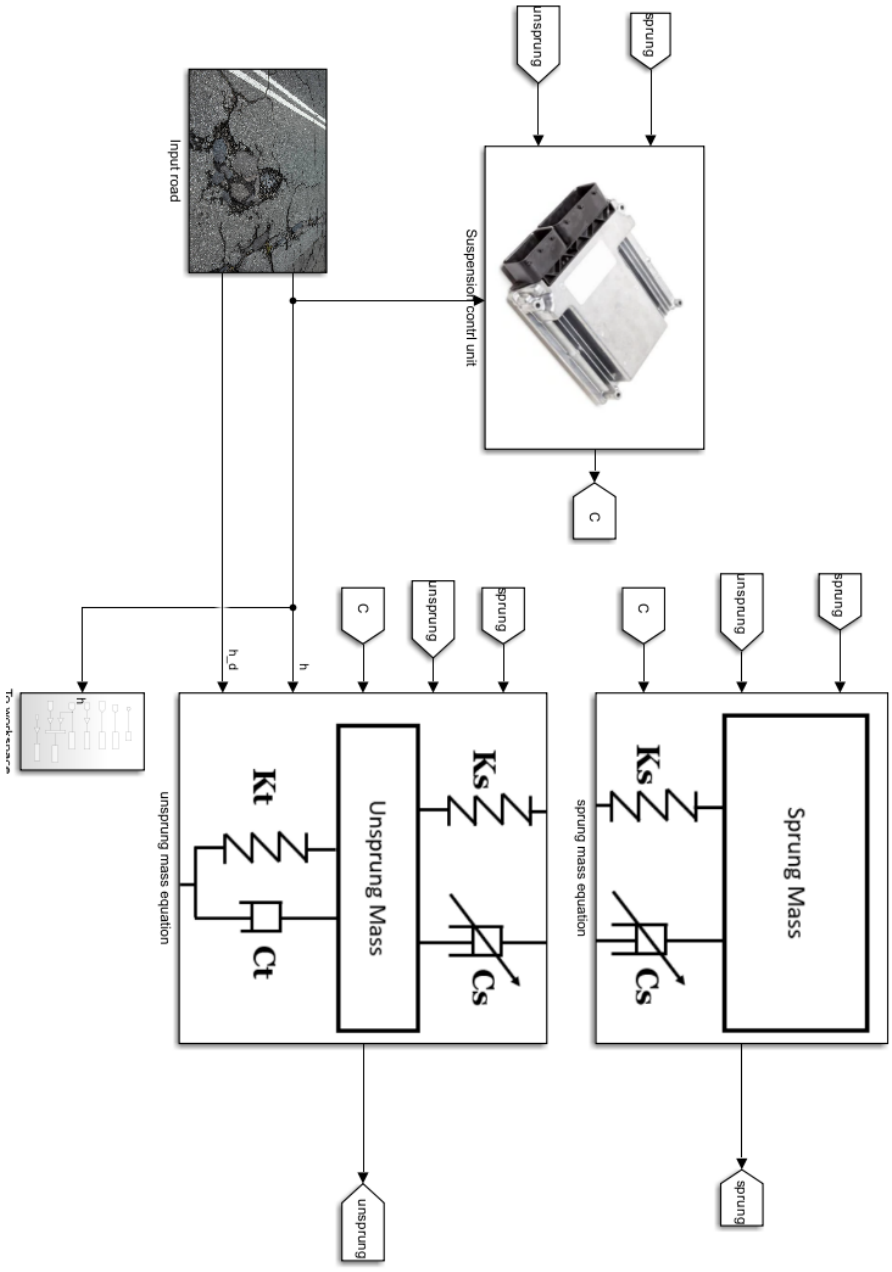

Figure 82: quarter-car vehicle model Simulink implementation

A.2 4DOF vehicle model

The 4DOF Simulink model is briefly described in this section. The 4DOF vehicle model is represented by the 4 differential equations contained in system 42. Each line describes the motion of one degree of freedom of the model, which as mentioned in 6.1 consist of the sprung mass vertical translation, the sprung mass pitch oscillation and the unsprung vertical motions.

$$\begin{cases} m\ddot{z}_s = k_{s,f}[z_{u,f} - (z_s + \theta a)] + k_{s,r}[z_{u,r} - (z_s - \theta b)] + c_{s,f}[\dot{z}_{u,f} - (\dot{z}_s + \dot{\theta} a)] \\ +c_{s,r}[\dot{z}_{u,r} - (\dot{z}_{u,r} - (\dot{z}_s - \dot{\theta} b)] \\ \\ J\ddot{\theta} = k_{s,f}[z_{u,f} - (z_s + \theta a)]a + k_{s,r}[z_{u,r} - (z_s - \theta b)]b + c_s[\dot{z}_{u,f} - (\dot{z}_s + \dot{\theta} a)]a \\ +c_s[\dot{z}_{u,r} - (\dot{z}_{u,r} - (\dot{z}_s - \dot{\theta} b)]b \\ \\ m_{u,r}\ddot{z}_{u,r} = -k_{s,r}[z_{u,r} - (z_s - \theta b)] + k_t(h_r - z_{u,r}) - c_s[\dot{z}_{u,r} - (\dot{z}_s - \dot{\theta} b)] \\ +c_t(\dot{h}_r - \dot{z}_{u,r}) \\ \\ m_{u,f}\ddot{z}_{u,f} = k_{s,f}[z_{u,f} - (z_s + \theta a)] + k_t(h_f - z_{u,f}) - c_s[\dot{z}_{u,f} - (\dot{z}_s + \dot{\theta} a)] \\ +c_t(\dot{h}_f - \dot{z}_{u,f}) \end{cases} \tag{42}$$

At each simulation step the Simulink scheme resolves for $\ddot{z}_s$,$\ddot{\theta}$, $\ddot{z}_{u,f}$ and $\ddot{z}_{u,r}$, the degrees of freedom of the model, and the respective speeds and motions variables are found by integrating. Coherently with the quarter-car model, also in this Simulink the variable damping c_s is defined in a specific block and fed to the vehicle plant. The remaining terms a, b, $k_{s,f}$, and $k_{s,r}$ are respectively the semi-front and rear wheelbase, and the front and rear suspension stiffnesses. In addition to these, the tyre parameters c_t and k_t are imposed as constant values. The Simulink layout resembles the quarter-car implementation, therefore each equation is resolved in separate subsystems and every variable is passed through 'Go To' blocks for sake of clarity and simplicity. The inputs once defined in a specific box are fed to the unsprung masses' subsystems. It is worth mentioning that the rear road profile is the same input as the front road, except for a delay equal to the time the vehicle spends to cover a path equal to the wheelbase. Such a hypothesis is generally respected since the wheels of a 2-wheeler are usually aligned or deviate marginally. Indeed, the steering angle is insignificant with respect to a four-wheel vehicle. Also in this case the simulation is implemented by imposing a fixed step and automatic solver.

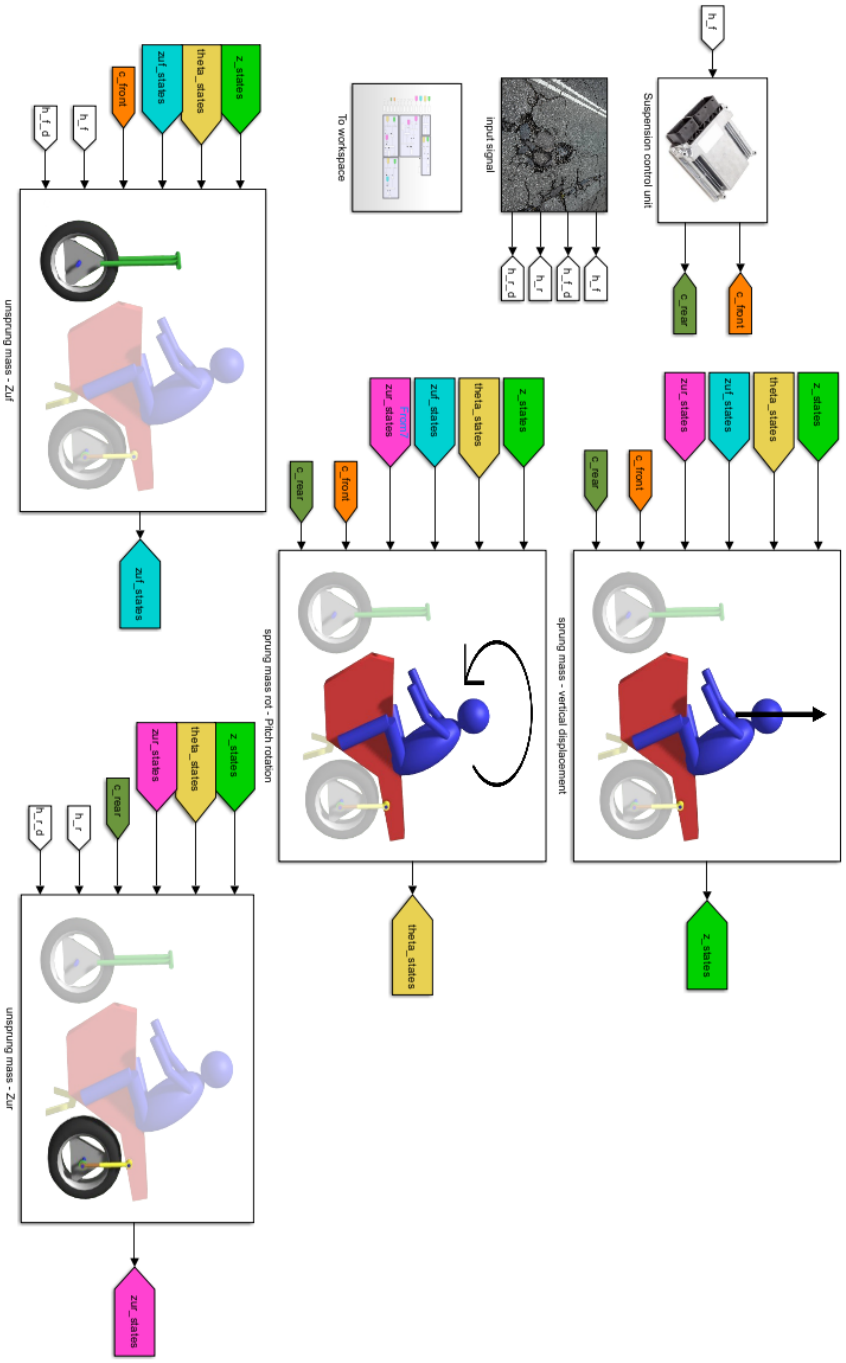

Figure 83: 4DOF model Simulink implementation

A.3 IPG MotorcycleMaker-Simulink model

In 7 the multi-body analysis of the vehicle equipped with the Hybrid control law is presented, and for coherence with the preceding models, the schemes adopted are reported in this subsection. The MotorcycleMaker simulator operates within a proprietary environment inaccessible to users. To facilitate a Simulink-MotorcycleMaker co-simulation, the IPG software house developed a dedicated SLX file. MotorcycleMaker's operational mechanism involves the iterative resolution of differential equations across multiple time steps, comprising equation resolution and subsequent updating processes. The Simulink file serves as an interface, granting users access to the updating process. Consequently, users can interpose their models into the signal flow directed to MotorcycleMaker, thereby overriding the signals computed internally by MotorcycleMaker. In figure 85 is reported the Simulink frame where the MotorcycleMaker equations are recalled through S-Function blocks. In this particular scenario, the objective is to override the signals related to suspension forces and substitute the standard suspension with the proposed Hybrid-controlled layout. An important difference concerning the previous models, is that in IPG the suspension-related quantities are not directly available. Therefore, the sensors supposed to be mounted on the bike are implemented into the IPG model. It is mentionable that if the sprung masses' quantities are directly retrievable from the accelerometers placed on the steering plate and the rear shock absorber-body mount, to compute the unsprung masses' kinematics the following Simulink scheme of figure 84 was necessary. In this manner it was possible to estimate the absolute velocity of the unsprung masses, as discussed in section 8. Here the signals coming from the sensors are first filtered, and successively the absolute unsprung speed is computed by adding to the sprung mass absolute velocity the relative speed of the two masses.

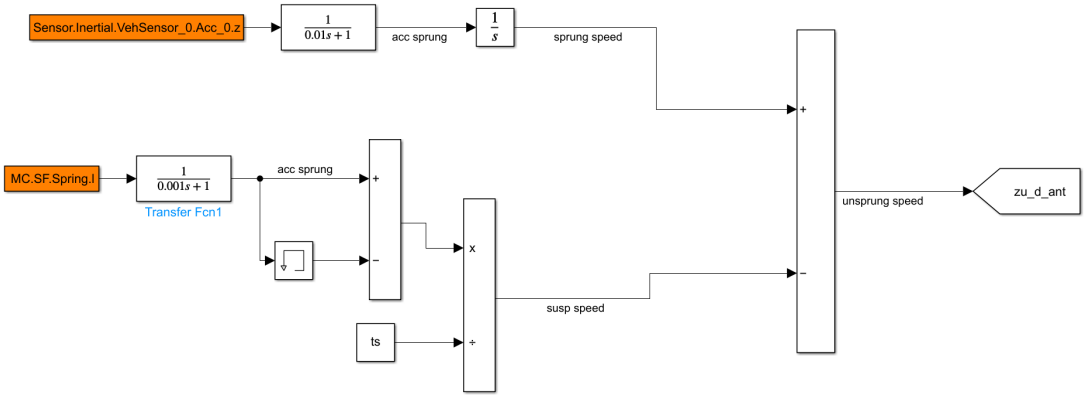

Figure 84: Derivation of the unsprung mass scheme

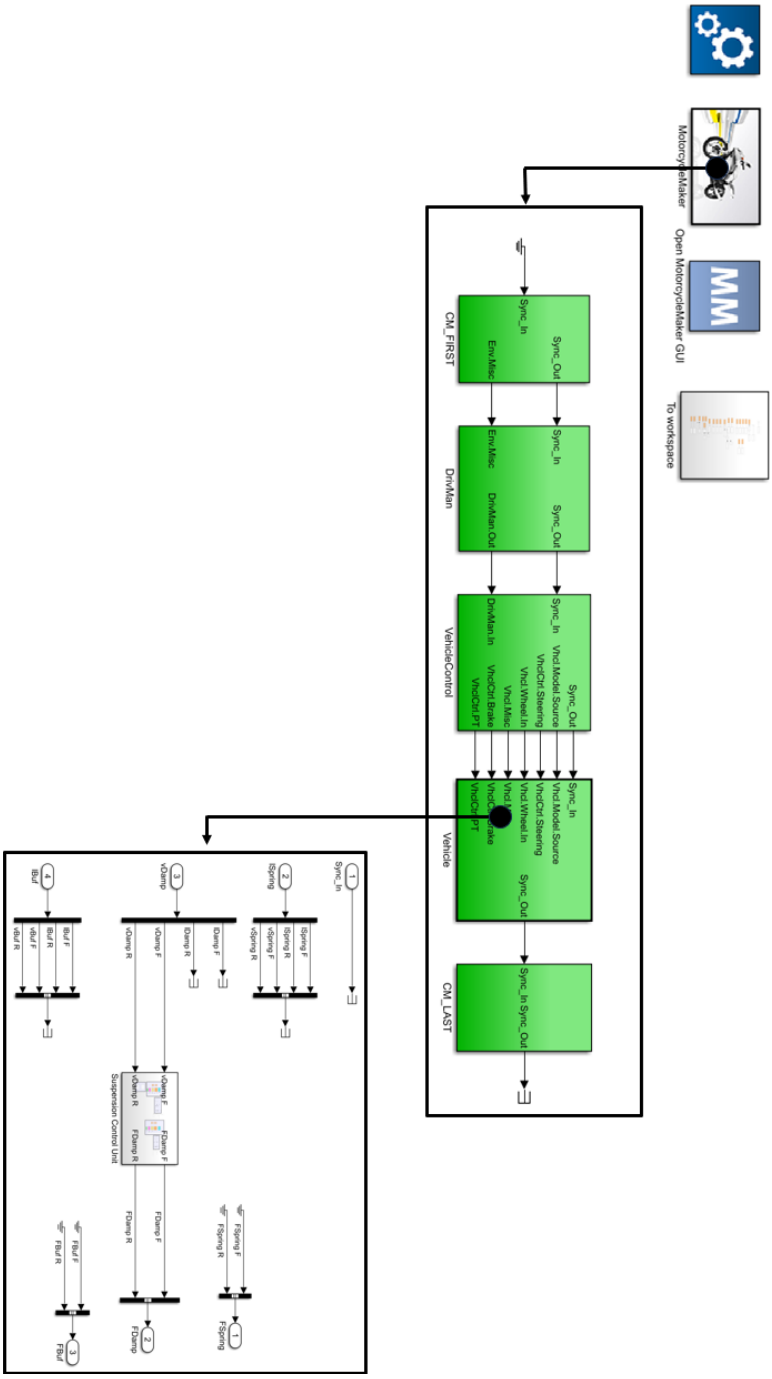

Figure 85: MotorcycleMaker-Simulink co-simulation scheme

A.4 Suspension control unit model

The SCU-Suspension Control Unit is the micro-controller where the Hybrid (and the competitive controllers) algorithm is implemented. In the Simulink models the controller's equations are enclosed in a specific subsystem, whose content is essentially unaltered and shared between the different models proposed. In figure 86 the MotorcycleMaker implementation of the SCU and the controllable damper is reported, and compared with the other models, the only variation regards the retrievement of the quantities essential to compute the algorithm, such as the accelerations and speeds of the vehicle masses. The damper model consists of the equation 40, and the SCU considers the different control laws taken into account in the project. More specifically, the Simulink scheme of the hybrid control algorithm is proposed in figure 87, where equation 24 is implemented as well as the two different logics of the Hybrid control law, the comfort-oriented and the handling-focused rationale. Figure 87 shows also the weighting function η block, where the orientation parameter is computed based on the acceleration perceived.

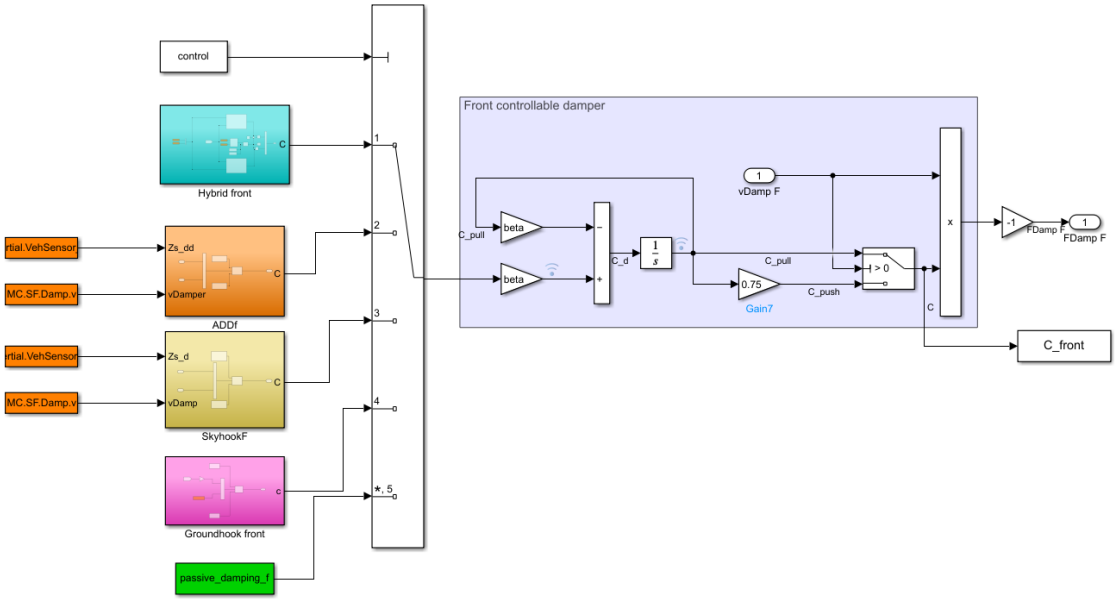

Figure 86: SCU and damper Simulink model

The damper is modelled to correctly simulate a softer compression in comparison with the rebound phase. Therefore, for sake of simplicity a proportional reduction in rebound is actuated by reducing selected damping by 25%. The final -1 gain is necessary to fit the MotorcycleMaker reference system.

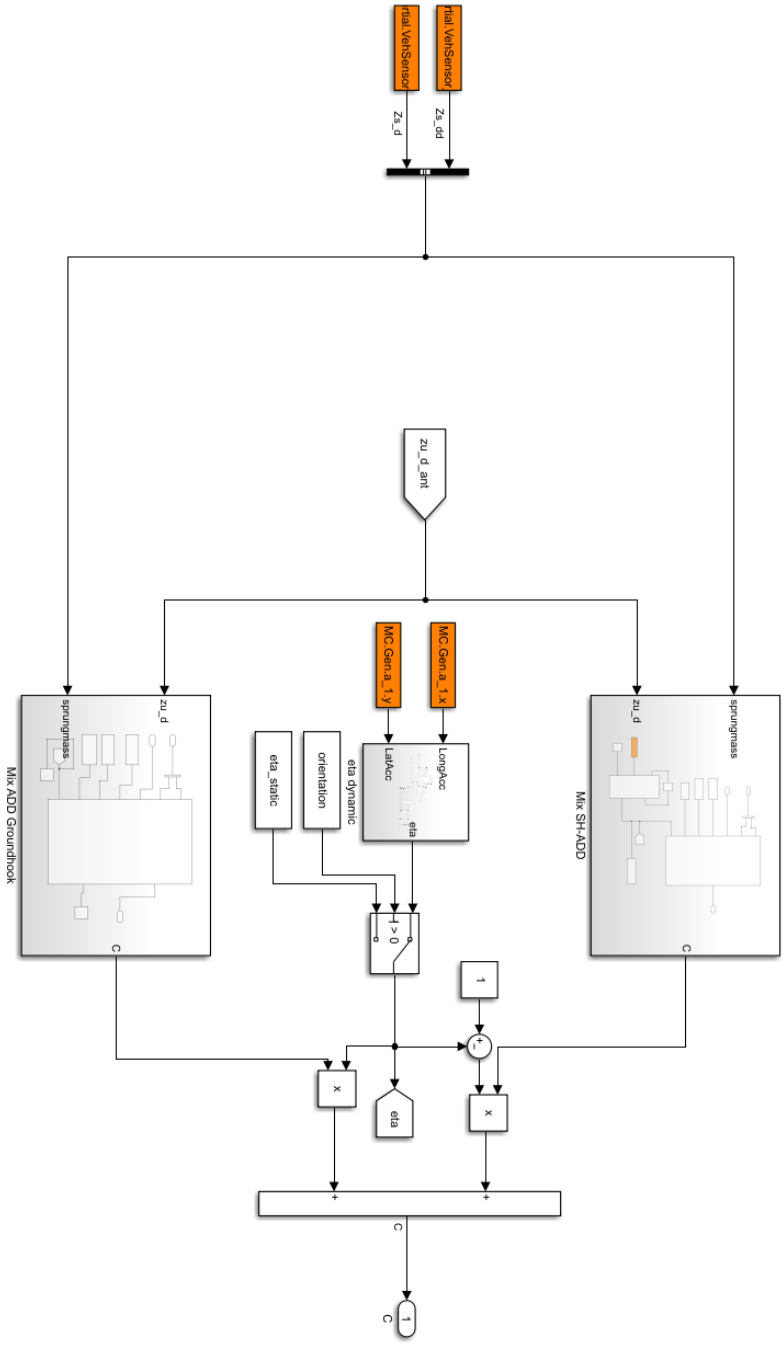

Figure 87: Hybrid controller Simulink scheme

To conclude the Simulink models analysis one of the two opposite-oriented control laws of the Hybrid rationale is presented. The comfort-focused strategy is reported in figure 88 where the algorithm is executed via Matlab function, as well as the frequency estimator function proposed in section 5.2. This block resembles a MATLAB script where the Fast Fourier Transform (FFT) is calculated, and equation 22 is expressed. The output is the instantaneous estimated frequency to feed the comfort strategy algorithm and implement correctly the Skyhook or the ADD strategies.

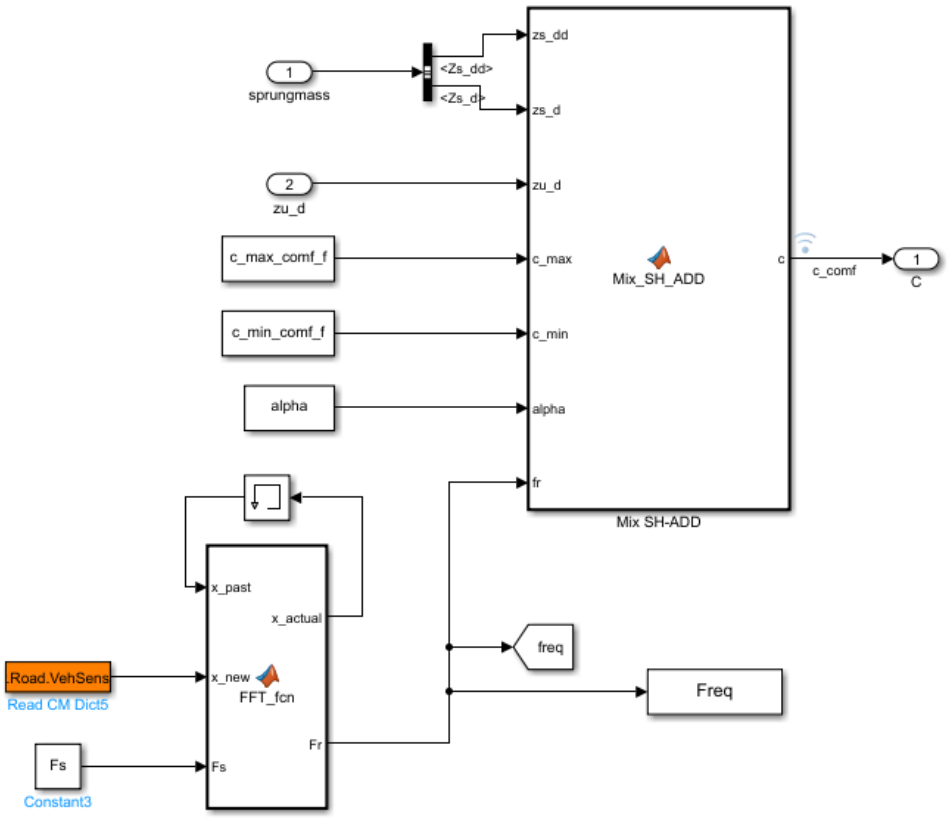

Figure 88: Simulink implementation of the front suspension comfort-oriented control law

The frequency selection function takes as inputs the sampling frequency and, as imaginable, the information regarding the road profile, in this case through a specific road sensor. Finally, the integration of the opposing handling-oriented control scheme is analogous, with the exception of the absence of the frequency estimator function.

References

[1] ZF commercial vehicle solutions. *Continuous Damping Control: Optimum Damping for Every Wheel on any Road*.

[2] Vittore Cossalter, Roberto Lot, and Matteo Massaro. Motorcycle dynamics. *Modelling, Simulation and Control of Two-Wheeled Vehicles*, page 168, 2014.

[3] Vittore Cossalter, Roberto Lot, and Matteo Massaro. Motorcycle dynamics. *Modelling, Simulation and Control of Two-Wheeled Vehicles*, page 181, 2014.

[4] Vittore Cossalter, Roberto Lot, and Matteo Massaro. Motorcycle dynamics. *Modelling, Simulation and Control of Two-Wheeled Vehicles*, page 219, 2014.

[5] Vittore Cossalter, Roberto Lot, and Matteo Massaro. Motorcycle dynamics. *Modelling, Simulation and Control of Two-Wheeled Vehicles*, page 200, 2014.

[6] Vittore Cossalter, Roberto Lot, and Matteo Massaro. Motorcycle dynamics. *Modelling, Simulation and Control of Two-Wheeled Vehicles*, page 203, 2014.

[7] Vittore Cossalter, Roberto Lot, and Matteo Massaro. Motorcycle dynamics. *Modelling, Simulation and Control of Two-Wheeled Vehicles*, page 210, 2014.

[8] Firth G Crolla DA and Horton D. *An introduction to vehicle dynamics*. Department of Mechanical Engineering, Leeds University, UK,, 1992.

[9] Giancarlo Genta and Lorenzo Morello. *The automotive chassis: vol. 2: system design*. Springer, 2009.

[10] Keith Howard. Active suspension. *Motor Sport Magazine*, 7 July 2014.

[11] Kawasaki Heavy Industries. *KECS-Kawasaki Electronic Control Suspension*.

[12] Mina Morad Saber Kaldas. Improvement of semi-active suspensions through fuzzy-logic and top mount optimization. *Shaker-Verlag*, 2015.

[13] Dean Karnopp, Michael J Crosby, and RA Harwood. Vibration control using semi-active force generators. *Journal of Engineering for Industries*, 1974.

[14] Ansar Mulla, Sudhindra Jalwadi, and Deepak Unaune. Performance analysis of skyhook, groundhook and hybrid control strategies on semiactive suspension system. *International Journal of Current Engineering and Technology*, 3:265–269, 2014.

[15] Ohlins. *Öhlins TTX 36 EC Supersport Shock Absorber KA 035*.

[16] Corina Sandu. Vehicle dynamics: Theory and applications. *Journal of guidance, control, and dynamics*, 33(1):287–288, 2010.

[17] Sergio M Savaresi, Charles Poussot-Vassal, Cristiano Spelta, Olivier Sename, and Luc Dugard. *Semi-active suspension control design for vehicles*. Elsevier, 2010.

[18] Sergio M Savaresi, Enrico Silani, and Sergio Bittanti. Acceleration-driven-damper (add): an optimal control algorithm for comfort-oriented semiactive suspensions. *ASME. J. Dyn. Sys., Meas., Control.*, 2005.

[19] Sergio M Savaresi and Cristiano Spelta. Mixed sky-hook and add: Approaching the filtering limits of a semi-active suspension. *ASME. J. Dyn. Sys., Meas., Control.*, 2007.

[20] AMA Soliman and MMS Kaldas. Semi-active suspension systems from research to mass-market–a review. *Journal of Low Frequency Noise, Vibration and Active Control*, 40(2):1007, 2021.

[21] AMA Soliman and MMS Kaldas. Semi-active suspension systems from research to mass-market–a review. *Journal of Low Frequency Noise, Vibration and Active Control*, 40(2):1008, 2021.

[22] AMA Soliman and MMS Kaldas. Semi-active suspension systems from research to mass-market–a review. *Journal of Low Frequency Noise, Vibration and Active Control*, 40(2):1009, 2021.

[23] AMA Soliman and MMS Kaldas. Semi-active suspension systems from research to mass-market–a review. *Journal of Low Frequency Noise, Vibration and Active Control*, 40(2):1013, 2021.

[24] Cristiano Spelta, Diego Delvecchio, and Sergio M Savaresi. A comfort oriented control strategy for semi-active suspensions based on half car model. In *Dynamic Systems and Control Conference*, volume 44182, pages 835–840, 2010.

[25] Cristiano Spelta, Sergio M Savaresi, and Luca Fabbri. Experimental analysis of a motorcycle semi-active rear suspension. *Control Engineering Practice*, 18(11):1239–1250, 2010.

[26] British Standard. Mechanical vibration and shock — evaluation of human exposure to whole-body vibration. Technical report, ISO-International Organization for Standardization, 1997.

[27] Takenori Terada, Kazuhiro Ichikawa, Hideyuki Kato, and Taro Iwamoto. A study of the control logic of electronically controlled suspension for motorcycle. Technical report, SAE Technical Paper, 2020.

[28] Johan Theunissen, Antonio Tota, Patrick Gruber, Miguel Dhaens, and Aldo Sorniotti. Preview-based techniques for vehicle suspension control: A state-of-the-art review. *Annual Reviews in Control*, 51:206–235, 2021.

[29] Alessandro Vigliani. Quarter-car model analysis. In *Vehicle Dynamics Simulation lecture*, 2023.